Gallium nitride photonic crystals

Roeling, E.M.

Award date:
2007

Gallium Nitride Photonic Crystals

Erik M. Roeling

March 2007

Abstract

Gallium nitride (GaN) is a wide bandgap semiconductor used for the fabrication of ultra-violet, blue or green light emitting diodes (LEDs) and lasers. GaN LEDs are becoming increasingly more important as solid state light sources. Most of the generated light inside a LED is trapped due to total internal reflection. For a GaN planar LED with refractive index of ~2.5, only 8% of the generated light is radiated to air.

Photonic crystals (PhCs) are periodic dielectric structures in one, two (2D) or three dimensions which can exhibit a photonic bandgap (PBG). They can be used to enhance the overall efficiency of LEDs through Purcell enhancement, redistribution of light emission or Bragg scattering of light.

The focus of this thesis is on GaN 2D PhCs. It is investigated how 2D PhCs can be used for enhancement of the external quantum efficiency of LEDs. Finite Difference Time Domain (FDTD) light extraction simulations are performed. A GaN 2D PhC with a PBG around the optical telecommunication wavelength (1.55 μm) is designed by 3D FDTD transmission simulations and subsequently fabricated. For the first time a GaN 2D PhC is characterized by optical transmission measurements.

This work has been performed as part of the Master of Science Degree in Applied Physics at the University of Technology Eindhoven (TU/e) under supervision of Prof. Dr. H.W.M. Salemink and Dr. R.W. van der Heijden.

Table of Contents

Chapter 1 Introduction

In 1946 E.M. Purcell [Purcell1946] predicted that the probability of spontaneous emission is increased when an atom is placed inside a wavelength size resonant optical cavity. This was the first step towards the control of the optical properties of materials. The concept of photonic crystals (PhCs) was simultaneously introduced by E. Yablonovitch [Yablonovitch1987] and by S. John in 1987 [John1987]. A PhC is a periodic arrangement of dielectric media in one, two or three dimensions which can exhibit a photonic bandgap (PBG). With PhCs properties of light can be controlled on the scale of its wavelength, including the realization of wavelength size cavities.

Solid state lighting is becoming increasingly important in today's society. General Electric invented the first (red) light emitting diode (LED) in 1968. It was made from gallium phosphide and the efficiency was about 1 lumen per watt [DOE2003]. For comparison, the efficiency of an incandescent light bulb is about 10 to 15 lumen per watt [Wikipedia2007]. Nowadays, LEDs with efficiencies of more than 100 lumens per watt - depending on color - are fabricated.

The applications of LEDs are numerous, e.g. in displays, beamers, traffic lights and automotive lighting (head-up displays, lighting and sensors). With the increasing amount of energy used in the world LEDs can reduce energy consumption and therefore CO_2 emissions.

In a 2003 report from the U.S. Department of Energy it is predicted that changing the incandescent light sources of traffic signals into LEDs could save 4.5 TWh a year. This is half the annual output of a large electrical power station. Converting all the light sources to LEDs in cars, trucks and busses would save 5.3 billion liters of gasoline and 4.2 billion liters of diesel a year in the USA (more than 30 days of oil flow in the Alaska pipeline at full capacity) [DOE2003].

Since the invention of the LED new materials are used and therefore new colors are available. For the fabrication of a blue LED, semiconductors such as zinc selenide (ZnSe) and the wide bandgap semiconductor gallium nitride (GaN) were investigated intensively. For a long time ZnSe was regarded as the most promising material of the two due to growth problems of GaN. The lifetime of blue ZnSe LEDs is however limited due to the creation and propagation of defects. In 1986 Akasaki et. al. succeeded to grow GaN on Sapphire using metal organic vapour phase epitaxy. They also experimented with p-type doping of GaN and in 1992 a GaN based blue LED was demonstrated. In 1994 the Japanese company Nichia introduced GaN based LEDs for the commercial market. These diodes exhibited high luminescence output. Nichia introduced the first GaN based laser just two years after that [Nakamura2000].

Although the efficiency of LEDs is relatively high compared to incandescent light bulbs, most of the light generated inside a LED will not be emitted due to total internal reflection. The efficiency of LEDs is expressed in the external quantum efficiency, which is a product of the injection efficiency (the ratio of the electron current to the total forward current in the quantum well region), the light generation

efficiency and the light extraction efficiency. For a planar LED a meager 4 to 9 percent[1], depending on the material, of the generated light can be extracted!

There are several ways to enhance the light extraction efficiency. Mostly this is done by changing the geometrical structure of the LED. A relative new method of enhancement of the light extraction efficiency is the use of PhCs.

The aim of this Masters Degree project is twofold. One goal is to investigate the use of PhCs for light extraction efficiency in particular in GaN LEDs. The other goal is to start experimenting with GaN PhCs.

GaN is an interesting material due to the wide bandgap and the operating wavelength regime (UV-blue-green). With the proper development of GaN PhC technology it is expected that more applications will emerge, like optical sensors in optical integrated circuits at visible wavelengths.

1.1.1 Thesis Outline

An introduction into light guiding and extraction is given in Chapter 2. The basic theory of PhCs and dielectric waveguiding is presented. The theory of waveguiding will later on be used in light extraction simulations. Furthermore, the enhancement of the external quantum efficiency by the use of PhCs is treated. Finally common techniques used to enhance the extraction efficiency in LEDs are discussed.

An introduction in the material properties of GaN is given in Chapter 3. The current status on GaN PhCs is treated subsequently.

Simulation results of light extraction in a material are presented in Chapter 4. The simulations are done with Crystal Wave, a simulation program specially designed for solving Maxwell equations in PhCs.

As a first experiment a GaN on sapphire PhC with a bandgap around the optical telecommunications wavelength (1.55 μm) is designed and fabricated. In Chapter 5 the design and fabrication, and measurement results are described.

The conclusions are presented in Chapter 6.

[1] $2 \cdot 1/\left(4n^2\right)$, with n the refractive index [Appendix I].

Chapter 2 Light Guiding and Extraction

In this chapter basic properties of dielectric wave guiding and PhCs are presented. Dielectric waveguides are used in experiments to direct light to and from PhCs. In light outcoupling simulations dielectric slab waveguides are used to simulate light outcoupling of a planar LED. The introduction into PhCs is largely a repetition of band theory in solid state physics. It will be explained in further detail how PhCs are used to enhance light extraction from a LED.

2.1 *Dielectric Wave Guiding*

It follows from Snell's law that a light wave impinging upon a boundary from one dielectric medium to another dielectric medium with lower refractive index can be totally reflected. For total reflection the angle between the incident light ray and the normal to the plane has to be larger than the critical angle. With this principle it is possible to guide a light wave through a high index slab that is surrounded by media of lower refractive index. In this section the principle of wave guiding is introduced by using ray optics [Saleh1991].

Mode Propagation

Consider a dielectric slab with refractive index n_{core} and thickness d, covered on both sides by a material with lower refractive index $n_{cladding}$ as shown in Figure 2-1. Light propagates through the high index layer in allowed modes which comply with the self consistency condition: a wave reproduces itself after reflecting twice.

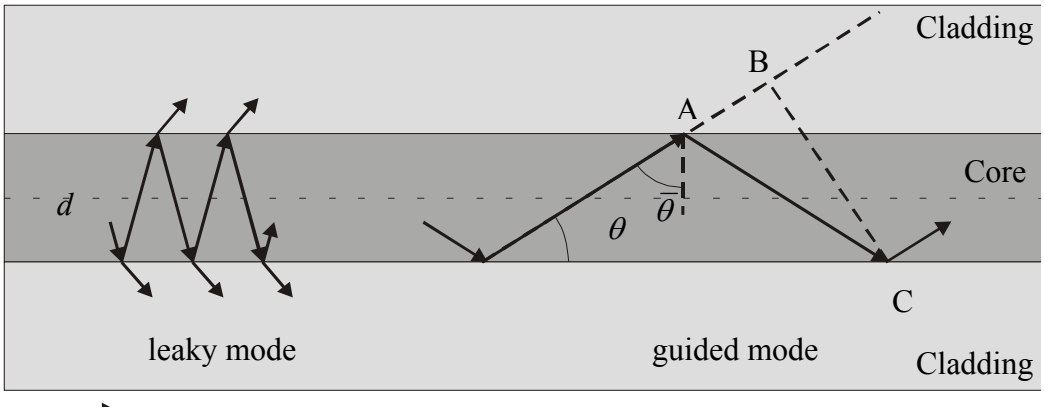

Figure 2-1: cross-section of a planar dielectric waveguide.

In a round trip the twice reflected wave lags behind the original wave with a distance of $\overline{AC} - \overline{AB} = 2d\sin\theta$. A phase shift φ_r is introduced for each reflection at a dielectric boundary. For self consistency the total phase shift between the two waves has to be zero or a multiple of 2π:

$$\frac{2\pi}{\lambda} 2d\sin\theta - 2\varphi_r = 2\pi m \qquad \textbf{[2.1]}$$

with λ the wavelength and m an integer. The modes are found by inserting the expression for φ_r for reflections at a dielectric interface. For light with transverse electric polarization (TE, electric field in plane) the self consistency condition is given by:

$$\tan\left(\pi\frac{d}{\lambda}\sin\theta_m - m\frac{\pi}{2}\right) = \sqrt{\left(\frac{\sin^2\bar{\theta}_c}{\sin^2\theta_m} - 1\right)} \qquad \textbf{[2.2]}$$

$\bar{\theta}_c$ is the complement of the critical angle and θ_m the mode angle. This expression is a transcendental equation which is solved numerically for θ_m. There is at least one intersection point and therefore one allowed mode in a dielectric waveguide, the fundamental mode. With decreasing wavelength the number of intersection points rises and with that the number of allowed modes.

In Figure 2-2 mode intensity profiles are shown for a 1 µm thick GaN slab with air claddings [Hammer2007]. The figure shows that a mode penetrates into the cladding layers. Higher order modes (longer wavelengths) do penetrate further into the claddings: the mode energy is spread towards the lower index claddings. A higher order mode is therefore less confined to the core layer than the fundamental mode.

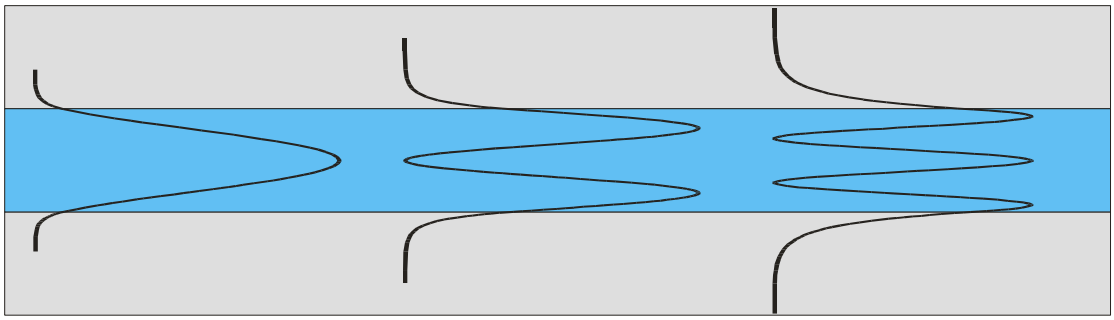

Figure 2-2: intensity mode profiles of the first three modes of a GaN slab with thickness of 1 µm for λ= 400 nm. The refractive index of GaN was 2.53 and of the claddings 1 [Hammer2007].

Effective Refractive Index

The propagation constant of mode m is defined as the parallel wavevector of that mode:

$$\beta_m = n_{core} k_0 \cos\theta_m \qquad \textbf{[2.3]}$$

with $k_0 = 2\pi/\lambda_0 = \omega/c$. λ_0 is the vacuum wavelength and c the speed of light. Equation [2.3] can also be expressed as:

$$\beta_m = n_{eff} k_0 = n_{eff}\frac{\omega}{c} \qquad \textbf{[2.4]}$$

n_{eff} is the refractive index of the core layer as felt by the mode m, with

$$n_{eff} = n_{core}\cos\theta_m \qquad \textbf{[2.5]}$$

The mode angle θ_m increases and the effective index n_{eff} decreases with rising mode order. Therefore higher order modes will be less confined to the core layer than the fundamental mode. This is already shown in Figure 2-2.

Group Velocity

The group velocity for a pulse of light of angular frequency centered around ω and propagation constant β is defined by $v = d\omega/d\beta$. The relation between β and ω, the dispersion relation, for TE polarized light is deduced from equation [2.2]:

$$\tan^2\left\{\frac{d}{2}\sqrt{\left(\frac{\omega}{c}\right)^2-\beta^2}-\frac{m\pi}{2}\right\}=\frac{\beta^2-\omega^2/c_{cladding}^2}{\omega^2/c_{core}^2-\beta^2} \qquad \textbf{[2.6]}$$

with c_{core} the speed of light in the core layer and $c_{cladding}$ the speed of light in the cladding layers.

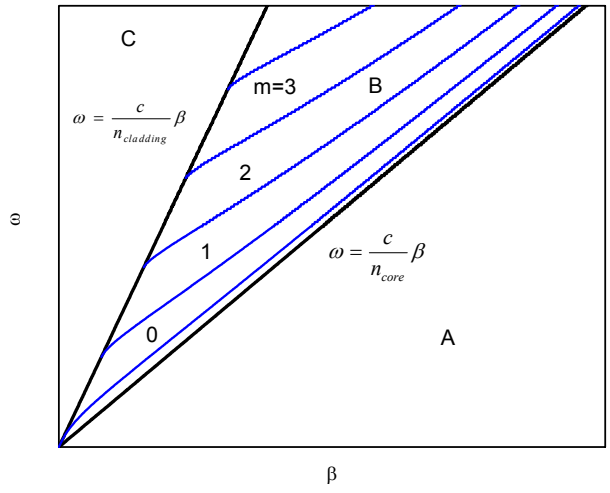

Figure 2-3: dispersion relation for a 1 µm thick GaN film surrounded by air. The refractive index of GaN is 2.53 (λ~400 nm).

Figure 2-3 shows the dispersion diagram for a GaN slab surrounded by air. The diagram is found by solving equation [2.6] with Mathematica. The figure shows that the group velocity of a mode decreases from $c_{cladding}$ to c_{core} and the effective index increases from $n_{cladding}$ to n_{core} for increasing propagation constant. For decreasing wavelengths a mode will therefore be more confined in the high-index core layer.

Leaky and Guided Modes

When light is guided in a dielectric waveguide it remains concentrated in the core layer and it cannot escape to the claddings. There are conditions where light can couple out from or into a dielectric waveguide. In the remainder of this section this will be explained by the introduction of the light cone [Inoue2004].

When a wave is refracting at the boundary between two dielectric media the parallel wave vector and energy are conserved: $k_{//1} = k_{//2}$ and $\omega_1 = \omega_2$. The light cone (or light line) of a uniform dielectric medium with refractive index n is given by:

$$\omega = \frac{c}{n}|k_{//}| \qquad \textbf{[2.7]}$$

The two black lines in Figure 2-3 are the light cones for the core medium and the cladding medium. Each light line divides the phase space $(\omega, k_{//})$ into two parts. Light with angular frequency $\omega = c_n/k$ traveling in the direction $\vec{k} = \vec{k}_{//} + \vec{k}_{\perp}$ can be found above the lightcone in phase space. No modes can exist below the light line.

Phase space in Figure 2-3 is divided into three distinctive areas A, B and C by the lichtcones of the core and cladding layers. In area A no modes exist in both media. In area B only modes guided by the core layer exist. These guided modes cannot couple to the cladding layers. In area C modes exist in the core and cladding layers. Light propagating in the core layer can therefore couple to cladding layers and vice versa. These modes are called leaky modes (Figure 2-1).

Concepts of waveguiding in a planar dielectric slab are shown. The properties of 2D ridge waveguides will however not be discussed. The main difference with the planar dielectric slab is that a mode is described in two directions, horizontally and vertically. The concept of the effective index is also used for 2D waveguides.

2.2 *Photonic Crystals*

Photonic crystals (PhC) are periodic arrangements of dielectric media in one (1D), two (2D) or three (3D) dimensions which can exhibit a photonic bandgap (PBG). They were simultaneously introduced by Yablonovitch [Yablonovitch1987] and John [John1987] in 1987. In Figure 2-4 examples of a 1D and 2D PhC are shown. A 1D PhC is also known as the Bragg reflector, or multilayer interference filter.

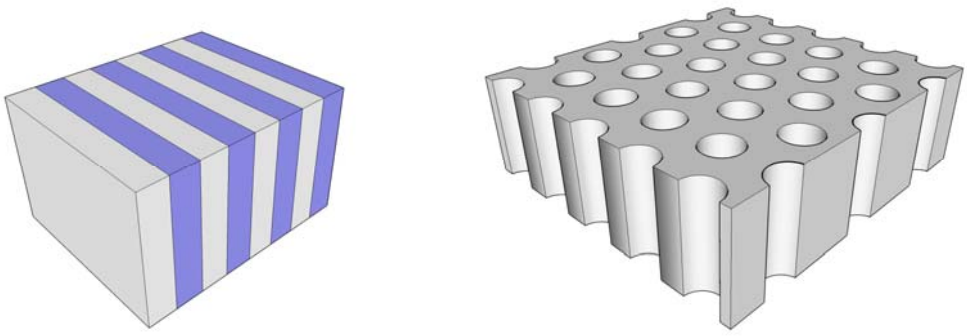

Figure 2-4: schematic drawing of a 1D PhC and a 2D triangular lattice PhC.

The Maxwell equations are at the basis of PhCs. To obtain the properties of a PhC the Maxwell equations are solved numerically with Crystal Wave, a commercial Maxwell solver. Universal properties of PhCs can directly be derived from the Maxwell

equations. In this paragraph an introduction is given in the electromagnetic theory of PhCs.

2.2.1 Master Equation

The Macroscopic Maxwell equations are given by [Jackson1962]:

$$\nabla \times \vec{E}(\vec{r},t) + \frac{\partial \vec{B}(\vec{r},t)}{\partial t} = 0 \qquad \textbf{[2.8]}$$

$$\nabla \times \vec{H}(\vec{r},t) - \frac{\partial \vec{D}(\vec{r},t)}{\partial t} = \vec{J}(\vec{r},t) \qquad \textbf{[2.9]}$$

$$\nabla \cdot \vec{B}(\vec{r},t) = 0 \qquad \textbf{[2.10]}$$

$$\nabla \cdot \vec{D}(\vec{r},t) = \rho(\vec{r},t) \qquad \textbf{[2.11]}$$

with $\vec{E}(\vec{r},t)$ and $\vec{H}(\vec{r},t)$ respectively the macroscopic electric and magnetic fields, $\vec{D}(\vec{r},t)$ and $\vec{B}(\vec{r},t)$the displacement and magnetic induction fields, $\rho(\vec{r},t)$ the free charges and $\vec{J}(\vec{r},t)$ the free currents.

PhCs composed of isotropic, lossless and linear dielectric media, free of currents and charges are considered. For these types of materials the Maxwell equations can be expressed in one single master equation [Joannopoulos1995]:

$$\nabla \times \left(\frac{1}{\varepsilon(\vec{r})} \nabla \times \vec{H}(\vec{r}) \right) = \left(\frac{\omega}{c} \right)^2 \vec{H}(\vec{r}) \qquad \textbf{[2.12]}$$

with $\vec{H}(\vec{r})$ the macroscopic magnetic field and $\varepsilon(\vec{r})$ the dielectric constant. Together with the condition $\nabla \cdot \vec{H}(\vec{r}) = 0$ it completely determines the macroscopic magnetic field inside the PhC.

Expression [2.12] is an eigenvalue problem for $\vec{H}(\vec{r})$ with a Hermitian linear operator $\theta = \nabla \times ((1/\varepsilon(\vec{r}))\nabla \times)$. It has an analogy with the Schrödinger equation in quantum mechanics. The solutions of the master equation are a set of harmonic modes $\vec{H}_{\omega_n}(\vec{r})$ with real and positive eigenvalues ω_n. Any linear combination of solutions is a solution itself and two modes $\vec{H}_1$ and $\vec{H}_2$ with different frequencies ω_1 and ω_2 are mutually orthogonal.

Bloch Theory

In quantum mechanics Brillouin zones and Bloch modes describe a system with translational symmetries. This is also used in electromagnetic theory to account for the periodic variation in dielectric constant.

Due to symmetries in a PhC the eigenfunctions $\vec{H}_{\vec{k}}(\vec{r})$ need only to be solved for the non-redundant k-space, the irreducible Brillouin zone. The eigenfunctions are

described in Bloch modes. In Bloch's theorem the eigenvector $\vec{H}_{\vec{k}}(\vec{r})$ can be written in the form:

$$\vec{H}_{\vec{k}}(\vec{r}) = e^{i\vec{k}\cdot\vec{r}} u_{\vec{k}}(\vec{r}) \qquad \textbf{[2.13]}$$

with $\vec{k}$ the propagation constant.

$$u_{\vec{k}}(\vec{r} + \vec{R}) = u_{\vec{k}}(\vec{r}) \qquad \textbf{[2.14]}$$

is a periodic function, with $\vec{R}$ a real space lattice vector.

The eigenfrequencies ω_k can exhibit gaps at the boundaries of the Brillouin zones: the PBG.

Scalability of Photonic Crystals

There is no fundamental length scale for the Maxwell equations other than the assumption that the system is macroscopic. The solution of a problem at one length scales determines the solution for all length scales. It is therefore possible to express the properties of a PhC in normalized frequencies a/λ (or $\omega a/2\pi c$) and normalized wavevectors $ka/2\pi$, with a the PhC lattice constant.

2.2.2 Two Dimensional Photonic Crystals

The PhCs discussed in this thesis are mainly 2D with a triangular lattice of holes (Figure 2-4). The main crystal directions are the ΓM and ΓK directions as shown in Figure 2-5.

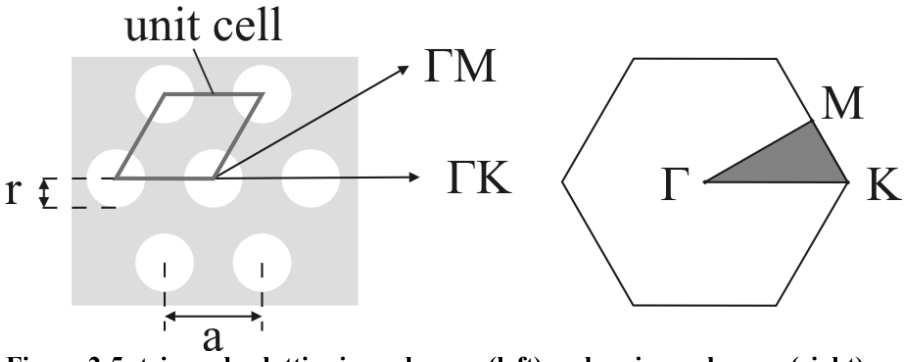

Figure 2-5: triangular lattice in real space (left) and reciprocal space (right).

2D PhCs will only guide light in the plane. In the vertical directions the light is not guided. Dielectric waveguides are therefore often used to confine the light in the plane.

The size and location of the PBG of the 2D PhC with a triangular lattice of holes depends on the air filling factors, i.e. on the r/a-ratio with r the radius of the holes and a the lattice constant. In Figure 2-6 a banddiagram is shown for a 2D GaN PhC with an r/a-value of 0.3. A gap in the ΓM or the ΓK direction is called a stopgap.

The parts of the stopgap that overlap in all directions is called the PBG. There is a PBG for TE polarized light for the 2D GaN PhC with a triangular lattice of holes as shown in Figure 2-6.

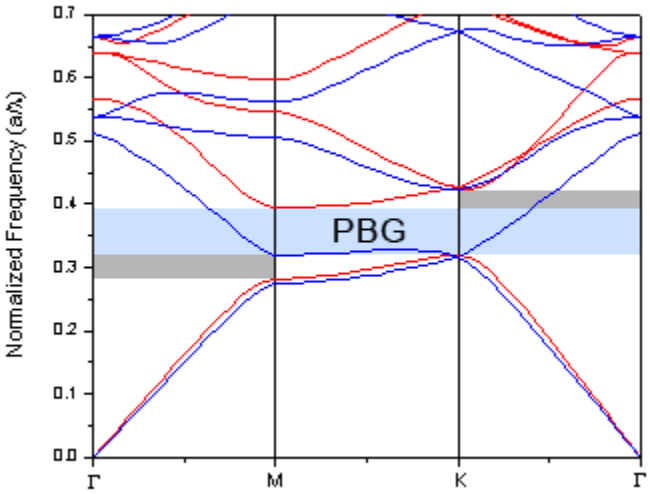

Figure 2-6: banddiagram for a 2D hexagonal GaN PhC for TE (red) and TM (blue) polarization. The refractive index of GaN was set to 2.31 [Hui2003a].

The lowest band is called the dielectric band and the second band the air band. In the dielectric band light tends to concentrate its displacement field in regions of high dielectric constant. As the modes must be orthogonal the displacement field of the second mode must be more concentrated in the air region. In Figure 2-7 the field distribution of the Bloch modes at the M-point in k-space of the dielectric and air band are shown. The light is TE-polarized.

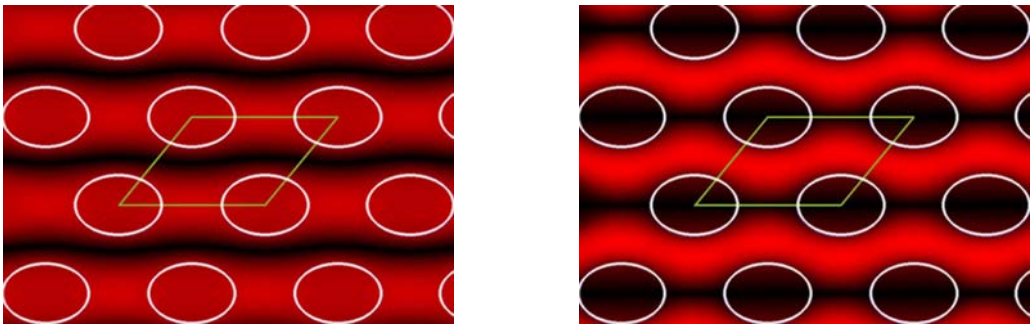

Figure 2-7: Bloch modes (amplitude magnetic field) of the 2D GaN PhC at the M-point in k-space for TE-polarized light. On the left the Bloch mode for the dielectric band on the right the Bloch mode for the air band. The rhomb depicts the unit cell.

For further reading on the theory of Photonic Crystals see the textbooks [Joannopoulos1995] or [Inoue2004].

2.3 *Photonic Crystal Light Outcoupling*

Light in a LED is generated inside a (multiple) quantum well (QW) by radiative recombination of an electron-hole pair. In a planar LED about $1/(4n^2)$ can escape through the top or bottom surface [Appendix I]. The remaining light will be trapped due to total internal reflection and eventually absorbed inside the structure. The recombination of an electron-hole pair can be non-radiative especially at defects in the structure.

The external quantum efficiency of a LED is the product of the material and optical coupling efficiency:

$$\eta_{ext} = \eta_{inj}\eta_i\eta_{opt} \qquad \textbf{[2.15]}$$

with η_{inj} the injection efficiency, η_i the light generation efficiency and η_{opt} the light extraction efficiency. The light generation efficiency is defined as the rate of radiative recombination to the total rate of recombination. The injection efficiency is the ratio between the electron current and the total forward current in the QW region. The light extraction efficiency is the rate of extracted light to the total generated light [Nakamura2000].

PhCs can enhance the external quantum efficiency in three different ways [Boroditsky1999-2]:

1. Enhancement of the spontaneous emission rate due to the Purcell effect. This effect competes with non-radiative recombination and affects the light generation efficiency.
2. Prohibition of light being emitted into guided modes due to the PBG. This affects the light generation efficiency as well as the light extraction efficiency.
3. Bragg scattering of generated light, to overcome the trapping of light due to total internal reflection. This competes with absorption and influences the light extraction efficiency.

Etching PhC holes through the QW can lead to an increase of non-radiative recombination and therefore to an adverse effect on light generation.

In this section the three ways for light enhancement will be discussed.

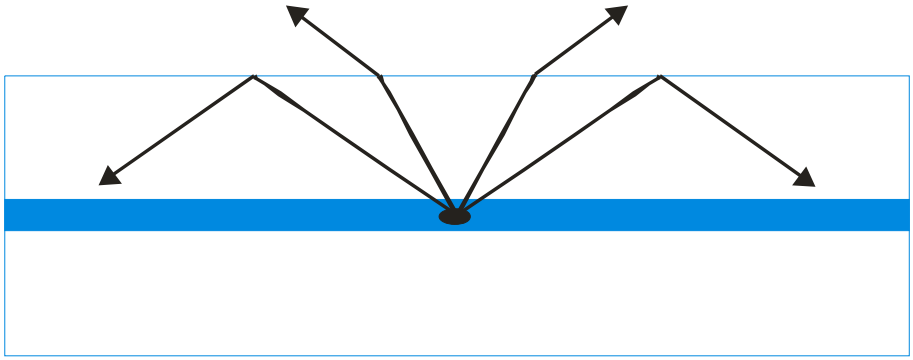

Figure 2-8: most of the light generated inside a QW (blue layer) will be trapped inside the material due to total internal reflection.

Purcell Effect

Purcell predicted that an atom in a wavelength size cavity can radiate much faster than in free space [Purcell1946]. A PhC can be used to fabricate the wavelength size cavity. The Purcell enhancement factor is given by:

$$f = \frac{3Qg(\lambda/2n)^3}{2\pi V_{cav}} \qquad \textbf{[2.16]}$$

with Q the cavity quality factor, V_{eff} the nanocavity mode volume, n the refractive index and g the electromagnetic mode degeneracy [Boroditsky1999]. The Purcell effect is a rate enhancement of spontaneous emission and therefore competes with non-radiative recombination.

For nitride materials with $n \sim 2.4$, $Q \sim 10-30$, $\lambda \sim 475$, $V_{cav} \approx 0.0024$ μm^3 and single mode degeneracy f is about 5.7 [Oder2003]. The quality factor Q is limited at room temperature by the material properties of the semiconductor. The internal quantum efficiency in GaN LEDs is about 60% [Watanabe2003]. From this it is expected that the overall improvement by the Purcell effect is limited.

Excitation in the Photonic Bandgap

Consider light generation in a PhC punctured QW as shown in Figure 2-9. If the emission wavelength of the QW coincides with the PBG no light can be emitted in the plane of the LED. Light can only be emitted into leaky modes. Because no modes can be excited in the PhC plane the spontaneous emission lifetime should increase and the overall emission rate is expected to decrease. As a result of the inhibition of modes in the plane of the PhC the emission in the direction normal the PhC will increase via redistribution of saved energy [Fujita2005].

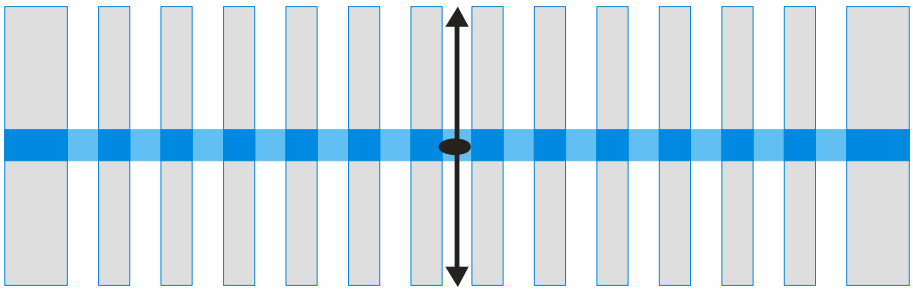

Figure 2-9: the existence of a PBG in the wavelength region of the light emission can prevent that light is emitted into guided modes.

Bragg Like Scattering

PhCs can Bragg scatter light from a high index material to a low index material. The 1D PhC acts in that case as a grating. Consider a 1D PhC slab surrounded by air as shown in Figure 2-10.

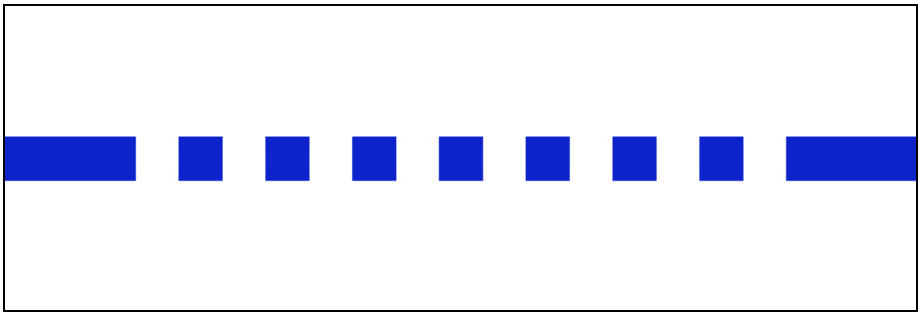

Figure 2-10: cross-section of a 1D PhC slab.

The relation between PhCs and light extraction can be qualitatively understood with Bloch theory [Krauss2006]. The Bloch modes for the electric field are given by:

$$E_k(r) = u_k(r)e^{-ikr} \qquad \textbf{[2.17]}$$

which may be Fourier transformed to

$$u_k(r) = \sum_G A_G e^{-iGr} \qquad \textbf{[2.18]}$$

where $G = m \cdot 2\pi/a \quad (m \in \mathrm{N})$ and k the parallel wavevector. Qualitatively the effect of a grating is found by taking only $G_0 = 0$ and $G_1 = 2\pi/a$ into account. The Bloch mode of the electric field becomes:

$$E_k(r) = A_0 e^{-ikr} + A_1 e^{-i\left(k-\frac{2\pi}{a}\right)r} \qquad \textbf{[2.19]}$$

The important cases are the one with parallel wavevector $k = \pi/a$ and the one with $k = 2\pi/a$.

For $k = \pi/a$ and $A_0 = A_1$ equation [2.20] will become a standing wave:

$$E_k(r) = A_0 e^{-i\frac{\pi}{a}r} + A_1 e^{-i\left(-\frac{\pi}{a}\right)r} = 2A\cos(\pi/a) \qquad \textbf{[2.20]}$$

this is the case where light is Bragg reflected in the plane and is the origin for the PBG. For $k = 2\pi/a$ it is found that the electric field is given by:

$$E_k(r) = A_0 e^{-ikr} + A_1 e^{-i(k-G)r} = A_0 e^{-i\frac{2\pi}{a}r} + A_1 \qquad \textbf{[2.21]}$$

A_1 has no parallel wave vector. This part corresponds to light extraction out of the plane of the PhC. The standing wave and the extractor principle are illustrated in the banddiagram of a 1D PhC (Figure 2-11). It shows that the 1D PhC for $k = \pi/a$ will work as a reflector, going from the point $k = \pi/a$ to $k = -\pi/a$ in the dielectric band. For the extractor the parallel wavevector will go from $k = 2\pi/a$ to $k = 0$ in the air band.

Frequency domain simulations for a 1D PhC membrane are performed in Crystal Wave. The results are shown in Figure 2-12. The fundamental mode of a dielectric slab waveguide is excited by a mode excitor, after which it couples into the 1D PhC slab membrane. The simulated structure is drawn on top of the simulation results. The reflector principle is shown in the left figure. The frequency used for this simulation matches with the frequency belonging to $k = \pi/a$. A standing wave is visible. The extractor principle is shown in the right figure. The used frequency belongs to the parallel wavevector $k = 2\pi/a$.

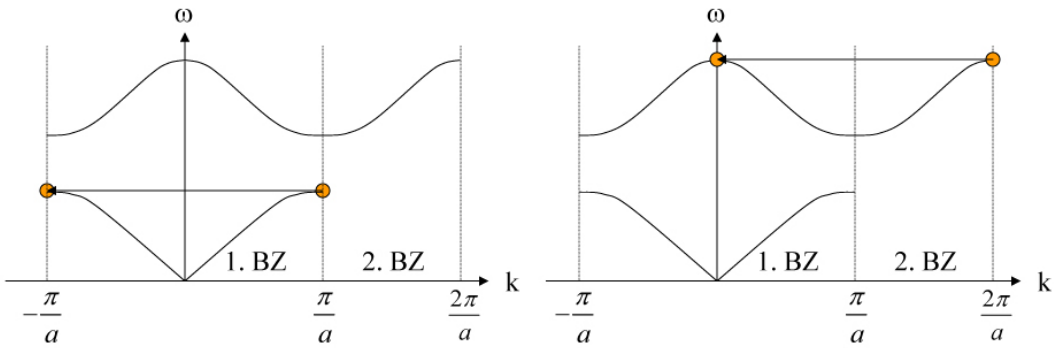

Figure 2-11: on the left the reflector and on the right the extractor principle explained with the banddiagram of a 1D PhC [Krauss2006].

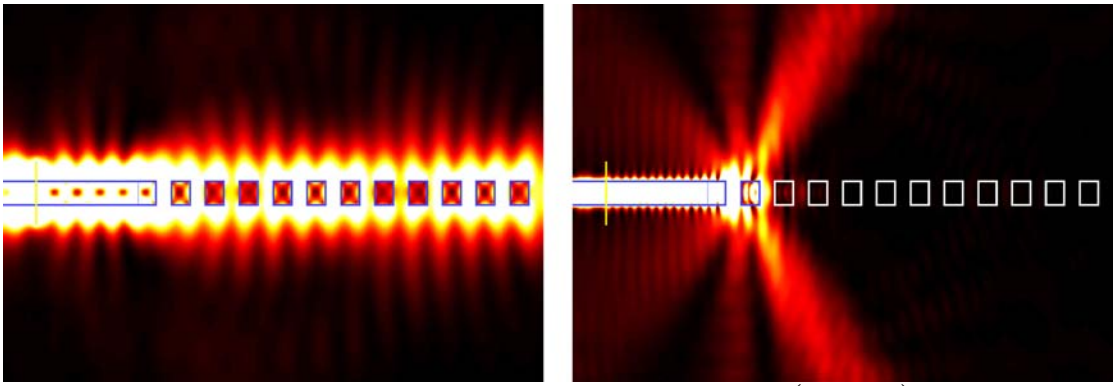

Figure 2-12: on the left frequency domain simulations for a reflector $(k = \pi/a)$ and on the right for a standing wave $(k = 2\pi/a)$. The simulations are performed with Crystal Wave, for a 1D GaN PhC slab of 350 nm thick with slits of 0.5 µm wide and 1 µm period.

The extraction principle of a 1D PhC is just described with Bloch theory for a parallel wavevector $k = 2\pi/a$. However, there are more wavevectors than $k = 2\pi/a$ for which light can couple out of the PhC slab.

Figure 2-13 shows the banddiagram for a 1D PhC with a filling fraction of 0.5. The red line in Figure 2-13 is the lightline for air. There are 2 distinctive areas in the diagram. Light propagating in a 1D PhC mode under the light line is not able to couple to continuum. These are the guided modes of the PhC. Light propagating in a mode above the lightline can couple to continuum. These are the radiative or leaky modes of the PhC.

The normalized frequency belonging to the parallel wavevector $k = 2\pi/a$ is about 0.64. This value is indeed lying above the lightline as shown in Figure 2-13. The normalized frequency belonging to $k = \pi/a$ is about 0.25. The $k = \pi/a$ point is lying below the lightline.

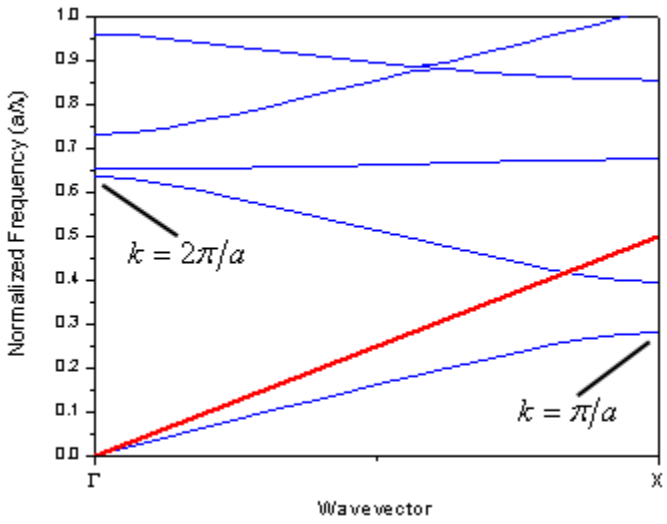

Figure 2-13: banddiagram for a 1D PhC.

A 2D PhC for light outcoupling is not just the superposition of a 1D PhC in two directions. This can be explained by the banddiagrams of a 1D and 2D PhC, shown in Figure 2-14. The dispersion relation of the air band for the 1D PhC is apart from the gaps almost equal to the dispersion of a plane wave in a homogeneous material with the relation $\omega = (c/n)k_{//}$ (green line). This band is also found in the dispersion relation of the 2D PhC (green line). However for the 2D PhC there are more bands present where guided light can couple to leaky modes. These extra bands originate from Bragg reflections into other directions than the direction of the incoming wave.

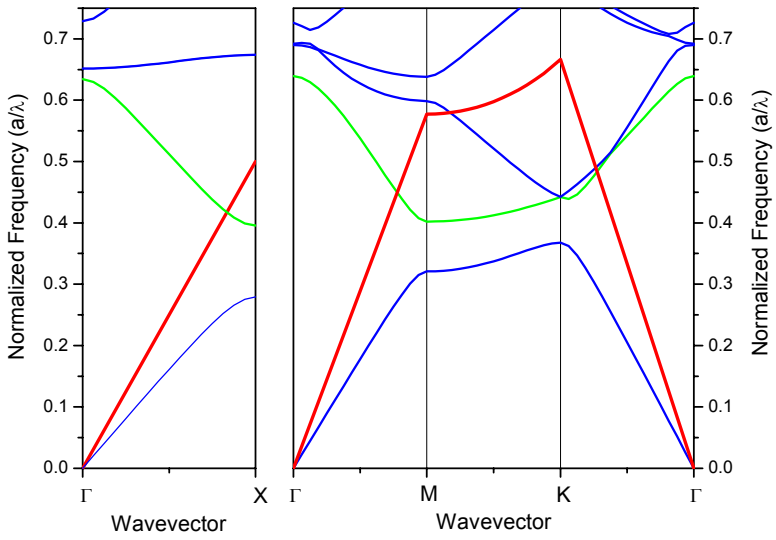

Figure 2-14: on the left the banddiagram for a 1D infinite PhC (Bragg reflector) and on the right the banddiagram for a 2D PhC. The red lines are the lightlines to air. The refractive index for the dielectric material in this calculation is about 2.

PhCs used for extraction by Bragg scattering of light do not have to be etched through a structure. Weak coupling of a periodic dielectric with the electromagnetic mode is sufficient. A shallow perturbation can be enough to scatter the (generated) light out of a device (Figure 2-15). Shallow etched PhCs used for light outcoupling are also called in- or outcouple gratings and are used to couple light in or out of a waveguide.

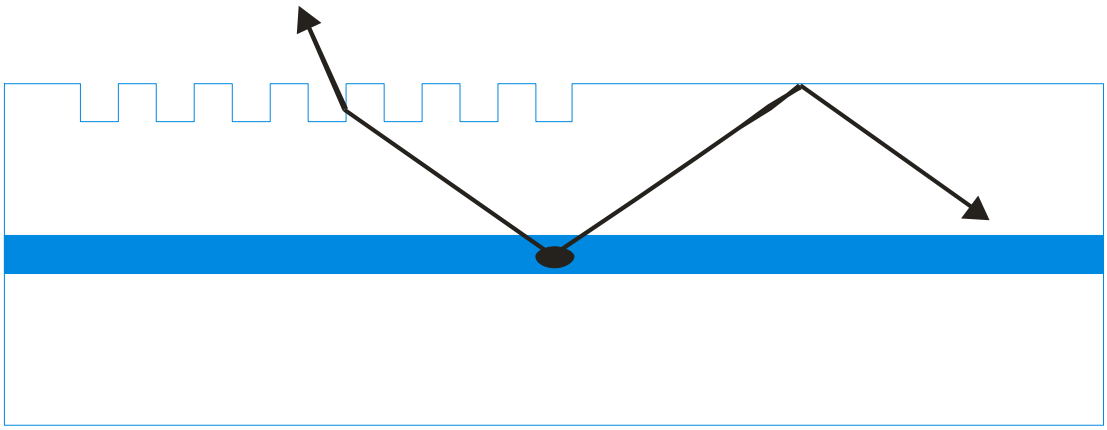

Figure 2-15: Bragg scattering at a shallow etched PhC at the surface of a device can enhance light extraction.

2.4 *Light Emitting Diodes*

PhCs can be used to enhance light extraction as is shown in the previous section. In this paragraph more conventional methods for increasing the light extraction efficiency are shown.

The geometrical shape of LEDs has a large influence on the light extraction efficiency. In Figure 2-16 a schematic picture of a planar LED is shown. From a planar LED only about $1/(4n^2)$ of the light generated inside will couple to air. This factor can be doubled if a reflector is placed across the bottom of the planar LED. In reality taking into account the Fresnel equations the amount of light that can couple out is even smaller. In Figure 2-17 the far field radiation profile of a planar LED is shown. This Lambertian profile shows that an increase in angle between the light ray and the normal to the plane leads to a decrease in output power.

A commonly used method for enhancing the output efficiency is changing the geometrical shape from a planar surface to a hemisphere or parabola. These geometries are shown in Figure 2-16. Their radiation profiles are shown in Figure 2-17.

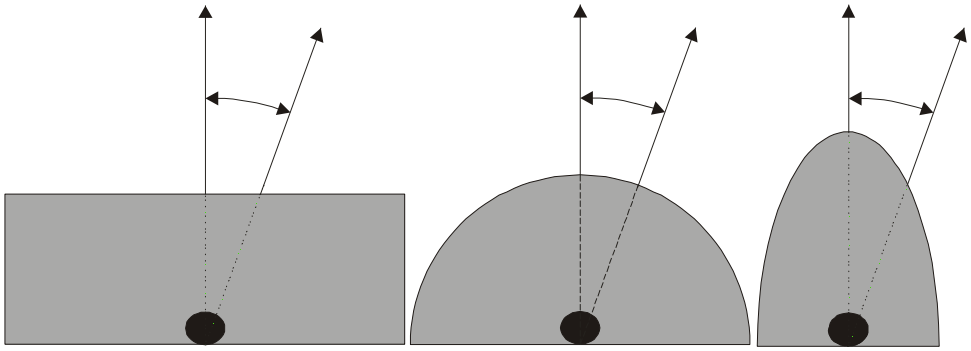

Figure 2-16: schematic drawing of planar, hemispherical and parabolic shaped LED [Schubert2003].

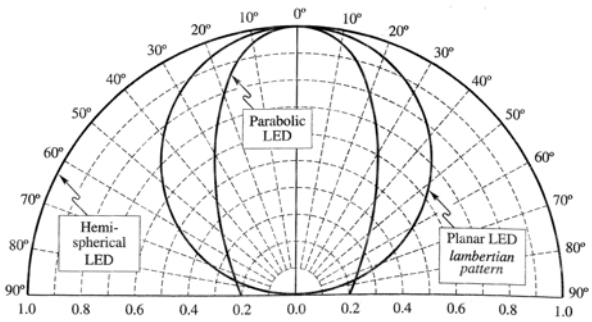

Figure 2-17: far field radiation profiles for the planar, hemispherical and parabolic shaped LED [Schubert2003].

Other geometries used are the rectangular parallelepipedal LED which has a total of five escape cones and a cylindrical LED with a top escape cone and a side escape ring [Schubert2003]. These geometries are pictured in Figure 2-18.

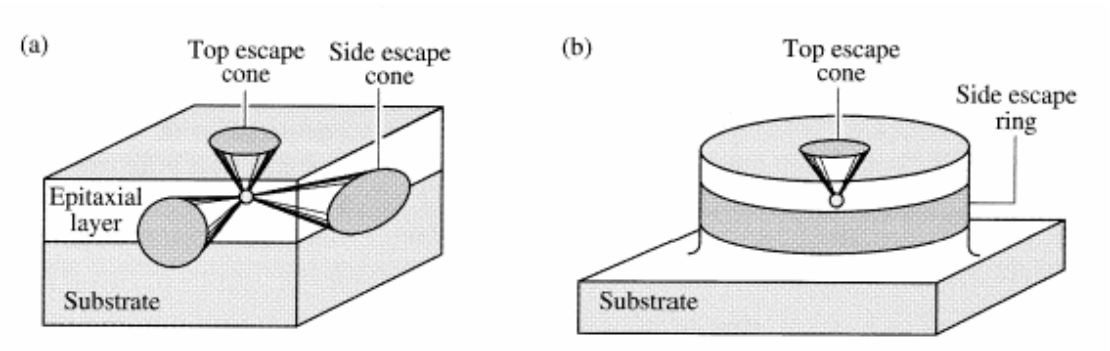

Figure 2-18: rectangular parallelepipedal LED (left) and a cylindrical LED (right) [Schubert2003].

Emission from a high power LED using a truncated inverted pyramid was reported in 1999 (Figure 2-19) [Krames1999]. The external quantum efficiency was determined to be higher than 50%. As the figure shows it is not straightforward to fabricate this type of LED. This is a disadvantage for mass production.

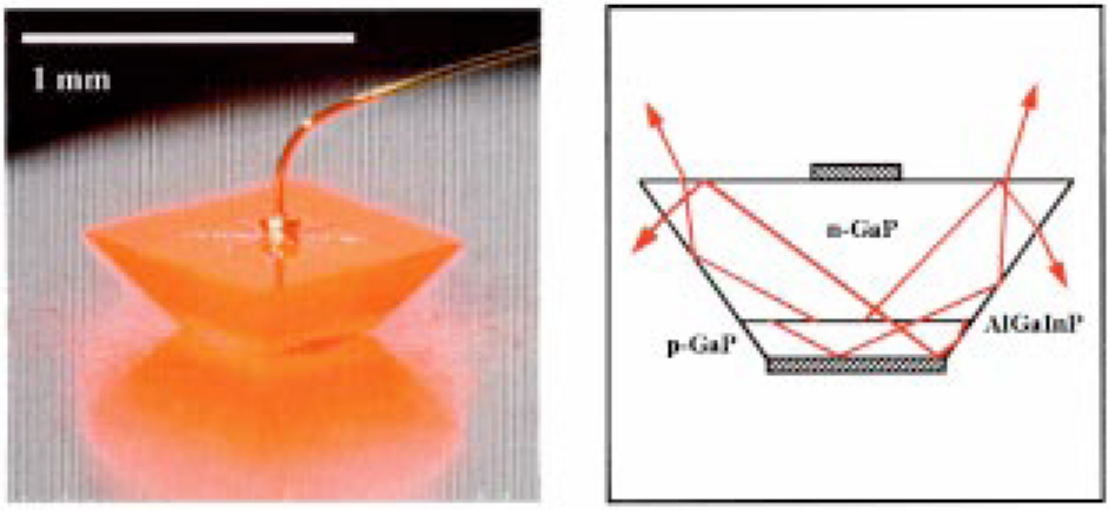

Figure 2-19: geometry of the truncated inverted pyramid LED. On the left side the LED under forward bias. On the right side a schematic drawing of how light can escape out of the pyramid [Krames1999].

Roughening the surface of the LED will also increase the outcouple efficiency. For a GaN LED the light outcoupling efficiency can double [Fujii2004].

Placing a LED between distributed Bragg reflectors (Figure 2-20) can also lead to an increase in the output efficiency [Rattier2002]. Light is emitted in a number of allowed quantized modes. Light emitted in a mode that is lying above the light line will escape. The efficiency scales as the number of modes above the light line divided by the total number of allowed modes. Light extraction efficiencies of 20 to 30 percent have been obtained.

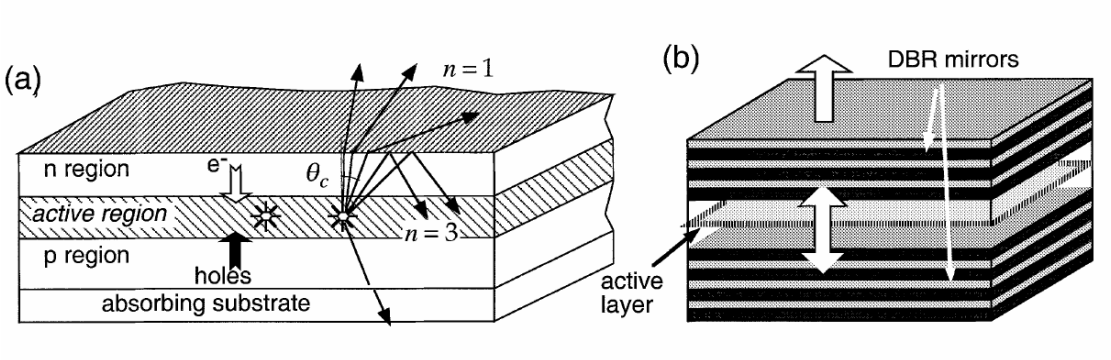

Figure 2-20: in a planar LED the majority of the photons that is generated are trapped by total internal reflection (left). By placing the structure between DBR mirrors higher efficiencies can be obtained (right) [Rattier2002].

Chapter 3 Gallium Nitride

The project is focused on GaN PhCs. In this chapter, GaN properties are given which are used for the light extraction simulations and the experiments. Furthermore an overview of worldwide conducted research on GaN PhCs is presented.

3.1 *Gallium Nitride*

GaN is a wide-bandgap III-V semiconductor. The direct bandgap makes it an interesting material for the use in solid state lighting. GaN can have two different crystal structures dependent on the substrate: wurtzite (α-GaN) or cubic (β-GaN). In Figure 3-1 a diagram is given for bandgap energy versus lattice constant for a number of important compound semicocnductors. The lattice constant of α-GaN is relatively close to that of aluminum nitride (AlN) and indium nitride (InN). These semiconductors are used for LEDs and lasers in the UV-blue-green wavelength region. In this project α-GaN is used for simulations and experiments. α-GaN will be abbreviated to GaN.

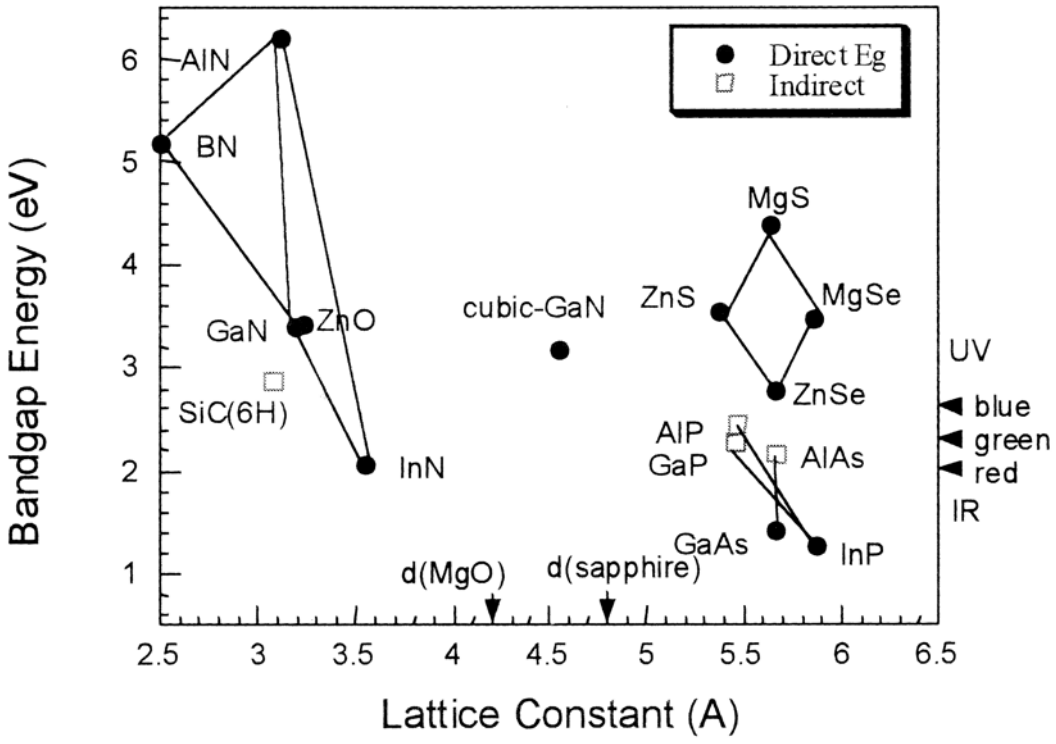

Figure 3-1: bandgap energy versus lattice constant for various semiconductors [Nakamura2000]. Note that the bandgap energy of InN is a point of discussion.

Growth of Gallium Nitride

Wurtzite GaN is grown on a c-plane sapphire (Al_2O_3) substrate. There is a large lattice mismatch between the two materials as shown in Figure 3-2. The lattice constants for GaN are $a = 3.189$ Å and $c = 5.182$ Å and for sapphire $a = 4.758$ Å and $c = 12.991$ Å. To compensate for the large lattice mismatch a GaN or AlN bufferlayer

is used. The bufferlayer is grown at a lower temperature than the actual GaN layer and has a thickness of about 50 nm. Thick GaN layers (~2 μm) are grown to obtain GaN which can be used in electronic devices. This thick layer is sometimes called the buffer layer [Nakamura2000].

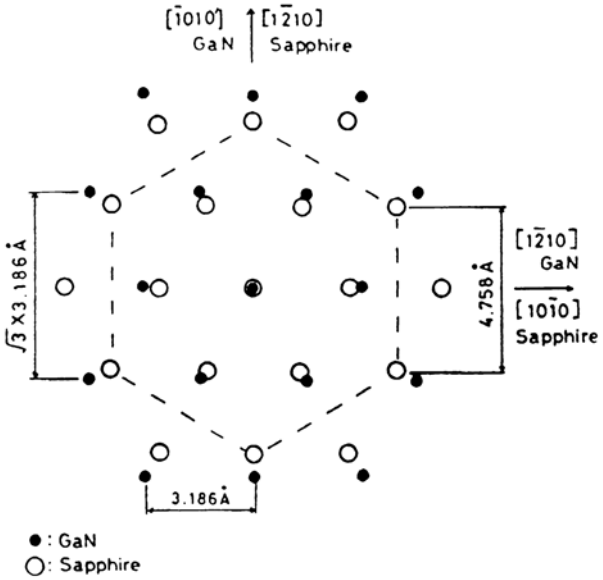

Figure 3-2: schematic illustration of GaN growth on a sapphire substrate [Nakamura2000].

Birefringence

GaN is birefringent. The ordinary axis is perpendicular to the c-axis and the extraordinary axis parallel to it. Around 400 nm wavelengths the refractive index of GaN is about 2.53 for the ordinary and about 2.58 for the extraordinary axis [Zhang1996]. The birefringence of GaN around the optical telecommunication wavelength is investigated in [Hui2003a] and [Hui2003b]. The refractive index for the ordinary axis is about 2.315 and for the extraordinary axis 2.357 at $\lambda \sim 1.55$ μm.

Cleavage Plane

Cleaving of GaN and sapphire is difficult. In Figure 3-3 a diagram of c-plane sapphire is shown. The r-plane is weaker than the vertical planes. When cleaving a diagonal-break side wall is typical. Another possibility is a breakout caused by polish-marks. The c-plane structure offers a hexagon of possible planes to break. If a polish mark is close-to-parallel to one of these planes it can offer a starting point for a cleave [Cook2006].

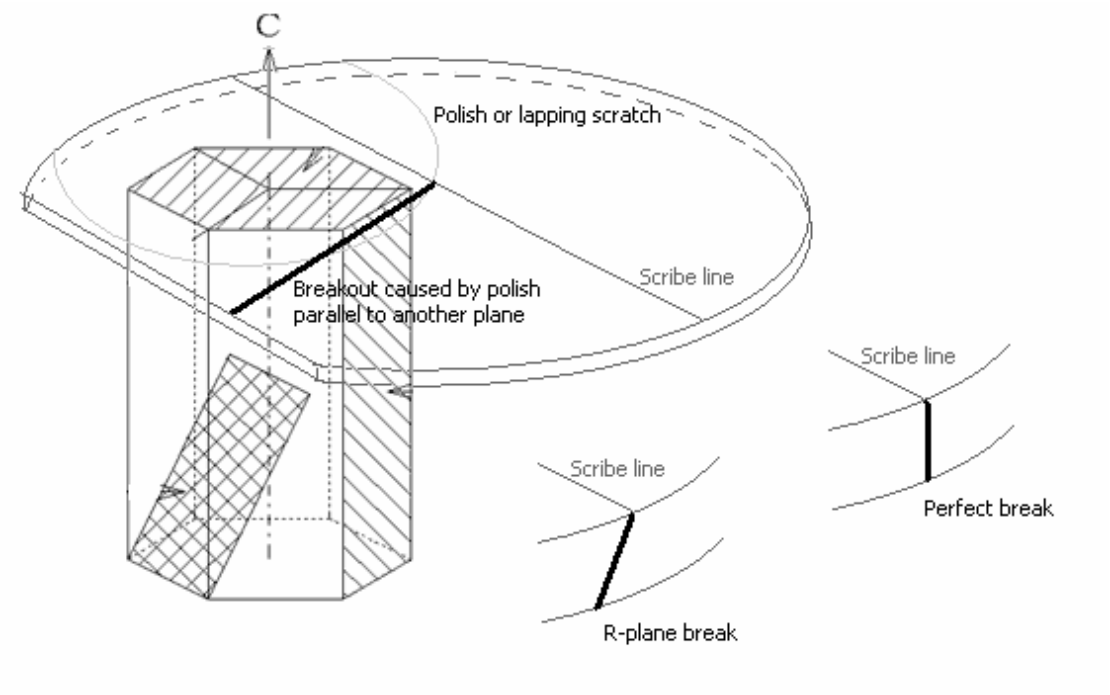

Figure 3-3: C-plane sapphire. Two typical break types are shown [Cook2006].

3.2 *Gallium Nitride Photonic Crystals in Literature*

Several groups are conducting research on GaN PhCs. The basic topic is the use of PhCs to enhance light outcoupling in GaN LEDs. Lately also work on GaN membrane PhC cavities is published. Below an overview is given about research results on GaN PhCs.

Gallium Nitride Photonic Crystals

In 1999 Coquillat *et al*. published findings on the photoluminescence (PL) characterization of triangular lattices of holes and pillars etched in a epitaxial grown 1.8 μm thick GaN layer. The PhCs have a periodicity of 1 and 2 μm. The filling factors for the PhC holes were between 0.19 and 0.25 and for the PhC pillars between 0.10 and 0.39. The PL peak is used to evaluate the damage introduced onto the semiconductor by the etching procedure. The main conclusion is that optical properties like emission intensity are maintained at 5 and 300 K after etching procedure. The results suggested that GaN is a favorable material system for the nanofabrication of miniature devices based on PBG effects [Coquillat1999].

Coquillat *et al*. also made the first observations of a 2D PhC band structure in a GaN on sapphire PhC in 2001 [Coquillat2001a], [Coquillat2001b]. PhCs with periodicity of 1 μm and filling factors of 0.19, 0.21 and 0.22 were etched in the 1.6 μm thick GaN layer. The holes reached a depth of 1.1 μm. The band diagram is obtained by measuring the transmission spectra for collimated white light incident on the surface of the PhCs under a range of angles. Sharp resonances observed in the reflection spectra are due to Bloch modes allowed to propagate through the PhC. This is allowed when energy and in-plane wavevector match those of the modes of the PhC. Only the part of the banddiagram above the lightline can be measured with this method. A white light source with wavelengths between 830 nm and 2.5 μm is used. The

transmission spectra were measured with a Fourier transform infrared spectrometer. The banddiagram is measured for TE as well as TM polarization in the ΓM direction.

A GaN PhC for 400 nm wavelengths with a square lattice of pillars is fabricated by Peyrade *et al*. [Peyrade2001]. The lattice constant, diameter and pillar height are respectively 270 nm, 160 nm and 600 nm. The sidewall angle of the pillars is 16 degrees (Figure 3-4). Reflection measurements were done at normal incidence at a cleaved edge of the sample. The measurements showed high reflectance for TM polarization around a wavelength of 405 nm. For TE polarization a slight increase was found around this wavelength. The reflectivity peak was interpreted to correspond with the simulated TM PBG as shown in Figure 3-5.

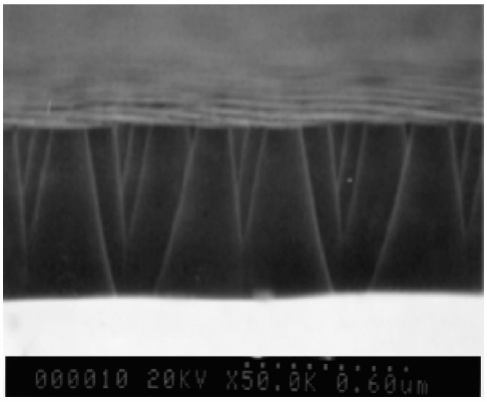

Figure 3-4: SEM image of the GaN PhC with a square lattice of pillars. The sidewall angle is 16 degrees [Peyrade2001].

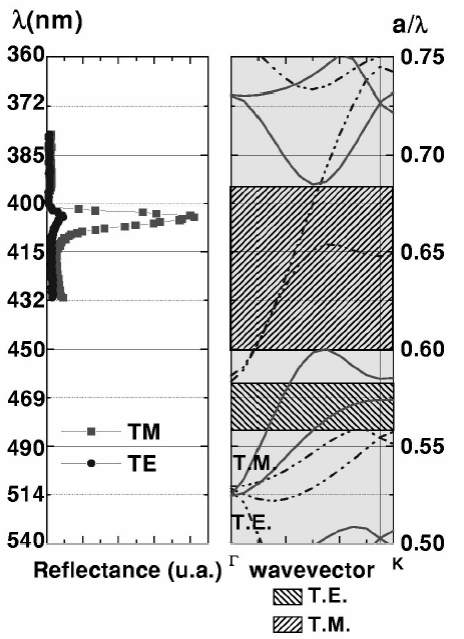

Figure 3-5: comparison of experimentally obtained reflectance spectra compared with a 2D plane waves band diagram [Peyrade2001].

Measurement of equifrequency surfaces in GaN on sapphire PhCs showed that 2D GaN PhCs can be used for efficient light outcoupling [Peyrade2003]. A triangular lattice of holes is etched in a thin single mode GaN planar slab waveguide on top of a sapphire susbtrate. The lattice periodicity is 500 nm and the filling factor is 0.22.

Collimated white light incidents on the surface of the 2D PhC over a range of two angles θ and φ, with θ the angle of incidence relative to the surface normal and φ the azimuthal angle between the plane of incidence and one of the axes of symmetry of the PhC. For certain angles light can couple to PhC modes above the lightline for air. The wavelength range over which is measured runs from 500 nm to 1100 nm.

All the measurements on GaN PhCs discussed above do have in common that the measurements are conducted above the lightline for air. In the last part of this section GaN membrane PhCs are discussed. The fabrication of high-Q GaN PhC membrane nanocavities would be interesting, for instance for GaN lasers. The fabrication of these membrane nanocavities is difficult as there is no conventional selective chemical wet etch technique available as there is for the fabrication of InP membranes [Choi2005].

In the nineties, after the progress made in the growth quality of GaN Minsky investigated the photoelectrochemical (PEC) etching technique for GaN materials [Minsky1996]. PEC etching can be selective to defects, dopants and band-gaps [Haberer2004]. At UCSB band-gap selective PEC etching is used for the fabrication of GaN PhC nanocavities membranes with a GaN/InGaN quantum well as active layer. An $In_xGa_{1-x}N/In_yGa_{1-y}N$ quantum well is used as the sacrificial layer. Quality factors up to 800 around a wavelength of 480 nm [Choi2005] and up to 300 [Meier2006] are reported.

Enhancement of Light Extraction Efficiency

Several results are published on the use of PhCs for light extraction enhancement in GaN LEDs for blue and UV wavelengths. The shallow etched (~100-250 nm) PhCs are designed to couple guided modes inside the LED into leaky modes. Purcell enhancement is not used to enlarge the external quantum efficiency. The maximum light extraction enhancement so far obtained for PhC LEDs is 2.5 for the UV and 1.5 for the blue wavelengths compared to unpatterned LEDs. These numbers might rise if techniques described in this section are combined in one single LED.

Near-field Measurements

At Kansas State University near field measurements are performed to investigate the use of a PhC with a triangular lattice of holes for light extraction efficiency. The lattice constant of the PhCs is 300 nm and the hole diameter 120 nm. AFM measurements show that the etched holes are about 200 nm deep penetrating the InGaN/GaN multiple quantum well (MQW). The MQW is pumped with 266 nm laser light. The light generation area is separated from the PhC region as shown in Figure 3-6. Emission intensity is collected by a near-field scanning optical microscope (NSOM) probe. Reference data is obtained by collecting emission intensity at an unpatterned area at equal distant from the pump location as the PhC area. In Figure 3-6 measurement results are shown. On the right side the influence of the PhC orientation is shown. It is found that the intensity level measured above the PhC region, with the NSOM in collection mode, is 20 times higher in the ΓM direction and 7 times higher in the ΓK direction compared to the unpatterned region. The measurement data further shows that almost no light is collected above the unpatterned reference area. This can be explained by the fact that when generated light reaches the reference area it will only travel in guided modes. There are no

disturbances at that area which means that no light can couple out. The intensity enhancement of 20 in the ΓM direction and 7 in the ΓK direction can therefore not be seen as indications for the increase in light intensity in electrically pumped LEDs. The measurements do however show that light extraction with PhCs is sensitive to the propagation direction of the light.

The emission wavelength of the MQW is 475 nm as show by the peak in the measured PL spectrum in Figure 3-6. As the period of the PhC is 300 nm the normalized frequency at this wavelength a/λ is 0.63. This value lies above the lightline for air. It can be concluded that the observed light intensity enhancement is due to coupling of guided modes to leaky modes.

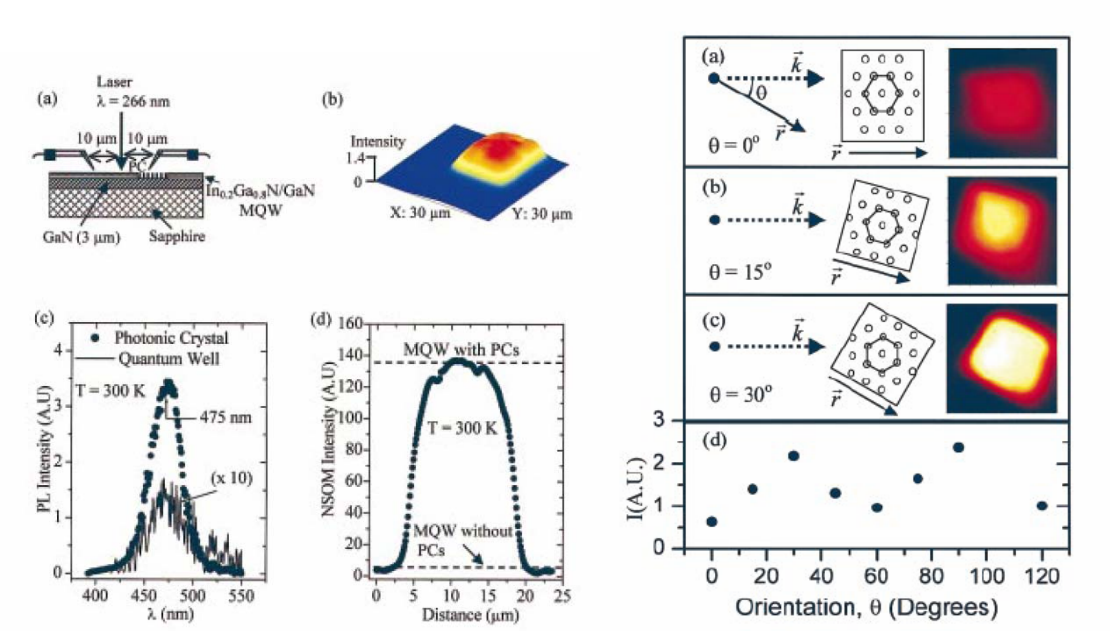

Figure 3-6: schematic set-up and measurement results from [Oder2003].

Gallium Nitride Photonic Crystal Light Emitting Diodes

An increase in power by 63% and 95% is found for respectively blue PhC LEDs and UV PhC LEDs compared to the unpatterned LEDs by Oder *et al*. [Oder2004]. The increase in intensity is shown by the optical microscope images in Figure 3-7. The holes with a diameter of 300 nm and a depth of about 200 to 250 nm are penetrating the p-type layers of the LED. The periodicity of the PhC is 700 nm. The observed light extraction enhancement is therefore due to the coupling of guided modes to leaky modes.

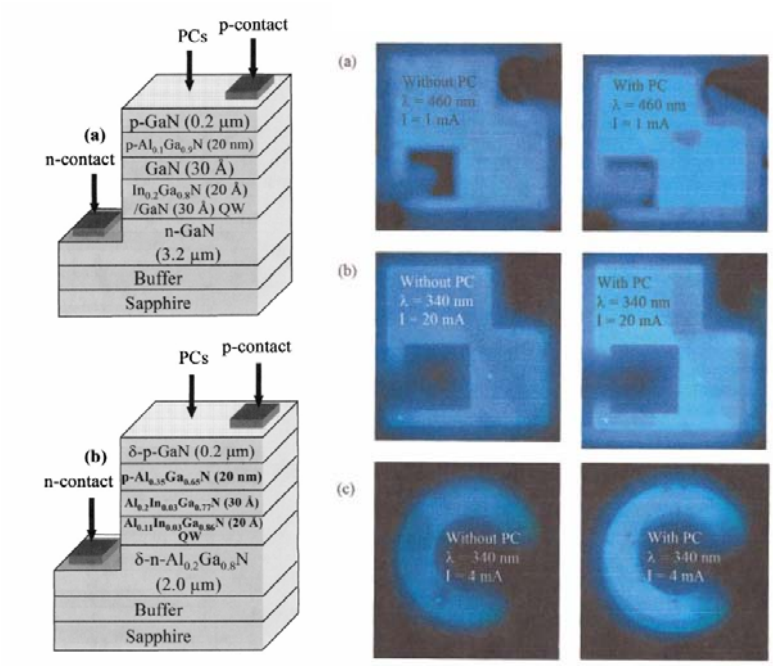

Figure 3-7: LED design for the 460 nm blue LED (top left) and the 340 nm UV LED (bottom left). On the right side optical microscope images of the blue and UV LEDs without and with PhC [Oder2004].

Shakya obtained a light extraction enhancement of 2.5 for a UV PhC LED compared to the unpatterned LED [Shakya2004]. In the LED design shown in Figure 3-8 the PhCs are etched around a hexagonal shaped p-contact with the ΓM direction of the PhC perpendicular to the edges of the contact. In Figure 3-6 it is shown that in this direction more light will couple out than when light is traveling in the ΓK direction [Oder2003]. The diameter and lattice constant of the PhCs varied respectively between d=100 nm and d=200 nm and a=300 nm to a=600 nm. Measurements results (Figure 3-9) show that extraction efficiency increases with increasing lattice constant. This implies that light extraction is dominated by Bragg scattering.

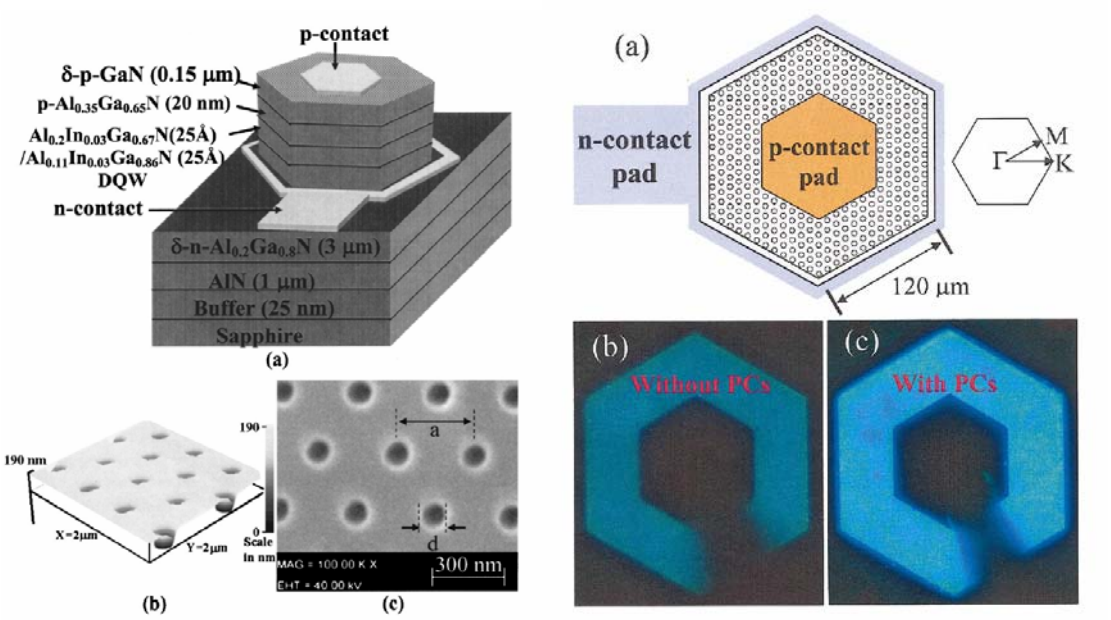

Figure 3-8: LED design and optical images of a LED without and with PhCs [Shakya2004].

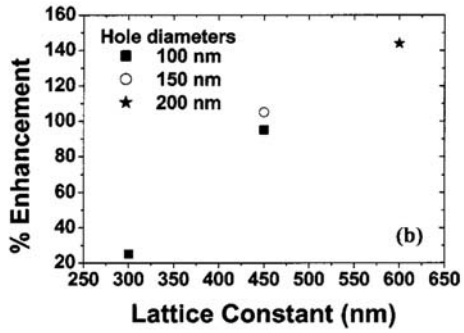

Figure 3-9: enhancement percentage versus lattice constant [Shakya2004].

Researchers at Sandia National Laboratory and Philips Lumileds Lighting produced GaN/InGaN blue PhC LEDs for investigating the far-field patterns for four different PhC lattices. The lattice constants and hole diameters were respectively 270 (PX1), 295 (PX2), 315 (PX3), and 340 (PX4) nm and 200, 220, 235, and 250 nm [Wierer2004]. The shallow etched holes (~100 nm) are placed away from metal contacts to avoid light-occlusion and absorption (Figure 3-10). An Al mirror is placed under the sapphire substrate to redirect light to the top of the device. The far-field radiation patterns of the PhC LEDs differs radically from the almost Lambertian profile for the LED without PhCs as shown in Figure 3-10. These experiments show that total light extraction and the directionality of light extraction strongly depend on the PhC parameters. The overall light extraction is increased with increasing lattice constant. For PX3 a light extraction enhancement of about 1.5 is obtained compared to an unpatterned LED.

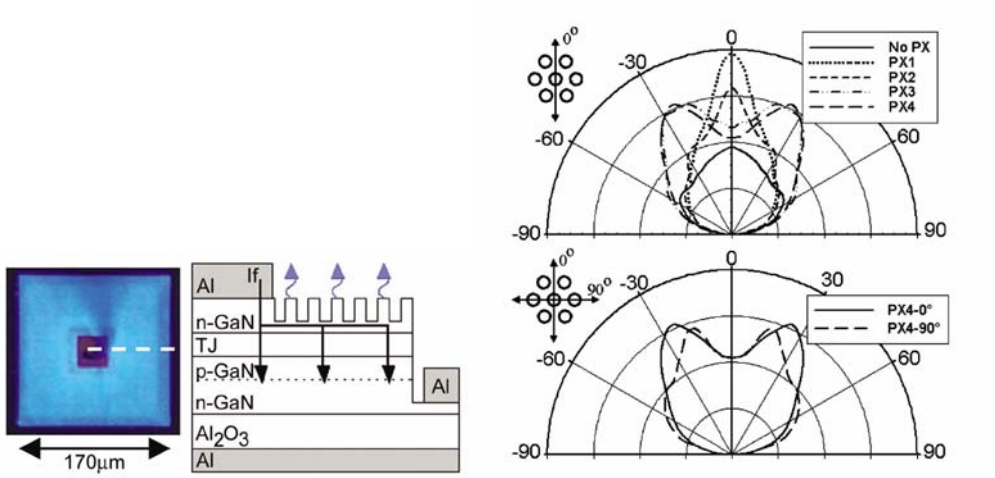

Figure 3-10: LED design (left) and measured far-field radiation patterns for several lattice designs [Wierer2004].

Band Structure Measurements

All the discussed LED structures are fabricated on top of a thick GaN layer on a sapphire substrate. The thick GaN layer is necessary to have GaN material which can be used for electronic devices. David *et al*. investigated which part of the generated light is extracted from a GaN LED by using PhC patterning [David2005], [David2006a]. Figure 3-11 shows the several paths which generated light can follow. About 6% of the generated light is emitted through the top. This is doubled when a mirror is placed under the sapphire substrate layer. The 88% left is trapped in the LED due to total internal reflection. About 22% of the generated light is able to escape to sapphire (substrate light) and 66% is guided within the GaN layers (guided light).

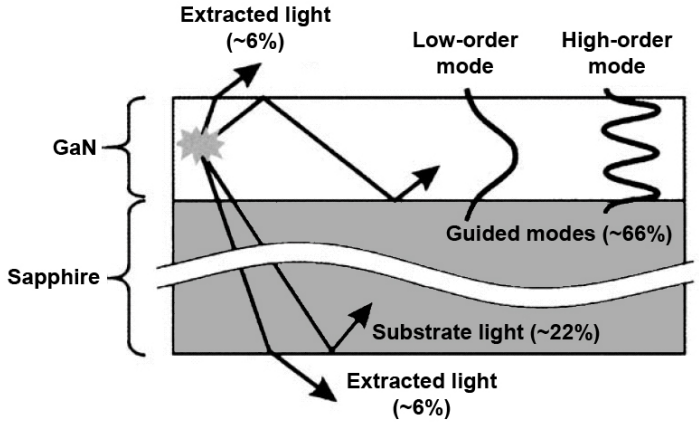

Figure 3-11: distribution of light in a GaN LED [David2006a].

A PhC used for Bragg scattering of light will have negligible influence on substrate light. The PhC only extracts guided light. An experiment is conducted to investigate how this guided light is extracted by PhCs. The used structure is as follows: sapphire substrate, a 2.5 µm thick GaN buffer layer, a 100 nm thick AlGaN layer, a 300 nm GaN cap layer including the MQW and on top a 40 nm thick SiO_2 (fabrication mask) layer. The PhCs are shallow etched (~120 nm) to minimize reflections when guided light starts interacting with the PhC (see inset Figure 3-12). The lattice constant is 200

nm. The emitted wavelengths will couple to PhC modes which lay above the lightline. These modes can couple to continuum. In Figure 3-12 the angular resolved photoluminescence spectrum in TE polarization is plotted for a PhC oriented in the ΓM direction. At angles between -90 and 0 degrees the spectrum of an InGaN QW emission in a thick GaN layer is shown. From 0 to 90 degrees the spectrum of the QW emission with shallow etched PhCs is shown. The inset of the figure shows that light guided to the left is diffracted into air to the right. The sharp slanting lines visible in the spectrum of the PhC LED show that the extraction enhancement is highly directional. This is typical for PhC light out coupling. From the emission spectrum the band structure could be deduced. This is shown on the left side in Figure 3-13. Two sets of bands are present, intense lines with a strong slope and weaker lines with a lower slope. For comparison a simulated band structure is plotted over the measured structure as is shown on the right side of Figure 3-13. Several simulated bands are not observed experimentally. These are the bands corresponding to the lower order modes. It is concluded that lower order modes are not coupled out because they are strongly confined to the center of the GaN layer and have little overlap with the PhC region.

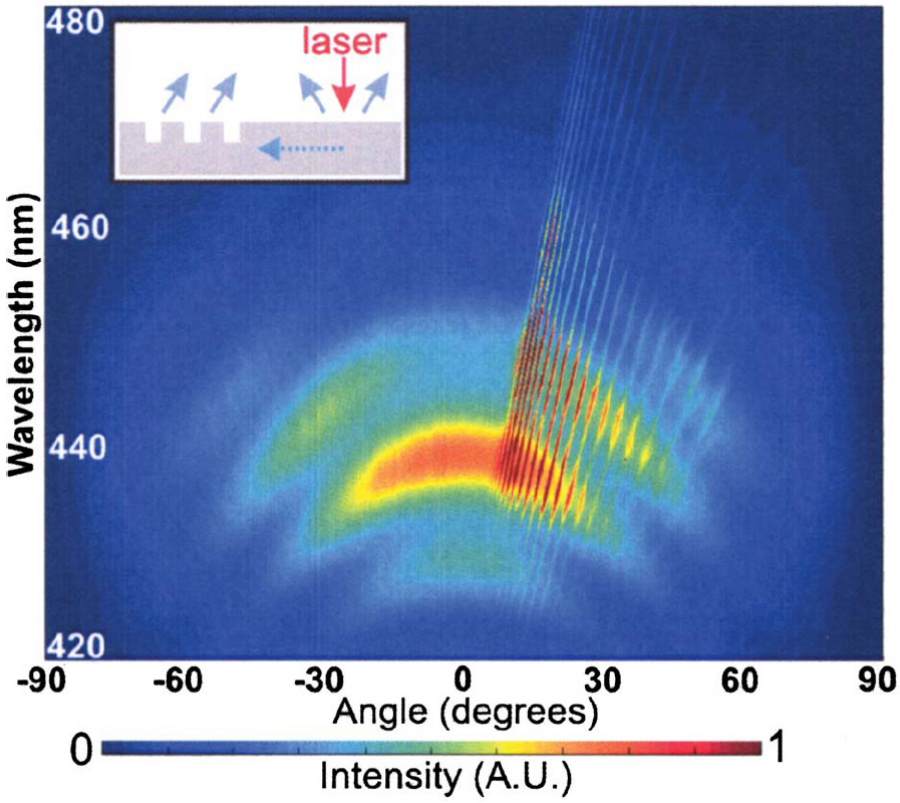

Figure 3-12: angular resolved photoluminescence spectrum [David2005].

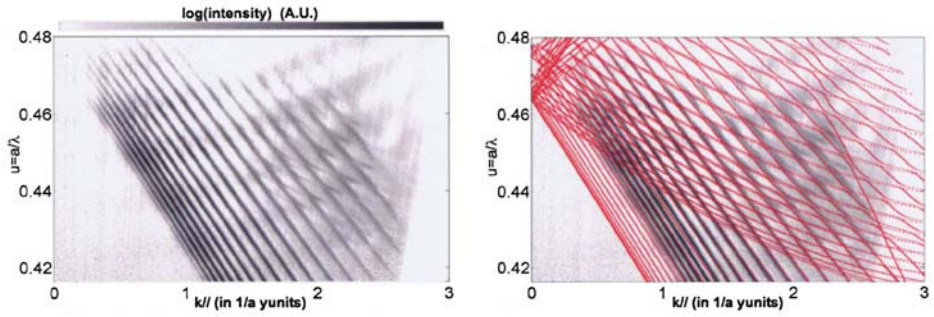

Figure 3-13: the measured band structure is shown on the right. In the left figure the measured and simulated band structure is plotted [David2005].

The observation of two types of bands in Figure 3-13 is specifically a 2D PhC effect and not a superposition of a 1D grating effect. The observation can be explained with the band diagram of a weak (low index contrast) 2D PhC (Figure 3-14a). In the considered region there are two bands: A and B. The dispersion of band A is close to a plane wave while the dispersion of band B is essentially a superposition of two plane waves. Each guided slab mode within the LED has its own corresponding banddiagram. Therefore there are two bands observed for each slab mode (Figure 3-14b). If the 2D PhC would act like a 1D grating coupler only band A would be measured.

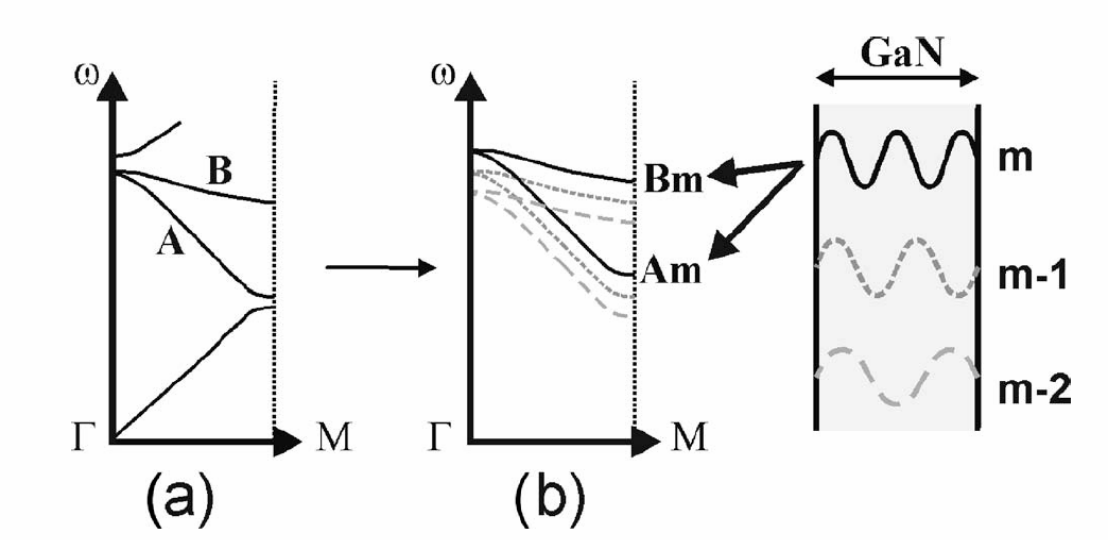

Figure 3-14: (a) 2D band structure of a PhC in the ΓM direction. (b) Band structure in a multi-mode waveguide. The frequency increases with increasing mode order [David2005].

Tailoring of Modes

The thick GaN layer (3~5 μm) can be regarded as a multimode waveguide. The diffraction efficiency depends on the mode order as shown above. Higher order modes will be extracted due to the interaction with the shallow etched PhCs while lower order modes will in general not be extracted. About 30% of the guided light is carried by the lower order modes. To redistribute the lower order modes a low index 800 nm thick AlGaN layer is grown on top of the GaN (buffer) layer. The low index layer is covered by a 600 nm thick GaN capping layer containing the p-n junction and the

active QW region. This structure is schematically shown in Figure 3-15. The AlGaN layer divides the thick multi-mode GaN waveguide, creating two new waveguides. Three types of modes are supported by the structure: capping layer modes (CLM), low-order modes in the thick GaN layer and high order modes which extend across the two waveguides. The AlGaN layer has no influence on the higher order modes as for these modes the effective index is much lower than the AlGaN layer index. Lower order modes in the GaN buffer exist but they have no overlap with the QW region. Little light will therefore be excited into these modes. With a thick enough GaN capping layer a high index cap layer mode (CLM) will be supported. This mode will have a large overlap with the QW region. Lower order modes will therefore be excited in the CLM. The CLMs have a large overlap with the PhC patterned region and will be extracted from the structure.

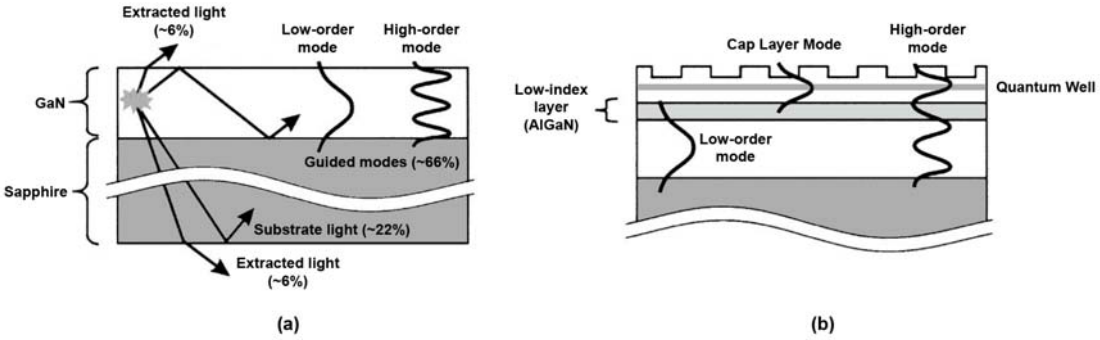

Figure 3-15: (a) the possible paths for emitted light in a conventional GaN LED. (b) Guided modes in a GaN LED with a low index layer and CLM [David2006a].

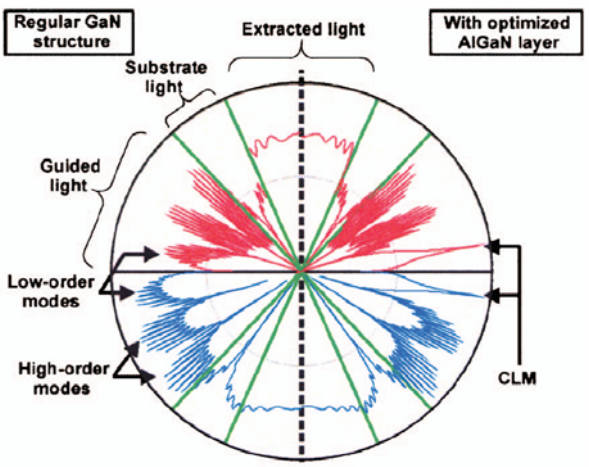

Figure 3-16: emission in a GaN PhC LED plotted as function of the polar angle. The left half shows the emission for the regular GaN PhC LED and the right half shows the emission for the GaN PhC LED with the low-index AlGaN layer. The green lines are the lightlines for air and for sapphire [David2006a].

In Figure 3-16 the emission in a GaN PhC LED with and without a low-index layer is plotted as a function of the polar angle. The figure shows that lower order modes are replaced by a CLM with the implementation of the low index AlGaN layer. The experimental results indicate a 70 percent enhancement in extraction efficiency. It is claimed that optimization of the structure could lead to higher enhancements.

PhC LED structures discussed so far are formed on an epitaxial grown thick GaN layer on top of a sapphire wafer. These LEDs are multimode and the lower order modes do not couple out. David *et al*. showed that the implementation of a low index layer can be used to redistribute lower order modes to leaky CLM [David2006a].

Another idea for improving light extraction efficiency is the fabrication of a thin GaN PhC LED [David2006b]. Such a structure will only support a few guided modes. LEDs with a thickness of 400 nm and of 1 μm are fabricated by David *et al*. The conventional thick GaN LED structure is covered with a gold layer and turned around after which it is bonded on a AlN ceramic substrate. The sapphire wafer, originally used as the substrate for growing GaN is removed by laser-lift off (LLO). The GaN layer is thinned down and a PhC with a triangular lattice is etched into the layer. The lattice constant is 215 nm and the filling factor is 0.38. The depth of the holes is about 250 nm. A schematic drawing of the LED is shown in Figure 3-17. The LED is characterized by angle-resolved electroluminescence spectroscopy. It is found that the effects due to the PhC are strongest in the 400 nm thick device. The guided modes in this device do have more overlap with the shallow etched PhC than in the 1 μm thick device. Metal absorption limited the efficiency of the fabricated LED. A better design should solve this issue.

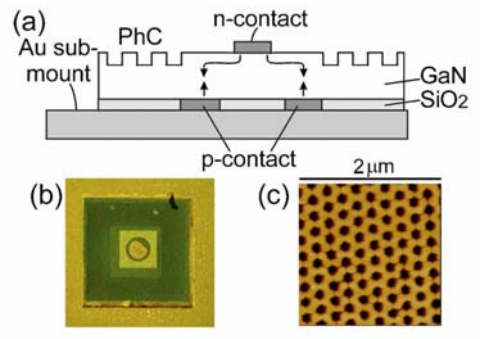

Figure 3-17: LED design (a) microscope image of the device (b) and atomic force microscope image of a PhC region [David2006b].

Pre-patterning of the Sapphire Substrate

Wang *et al*. also used LLO for the fabrication of a GaN PhC LED. The fabrication process is schematically pictured in Figure 3-18. A triangular PhC lattice is etched into the sapphire substrate before the epitaxial growth of the GaN layers. The holes in the patterned sapphire substrate (PSS) are 1 μm deep and 3 μm in diameter. The lattice constant is 6 μm. After growth of the GaN layer a 100 μm thick Cu layer was electroplated. The LED structure is flipped and the PSS is removed by LLO. GaN micropillars are left at the surface of the device. When PhC holes or pillars are etched in a pre-fabricated LED the etching process can damage the device. The advantage of this method is that the PhCs are etched before growing GaN. The LEDs will therefore not be damaged due to the PhC etching. The GaN pillars are however not perfectly straight. During the growth of GaN voids appeared between the sidewall of the holes (SEM-image Figure 3-18b). Room temperature electro luminescence measurements showed an increase of 39% in intensity compared to an unpatterned LED.

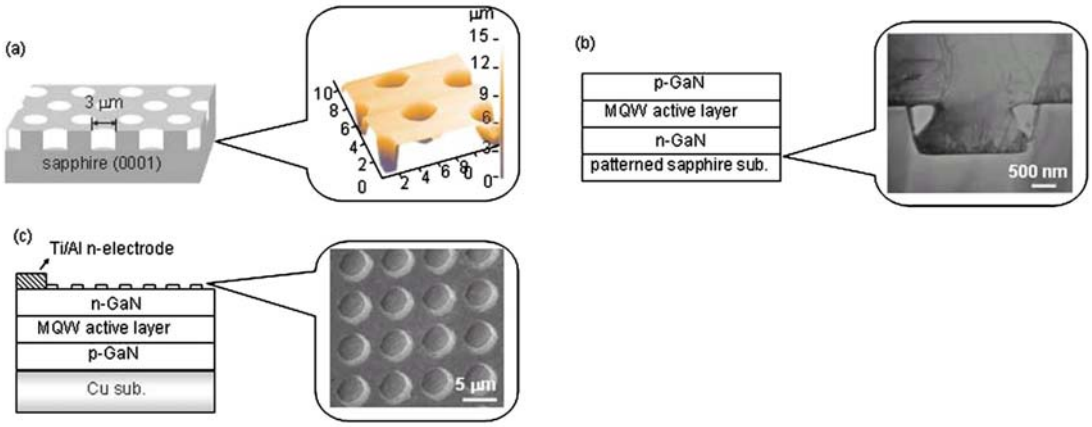

Figure 3-18: schematic overview of the fabrication method and LED design [Wang2006]. Voids in GaN are visible in the SEM image at (b).

GaN Photonic Quasicrystal LEDs

Zhang et.al [Zhang2006] used photonic quasi crystals (PhQCs) for the enhancement of light extraction for GaN-based LEDs. The quasicrystals were etched with a Focused Ion Beam (FIB) (Figure 3-19). The extraction enhancement for a octagonal PhQC (8PhQC), a dodecagonal PhQC (12PhQC), and a triangular PhC were investigated by electro luminescence measurements. Results show that a 1.7 and 1.4 higher emission is obtained for the respectively 12PhQC and 8PhQC compared to the PhC patterning. This increase in light outcoupling efficiency is attributed to the higher rotational symmetry in the PhQC compared with the PhC which leads to an isotropic bandgap. Extraction is therefore less dependent on the orientation as with PhCs as shown by Oder *et al*. [Oder2003]. A total enhancement of 2.5 is obtained for the 8PhQC compared to the unpatterned device.

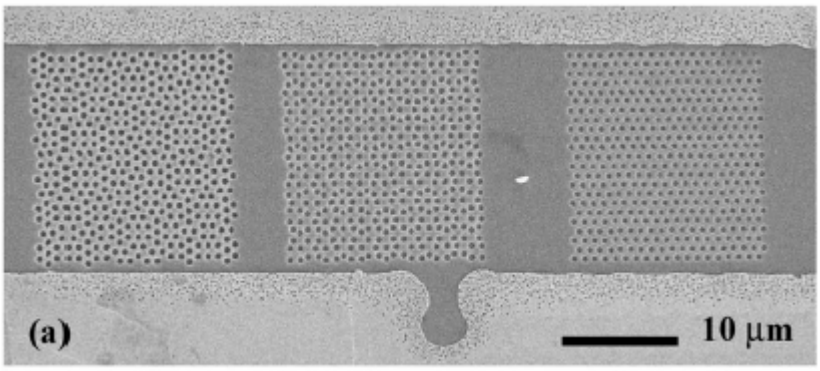

Figure 3-19: from left to right: SEM image of the 12 PhQC, 8PhQC and triangular lattice PhC [Zhang2006].

3.3 *Conclusions*

The measurements done at the GaN PhCs, except for the PhC membranes are all done above the lightline for air. For the fabrication of GaN membrane cavities PEC etching is necessary as there is no chemical wet etch available. So far quality factors up to 800 are obtained experimentally.

PhCs can be used to enhance light extraction in GaN LEDs. Enhancement factors of 2.5 for UV LEDs and 1.5 for blue LEDs are obtained. These numbers might increase by using combinations of obtained results.
It is shown by Shakya *et al*. [Shakya2004] and Wierer *et al*. [Wierer2004] that light extraction enhancement can be increased or decreased by changing the PhC lattice constant and the diameter of the holes.
Experiments done at UCSB showed that with a conventional GaN PhC LED (thick GaN layers and shallow etched holes) the excited lower order modes do not interact with the PhC. These modes are therefore not extracted from the LED. This problem was solved by using a low index AlGaN layer with on top a GaN capping layer [David2006a]. A 70% increase was observed compared to the GaN PhC LED without capping layer.
Oder *et al*. showed that the directionality of the PhC is important for light extraction enhancement [Oder2003]. More light will couple out when propagating in the ΓM direction than when propagating in the ΓK direction. Zhang *et al*. published results on the use of PhQC. For an octagonal PhQC the light extraction efficiency was 1.4 and for the dodecagonal 1.7 times higher than for a triangular lattice PhC.

Chapter 4 Light Outcoupling Simulations

PhCs can be used on three different ways to enhance the external quantum efficiency of LEDs. In this chapter a simulation scheme is discussed with which two of these methods can be investigated: the prohibition of emission into guided modes and Bragg scattering of light. 2D finite difference time domain (FDTD) simulation results are presented.

4.1 *Crystal Wave*

The simulations are performed on four clustered Dell Precision 490 computers running Crystal Wave 4.0. Each computer contains an Intel Xeon 5130 2.0 GHz processor and 4 gigabyte (GB) of DDR2 553 Quad Channel internal memory. The general user interface (GUI) computer is running on Windows XP service pack 2, the three other computers are running on Windows x64. A maximum of 15 GB internal memory can be used for running the operating systems and Crystal Wave (3 GB on the GUI and 4GB on each of the x64 machines).

The simulation software, Crystal Wave, is a commercial program developed by Photon Design (Oxford England) for designing and simulating PhCs. It can perform 2D and 3D FDTD simulations as well as Frequency Domain (FD) simulations. Band diagrams can be solved in 2D and 3D by the Plain Wave Expansion (PWE) method. For light outcoupling simulations the FDTD method is used. This method is shortly described in the remainder of this section.

4.1.1 Finite Difference Time Domain

FDTD is a popular simulation method in electromagnetism. Simulations are performed in the time domain which makes it possible to perform simulations covering a wide frequency range. The underlying principle of this method can be deduced from the Maxwell equations (Equations 2.8-2.11) [Wikipedia2007].

The change in electric field in time depends on the curl of the magnetic field. The electric field at a specific moment is therefore dependant on the stored electric field and its change in time. The change in magnetic field in time depends on the curl of the electric field. The stored magnetic field and the change in time will give the magnetic field at a certain moment. In FDTD simulations the electric and magnetic field are calculate in a leapfrog manner. First the electric field is calculated, the next time step the magnetic field and then again the electric field and so on.

The Maxwell equations are solved numerically, space and time are discrete. The space over where the simulation runs is divided into a grid. The time over where the simulation runs is divided in steps. The smaller the grid size and time steps the better the simulation corresponds with the actual case. In CrystalWave the time step size is coupled to the grid size. This is done to make sure that the used algorithms are stable and to run the simulation in the shortest time possible. As a rule of thumb, the smallest structure must at least be divided into ten grid cells. [CrystalWave2007]

An advantage of FDTD simulations is that the response of a system over a broad range of frequencies can be solved in one single simulation by Fourier transforming

the time results. Furthermore, the electric and magnetic fields are calculated in every grid cell. It is therefore possible to see the electric field, the magnetic field and the intensity evolve in time.

The main disadvantage of FDTD is the duration of the simulation. To see the response of a system the fields must be calculated at each grid cell and for every time step for the whole duration of the event. Another disadvantage is the large amount of internal memory necessary to run 3D simulations.

4.2 *Light Outcoupling Simulations*

FDTD simulations are performed to investigate how PhCs can be used for light extraction enhancement. It is chosen not to start with the simulation of light extraction in complicated structures like LEDs, but rather follow the approach used by Fan *et al*. [Fan1997]. In this approach the problem is simplified to light extraction in a dielectric slab surrounded by air. The same kind of simulation is also performed by Fujita *et al*. [Fujita2005].

Fan *et al*. performed 3D FDTD simulations for light extraction in a PhC slab and compared that with extraction in a planar dielectric slab (Figure 4-1a and Figure 4-1c). A point dipole source exciting a Gaussian intensity profile in time and polarized in the plane of the slab is used for simulating light generation inside a QW. The excitor is placed in the middle of the slab. The extraction efficiency is defined as the fraction of emitted flux through the top and bottom surfaces of the slab to the total emitted flux. The results are compared with corresponding dispersion relations. The focus is on TE guided modes since light emitted in a QW, sandwiched between two dielectric layers will have similar polarization.

The simulation results are shown in Figure 4-1. In Figure 4-1b the dispersion relations of dielectric slab modes is compared with the output efficiency. A peak is visible at $0.58c/a$. This coincides with the appearance of the second even mode. Due to reasons of symmetry, light can only couple to the even modes. For increasing frequency the density of leaky modes increases. As a result, the output efficiency will increase. At the frequency $0.58c/a$ the second even mode appears in which part of the emitted light is radiated. This leads to the observed decrease in output efficiency.

In Figure 4-1d the banddiagram of the PhC made by perforating a hole pattern in the slab of Figure 4-1a is compared with the output efficiency of a light emitter in this PhC. At the dielectric band edge for TE polarization, a sharp increase in the output efficiency is visible. A small dip occurs at the air band edge. The increase in output efficiency in the TE gap is due to the simultaneous inhibition and redistribution of spontaneous light emission. Because of the zero mode density for modes in the PhC slab, no light is emitted in the plane. After the small dip the output efficiency will remain high. This has to do with light extraction due to coupling to radiative modes above the lightline. The results show that the approach used by Fan *et al.* simulates two 2D PhC effects: Bragg scattering of light and the inhibition and redistribution of light.

The simulated output efficiency of the dielectric slab can be compared with that of the PhC. It shows that by using a PhC a large increase in output efficiency can be obtained.

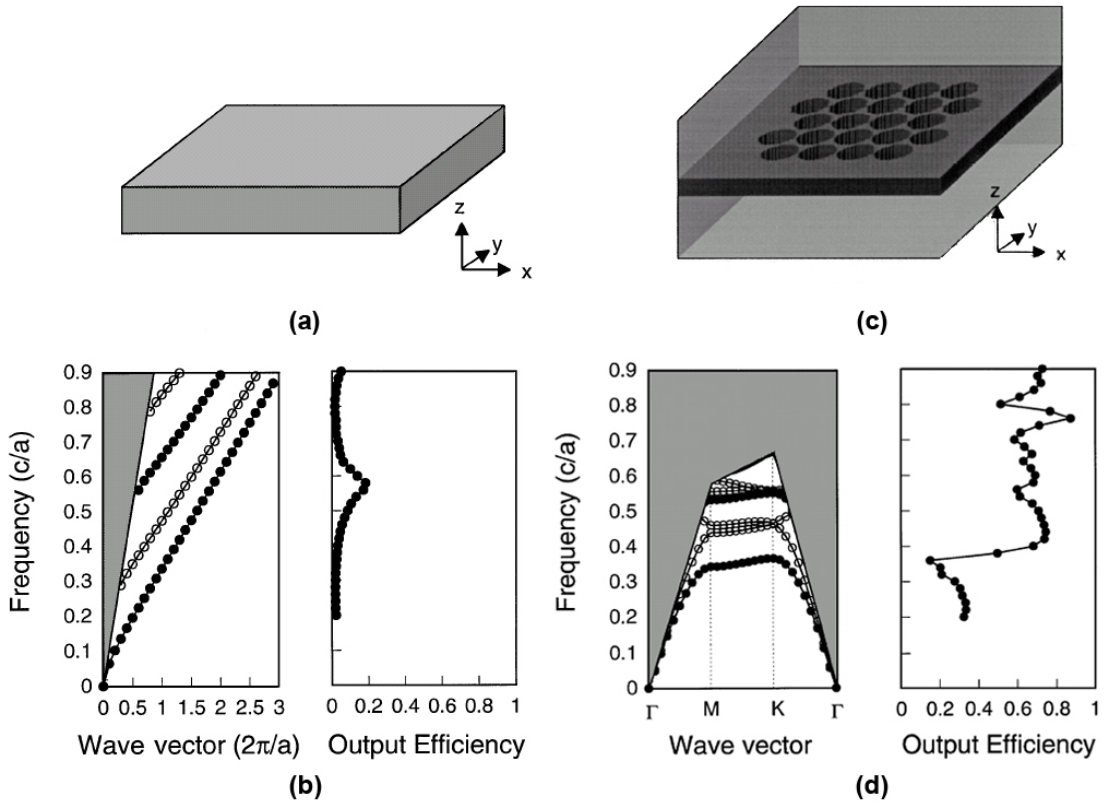

Figure 4-1: (a) and (c) simulation set-up. (b) output efficiency simulations compared with the dispersion diagram for a dielectric slab. (d) output efficiency simulation of a 2D PhC compared with its dispersion diagram [Fan1997].

Differences between 2D and 3D FDTD light extraction simulations are shown in section 4.2.1. The simulation set-up in Crystal Wave is presented in section 4.2.2.

4.2.1 2D versus 3D FDTD Simulations

The FDTD simulations described by Fan *et al.* are 3D. Crystal Wave can perform 2D and 3D FDTD simulations. In this section differences between 2D and 3D light extraction simulations are shown.

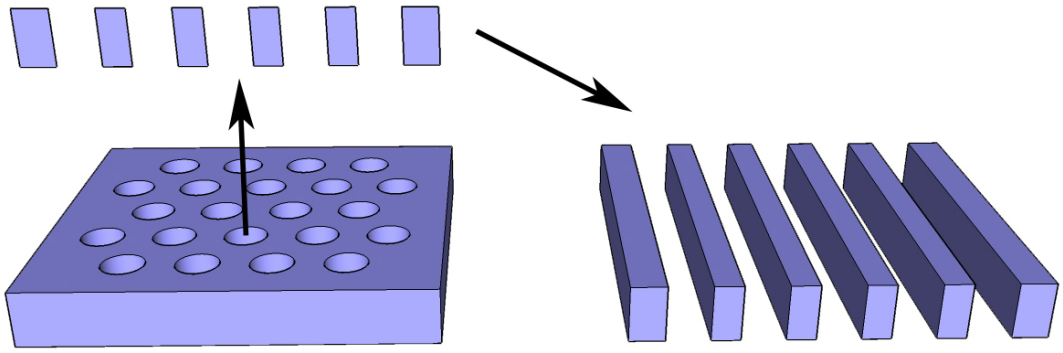

Figure 4-2: for a 2D FDTD simulation light extraction is simulated in a cross-section of the 2D PhC. The 2D PhC is therefore simulated as a 1D PhC.

For 2D FDTD light extraction simulations the light extraction is calculated in a cross-section of the (2D PhC) slab. As a result, the 2D PhC slab is simulated as a 1D PhC slab (Figure 4-2).

Since a 2D slab is isotropic the dispersion can be obtained from a 1D calculation. However, for 2D FDTD simulations the 2D PhC is seen as a 1D PhC. The dispersion relations of a 2D PhC essentially differs from a 1D PhC. There are more available bands to couple to for the 2D PhC than for the 1D PhC. These bands are not available in the 2D FDTD simulation. This difference is already discussed in the two previous chapters.

A second difference between 2D and 3D simulations is that the simulated output efficiency will be higher for 2D than for 3D simulations. In a planar slab about $1/2n^2$ of the generated light can escape to air through the top and bottom surfaces [Appendix 1]. For the 2D simulation about $4\theta_c/360$ of the generated light will couple to air, with θ_c the critical angle in degrees (Figure 4-3). This results in output efficiencies of approximately 8% for the 3D and 26% for the 2D simulations for $n \sim 2.5$.

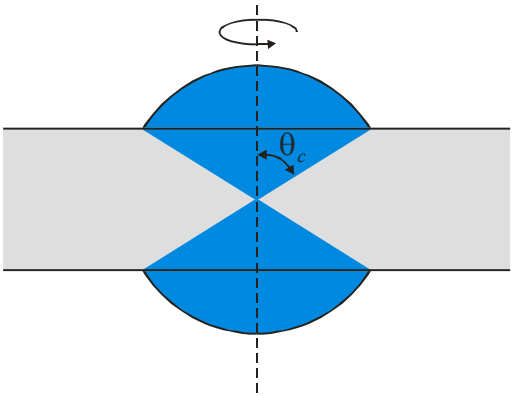

Figure 4-3: extraction cone in a dielectric slab. For 2D simulations a fraction of $4\theta_c/360$ can escape, while for 3D simulations just a fraction of $1/2n^2$.

It can be concluded that a 2D FDTD simulation will give too optimistic output efficiencies and that PhC outcoupling effects that are essentially 2D are not taken into

account. Light extraction simulations must therefore be 3D. 2D FDTD simulations are however carried out for the dielectric slab. Although these simulations are not realistic they may be carried out in a reasonable time and tell how Crystal Wave can be used for light extraction simulations. They also serve to reveal general qualitative features and trends of light extraction from dielectrics.

4.2.2 Simulation Set-up

Figure 4-5 shows a schematic overview of the set-up for 2D FDTD simulations. A dielectric slab with refractive index n_{slab} and thickness d is surrounded by air. A dipole excitor with in plane polarization is placed in the middle of the slab.

Sensors are placed in a square around the dipole excitor to register the flux (W/THz) through a line. The sensors are placed in the vicinity (~6 µm) of the dipole excitor to keep the calculation requirements within the specifications of the computer cluster. The direction of positive flux is defined outwards.

Eight sensors are used in total. Two of them register the light that is guided in the slab. Six sensors register the fraction of light that is coupled out of the slab. The output efficiency is obtained by dividing the extracted power by the total input power.

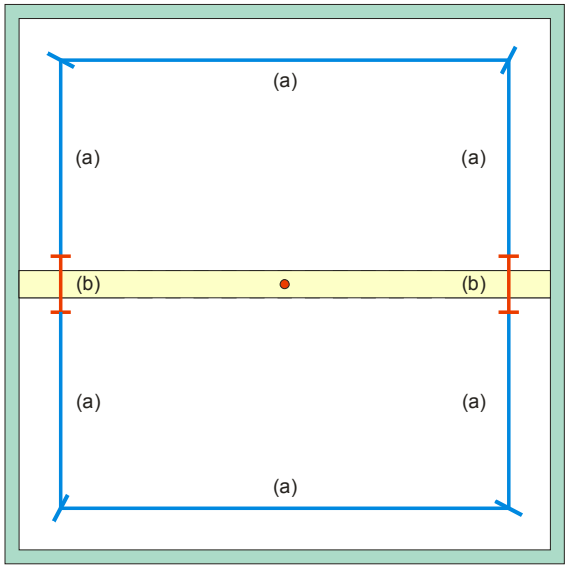

Figure 4-4: Crystal Wave set-up for 2D FDTD simulations. Sensors (a) register the extracted light. Sensors (b) register the guided light.

A schematic drawing for the 3D FDTD simulation set-up is shown in Figure 4-5. Fourteen sensors are placed around the center of the slab, forming a closed cube. Ten sensors (yellow) register the amount of light that is coupled out of the slab. Four sensors (orange) register the amount of guided light.

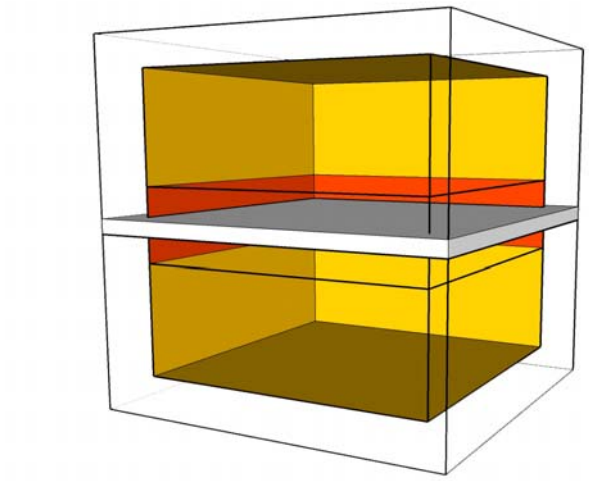

Figure 4-5: schematic 3D drawing of the simulation set-up for 3D FDTD simulations.

4.3 *First Simulation Results*

In this section the first simulation results are presented.

4.3.1 Dispersion Relation of a Dielectric Slab Waveguide

The dispersion relation of a dielectric slab waveguide is calculated with Mathematica, using the ray optics approach introduced in Chapter 2. To verify the Mathematica program the dispersion relation of a slab with refractive index $n = 3.5$ is calculated and compared with the dispersion relation of Figure 4-1b. The result is presented in Figure 4-6. As the figure shows the Mathematica calculation and the calculation done by Fan *et al.* do not match. A third computer program, CAMFR is used to calculate the dispersion diagram of the slab. CAMFR is developed by Ghent University and uses PWE to calculate dispersion diagrams [Ghent2007]. The results of the CAMFR calculations do exactly match with the Mathematica calculations as shown in Figure 4-6. The difference between the Mathematica and CAMFR calculations on one side and the calculations by Fan *et al.* on the other side can not be explained. The Mathematica program will be used to calculate the dispersion relations of a dielectric slab waveguide.

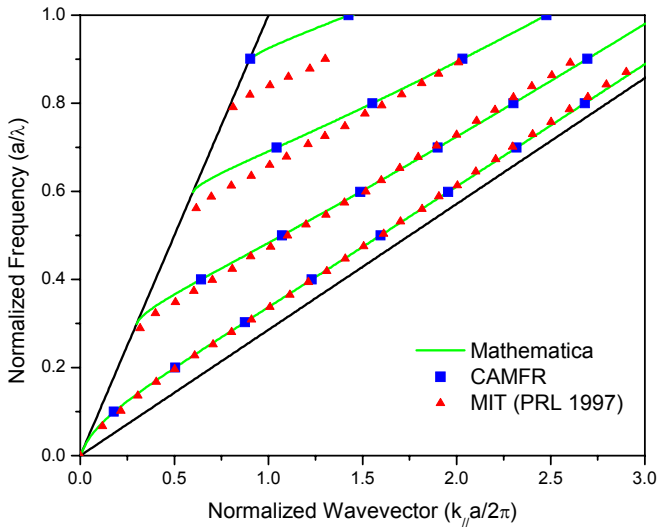

Figure 4-6: dispersion relation of a GaAs slab calculated by Mathematica, CAMFR and by Fan *et al.* (MIT).

The dispersion relation of a GaN slab for TE polarized light is shown in Figure 4-7. The slab has a thickness of $0.5a$ and a refractive index of 2.53. Even and uneven modes are marked.

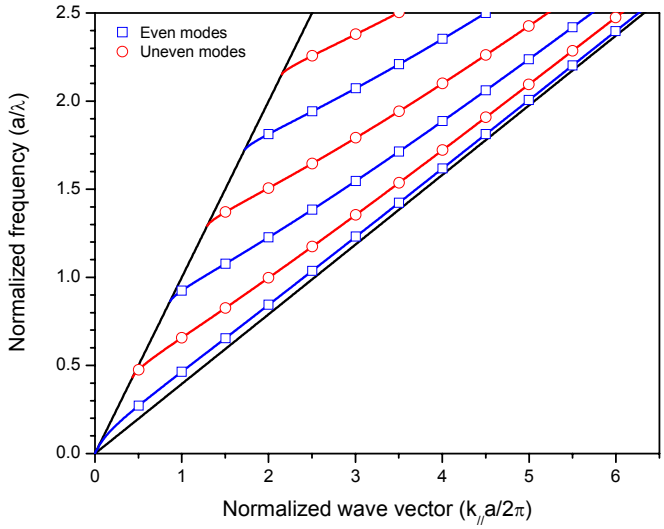

Figure 4-7: dispersion relation of a GaN dielectric slab waveguide. The open squares correspond to the even modes while the open circles correspond to the uneven modes. The refractive index used in this calculation is 2.53. The thickness d of the slab is $0.5a$.

4.3.2 2D FDTD Simulations

In this section the 2D FDTD simulation results for light extraction from a dielectric slab with thickness a are shown. The refractive index used for these calculations is 2.53, the refractive index for GaN around 400 nm [Zhang1996].

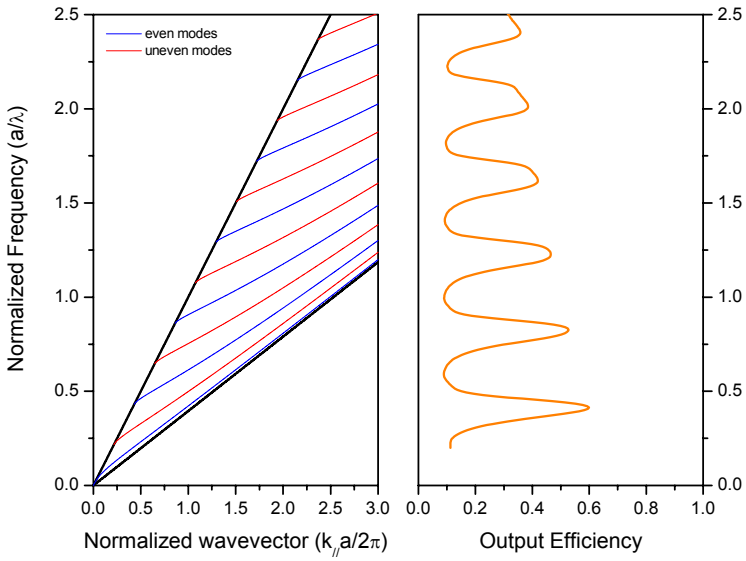

Figure 4-8: the dispersion relation of a planar slab is compared with the simulated output efficiency. The slab thickness is 500 nm and the simulation grid size 2 nm.

In Figure 4-8 the output efficiency of a planar dielectric slab is compared with its corresponding dispersion relation. The thickness of the slab is 500 nm and the simulation grid size 2 nm. The excitor is exactly placed in the middle of the slab. The location of the first peak in the output efficiency matches with the appearance of the second even mode. This is the same result as in the simulations performed by Fan *et al.* [Fan1997]. Emitted light can only couple to the even modes due to reasons of symmetry. With the excitor placed in the center, there must be an anti-node at the center. With increasing frequency the density of radiative modes increases. More light can couple out and the output efficiency will increase. With the second even mode appearing the emitted light can couple to two even modes. Therefore the output efficiency will decrease again. The second and higher peaks in the output efficiency graph however, do not coincide with the appearance of the new even modes. To investigate if this is caused by the simulations, the slab thickness, grid size and location of the dipole excitor is changed.

Note that the output efficiency in Figure 4-8 is higher than the output efficiency from the 3D FDTD simulations performed by Fan *et al.* (Figure 4-1b). This was already expected.

Slab Thickness

The influence of the slab thickness is investigated. The output efficiencies for slabs with thicknesses of 0.5, 1.0, 2.0 and 4.0 μm are simulated. The simulation grid size is

20 nm. The results are shown in Figure 4-9. Because the wavelength range is kept constant, the normalized frequency range a/λ increases with increasing a.

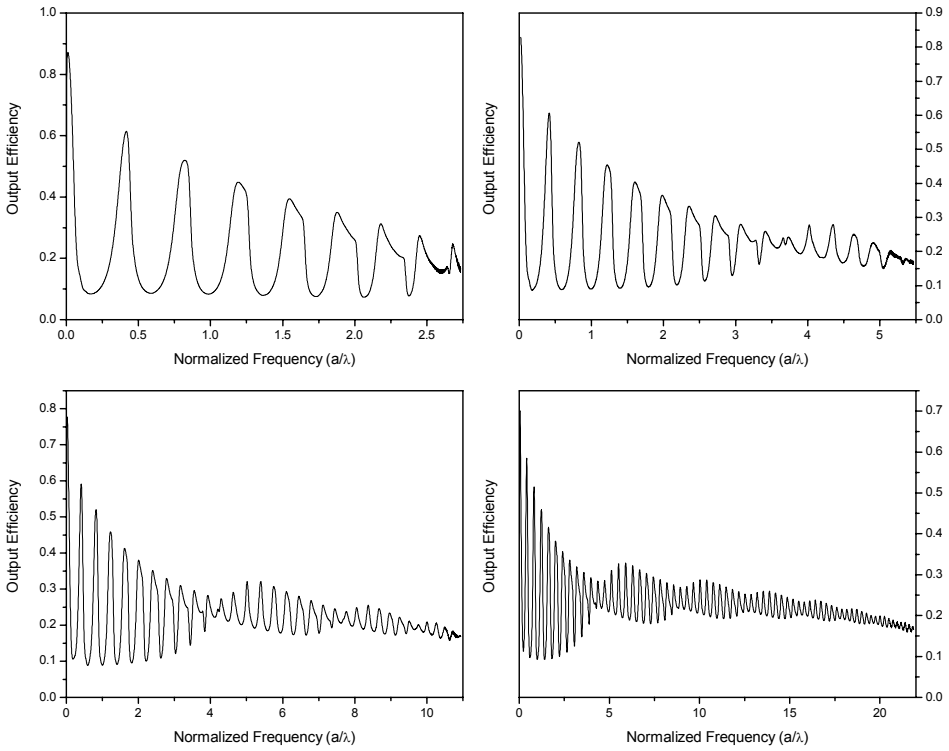

Figure 4-9: output efficiency versus normalized frequency for a 0.5 (top left), 1.0 (top right), 2.0 (bottom left) and 4.0 µm (bottom right) thick slab. The simulation grid size is 20 nm.

The figure shows that a beat appears in the output efficiency diagram for increasing normalized frequencies. The origin of this beat is unclear. In Figure 4-10 the simulated output efficiencies of the slabs are compared. For normalized frequencies up to about 1.5 the output efficiencies are matching. Above this value the graphs start to deviate from each other.

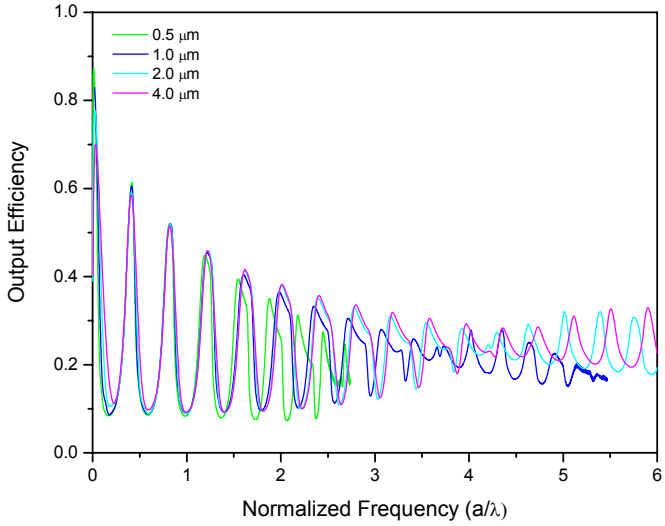

Figure 4-10: output efficiency versus normalized frequency for different slab thicknesses. The simulation grid size is 20 nm.

Simulation Grid Size

The influence of grid size is investigated. In Figure 4-11 the output efficiency for a 1 μm thick slab is shown, simulated with a 5 nm grid size and with a 20 nm grid size. The graphs overlap for normalized frequencies up to 1.5. The peaks in the output efficiencies are shifted to lower frequencies for the 20 nm grid size simulation compared to the 5 nm grid size simulation.

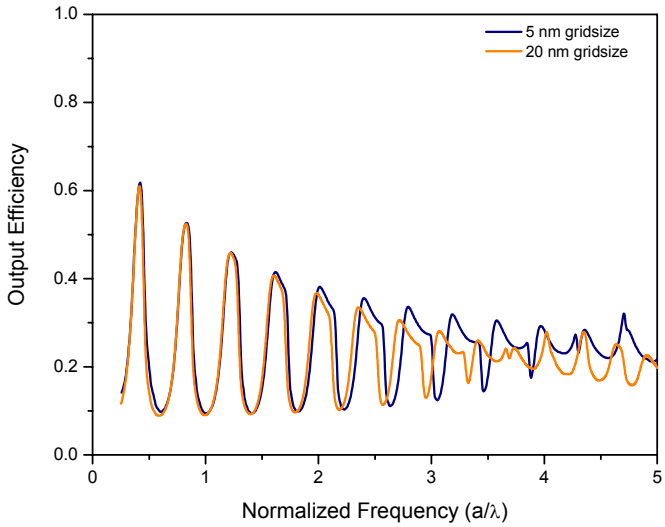

Figure 4-11: output efficiency for 1 μm thick slab simulated with a grid size of 5 nm and of 20 nm.

Figure 4-12 shows the output efficiency for a 500 nm thick slab, simulated with a 2 nm and 1 nm grid size. Up to $a/\lambda = 4$ the graphs match. For higher normalized frequencies extra fringes appear in the output efficiency for the simulation with 1 nm grid size.

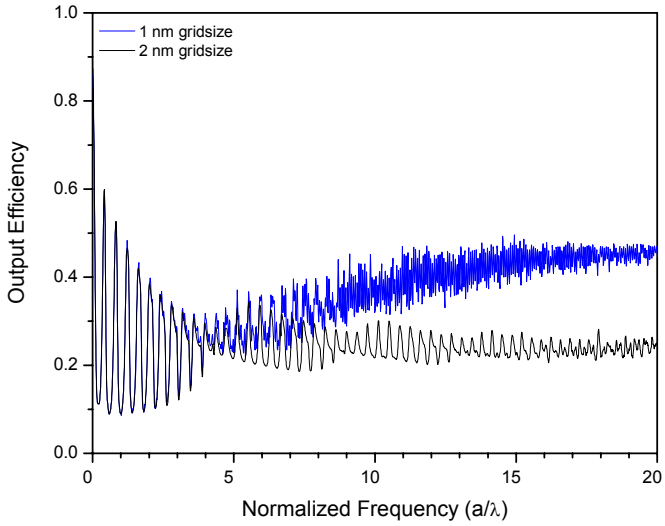

Figure 4-12: output efficiency for a 500 nm thick slab simulated with a grid size of 1 nm and of 2 nm.

Location Dipole Excitor

It might be possible that the peaks in the output efficiency do not match with the appearance of the even modes in the dispersion relation if the dipole excitor is not simulated exactly in the middle of the slab due to the discrete calculation space. Therefore the output efficiency of a 500 nm thick slab is simulated with the dipole excitor placed in the center and 2 nm of the center of the slab. The grid size was set to 2 nm. The results are shown in Figure 4-13. Although there is a difference in output efficiencies for these two simulations for normalized frequencies of 1.5 and higher, the peaks do exactly coincide.

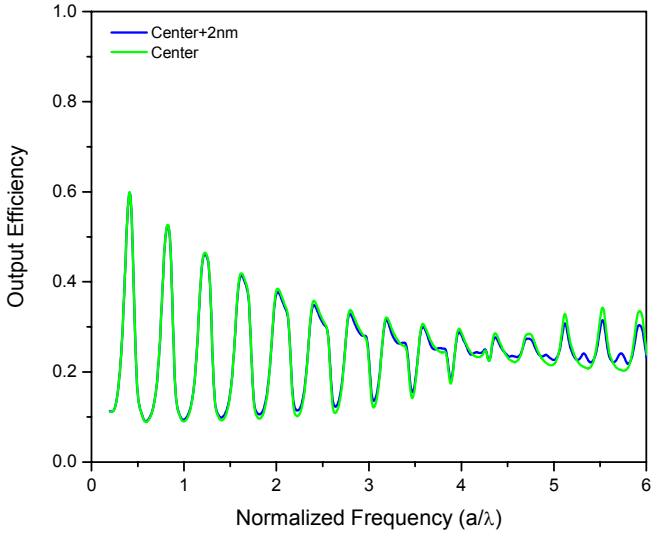

Figure 4-13: output efficiency for a 500 nm thick slab, with the dipole exciter placed in the center and 2 nm off the center of the slab. The simulation grid size is 2 nm.

To verify the coupling to even modes only due to the symmetric location of the dipole excitor, we now place the excitor at one quarter a of the slab edge. Due to symmetry reasons it is expected that light can couple to some uneven and even modes. In Figure 4-14 the mode profiles of the first five modes are shown. Emitted light can only couple to a mode when an anti-node is present. With the dipole exciter placed on one quarter a of the slab edge light can couple to the first uneven mode, but not to the second uneven mode. The simulation results presented in Figure 4-15 verify coupling to some even and uneven modes.

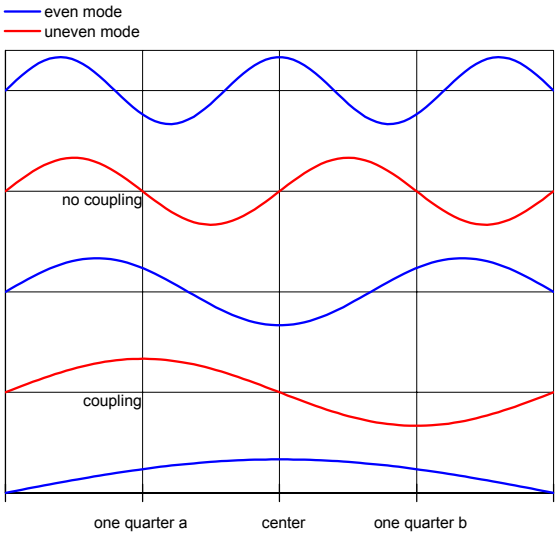

Figure 4-14: schematic representation of the mode profiles of the first five modes.

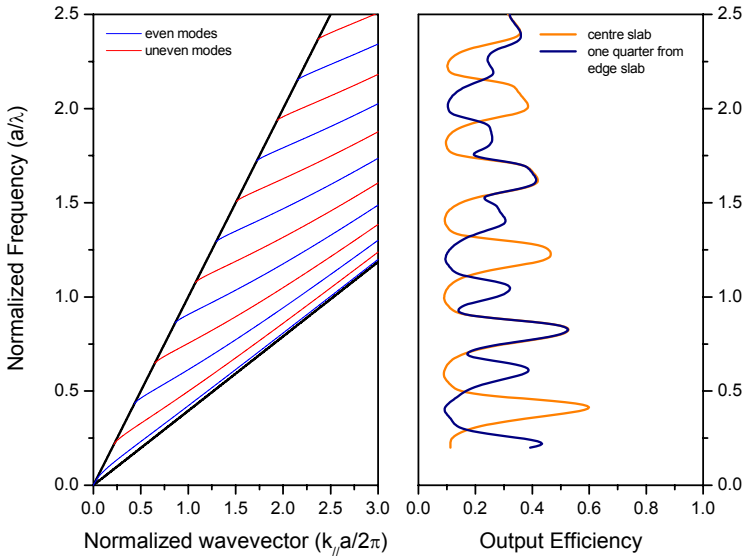

Figure 4-15: dispersion relation for a dielectric slab compared to the output efficiency diagrams for a 500 nm thick slab with the excitor placed in the center and on one quarter of the edge of the slab. The grid size is 2 nm.

Crossflux

The sensors in the simulation set-up are placed in a closed square around the center of the slab (Figure 4-4). It would be easier to place one sensor just above and one just below the surface to register the amount of extracted light. Four sensors can be removed and the calculation space can be made smaller. As a result, less internal memory and time would be needed to run the simulation. Crystal Wave however has a problem with registering flux passing through a sensor, for fields not propagating perpendicular to it. Guided light, not propagating through a sensor but with the evanescent tail in the sensor, may be registered as outgoing and ingoing flux. For large angles between the incident wave and the normal to the sensor this cross-flux can lead to significant errors [CrystalWave2007].

The output efficiency diagram for a simulation with sensors placed 50 nm above and below the sample is shown in Figure 4-16. The line sensors register the net, positive and negative flux through a surface. The figure shows that a large negative flux is measured. In reality light is radiated outwards and will not reflect outside the dielectric slab: there is no negative flux. To minimize cross flux the sensors are therefore placed in a square for 2D FDTD and in a cube for 3D FDTD simulations around the center of the slab as shown in Figure 4-4 and Figure 4-5. In Figure 4-17 the net, positive and negative output efficiency for a slab is shown. The sensors are placed in a square around the dipole excitor. The figure shows that no negative flux is recorded.

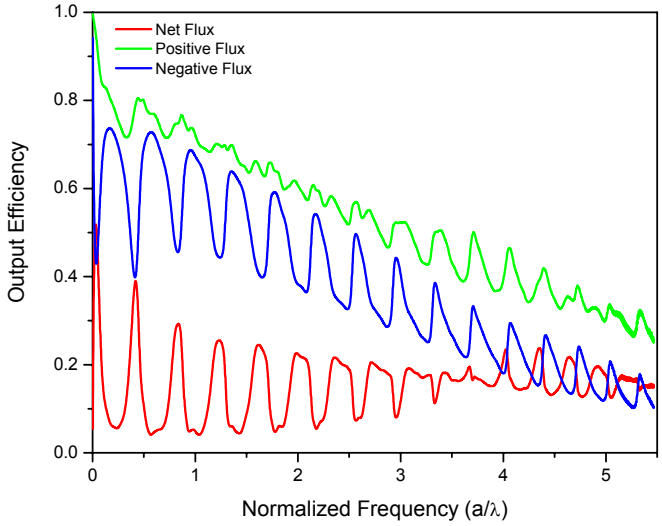

Figure 4-16: output efficiency for a 1 µm thick dielectric slab. The sensors registering the extracted light are placed 50 nm above and below the slab. The simulation grid size is 20 nm.

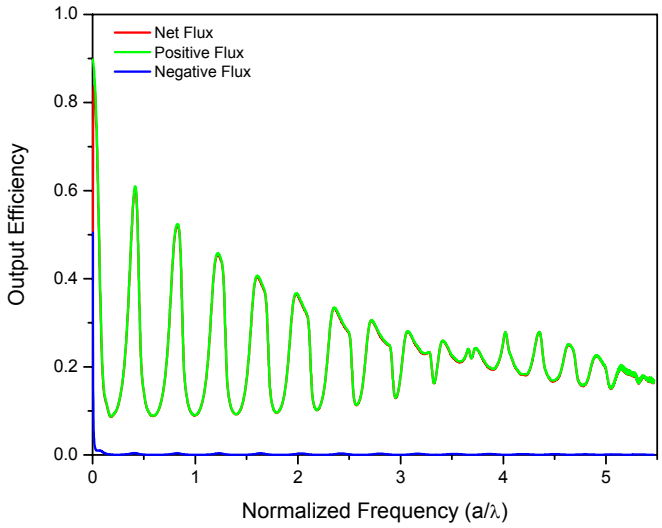

Figure 4-17: output efficiency for a 1 µm thick dielectric slab. The sensors registering the extracted and guided light are placed in a square around the center of the slab (Figure 4-4). The simulation grid size is 20 nm.

4.3.3 3D FDTD Simulations

Attempts have been made to perform 3D FDTD light extraction calculations with the cluster version of Crystal Wave. No reasonable results were obtained thus far. The program failed to perform 3D FDTD simulations for grid sizes smaller than 20 nm. This is about the grid size needed for the simulations. The reasons for the failure are attributed to software bugs in the newly developed 3D version of Crystal Wave.

Photon Design delivered a patch to repair the program. It is now possible to perform 3D FDTD simulations with a grid size smaller than 20 nm. However, a new problem occurs during the final calculation step, the Fourier transform. In the old version this

would take a few minutes to an hour. In the updated version this can take a few minutes to a few days depending on the amount of sensors used in the structure and their sizes. For light out coupling simulations where large sensors are used the Fourier transform can take a few days. A quick test showed that during this time the program sometimes crashes. The new version is not thoroughly tested yet. This should be done before any conclusions can be made about the usability of the program for 3D FDTD light extraction simulations.

4.4 *Conclusions*

The simulation set-up used by Fan *et al.* [Fan1997] will simulate PhC light extraction due to Bragg scattering and the inhibition and redistribution of modes. For correct modeling the simulations must be 3D. The cluster version of Crystal Wave 4.0 is used to perform 2D FDTD simulations. To minimize cross flux the sensors must be placed in a square around the center of the slab. The 2D FDTD simulations of the light outcoupling in a dielectric slab with the exciter placed in the center of the slab show that an increase or decrease in output efficiency goes together with the appearance of an even mode. This is in agreement with the results of Fan *et al.* The positions of the peaks in the output efficiency do however not exactly match with the appearance of an even mode, particularly at higher order modes. For $a/\lambda > 1.5$ the 2D FDTD simulations results for changing grid size and/or slab thickness start to deviate from each other.

The usability of Crystal Wave for 3D FDTD light extraction simulations must be further investigated.

Chapter 5 Experiments with Gallium Nitride Photonic Crystals

Interesting applications in GaN like LEDs work in the UV-blue-green wavelength region as is shown in Chapter 3. GaN PhCs used in these applications consist of either shallow etched holes for enhancement of light outcoupling or of thin membranes.

As a first experiment, a GaN PhC is designed which works at the optical telecommunications wavelength. Although the main applications of GaN PhCs are in the visible wavelength region, there are several good reasons to start with this experiment. The holes needed for a PhC with a PBG in the IR are larger and therefore easier to fabricate than for a PhC with a PBG around the UV-blue. Furthermore, there is experience with PhCs working in this wavelength region. For instance indium phosphide (InP), silicon (Si) or gallium arsenide (GaAs) PhCs. Finally, a set-up which can perform transmission measurements in the infrared (IR) is available. The experience acquired with these experiments can eventually be used for GaN PhCs working in the UV-blue-green wavelength region.

In this chapter the experimental results of the GaN PhCs with a triangular lattice of holes are given. For the first time the transmission of a GaN PhC is measured. These are also one of the very few experiments in GaN PhCs conducted below the light line for air.

5.1 *Gallium Nitride Photonic Crystal Design*

There are several types of 2D PhCs. There are PhCs with a low index contrast between the core and claddings and deeply etched holes. These PhCs are for instance made from InP/InGaAsP/InP. The second type are the free standing membranes with high index contrast between core and cladding layers made from for instance GaN, Si or InP. Finally, there are the PhC semi-membranes. These PhCs are basically high refractive index PhC membranes on top of a low index material. They are made from for instance Si on top of SiO_2. In this section the design of the GaN PhC is discussed.

Layer Structure

There are two important design criteria for the layer structure of the GaN PhCs. The first criterion is that the layer structure in which the PhC is etched must be single mode in the vertical direction. Secondly, the (fundamental) vertical mode profile should have a width comparable to the hole depth (Figure 5-1). These two criteria are drawn up to minimize out of plane losses due to scattering of light [Bogaerts2001]. Possible layer structures for the GaN PhCs are discussed below.

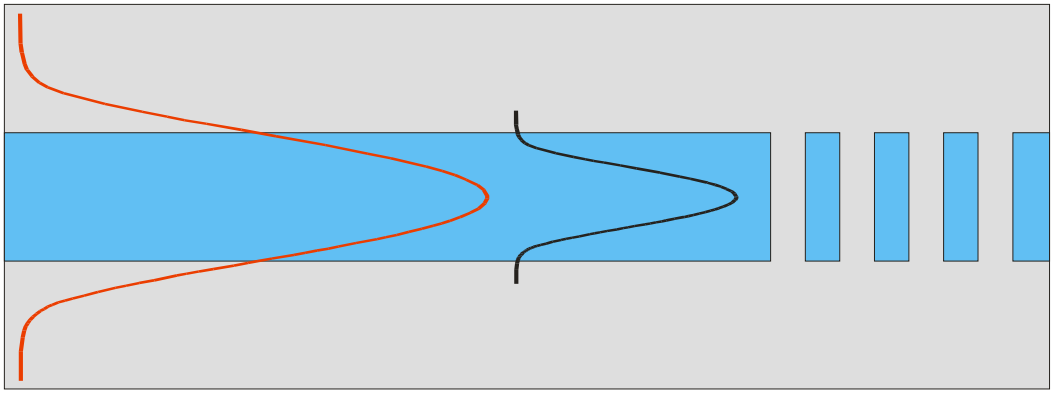

Figure 5-1: the vertical intensity mode profile must be localized within the holes. To minimize out of plane losses the vertical mode profile must be localized within the location of the holes (black line). High losses can occur if the vertical mode profile is extending in the cladding layers (red line).

The first option is to create a free standing GaN membrane. These membranes are fabricated by PEC etching (see section 3.2).

The second option is to use aluminum nitride (AlN) and indium nitride (InN) as respectively cladding or core layer. These two semiconductors are used to create alloys with GaN. The index difference for GaN and AlN for 1.55 µm is quite small, about 2.31 compared to 2.1. A layer structure of AlN and GaN will lead to a PhC with low index contrast and deep etched holes. InN is a controversial material to use. There are still ongoing discussions about the real value of the bandgap of InN. The lattice mismatch between InN and GaN is large, about 3.54 Å (a-axis) versus 3.19 Å (a-axis) [Ioffe2007].

The final option is to use the substrate, sapphire as a cladding layer. GaN is grown on sapphire, which is transparent and has a refractive index of 1.77 [MellesGriot2007] around $\lambda = 1.55$ µm. The index contrast between GaN (2.31) and sapphire (1.77) is much larger than between GaN (2.31) and AlN (2.1). It is not possible to etch structures into sapphire. Only a semi-membrane type of PhC can be fabricated with this layer structure.

It is not possible to etch deep holes (several micrometers deep) in GaN with the current state of technology. Fabrication of a PhC with low index contrast between core and cladding layers and deep etched holes is therefore not possible. The fabrication of a PhC membrane is also dropped as there is no experience with PEC etching. The best option is therefore to create a PhC semi-membrane of GaN on top of sapphire. Note that Coquillat *et al.* and Peyrade *et al.* already used sapphire for their GaN PhCs as shown in Chapter 3 [Coquillat2001a], [Coquillat2001b], [Peyrade2003]. Their experiments were however conducted above the lightline to air.

Figure 5-2 shows the vertical intensity profile of a GaN on sapphire waveguide [Hammer2007]. The width of the waveguides is chosen to be 2.5 µm. The same width used for our InP waveguides [VanDerHeijden2006]. The GaN layer for the mode calculation is chosen to be 650 nm thick as this is still single mode in the vertical direction. The second criterion for the design of the PhC was that the holes must cover the mode profile as far as possible to prevent losses. For the semi-membrane PhC this criterion is not fully met. The mode will still be present below the holes. This might

lead to extra losses in the PhC. In the next sections it is further investigated if the GaN on sapphire layer structure can be used for the fabrication of a GaN PhC.

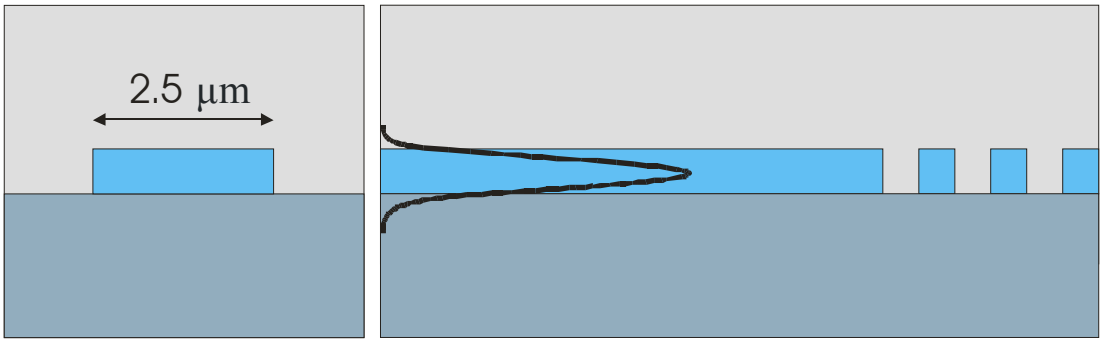

Figure 5-2: vertical intensity mode profile for a sapphire-GaN-air waveguide. The GaN layer is 650 nm thick and the width of the waveguide is 2.5 µm. The waveguide is single mode in the vertical direction. In the horizontal direction there are four modes [Hammer2007].

Gapmap Photonic Crystal

A gapmap is calculated for a 2D PhC with a triangular lattice of holes. For the calculation of the gapmap the effective index for the fundamental mode of the GaN-sapphire waveguide is used at $\lambda = 1550\,\text{nm}$. The gapmap will serve as a guide for the bandgap in the actual PhC. The gapmap is calculated for TE polarized light and the refractive index of GaN was set to 2.14 [Hammer2007]. The results are shown in Figure 5-3.

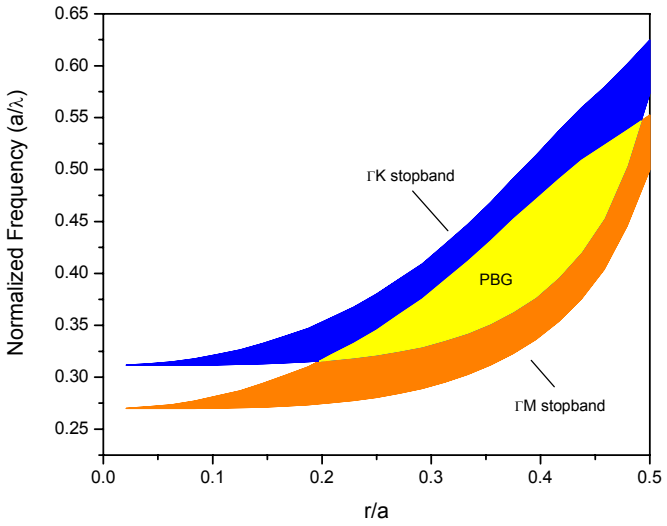

Figure 5-3: Gapmap for a 2D PhC for TE polarization. The effective index used in the calculation is 2.14, the index of the fundamental mode of the GaN-sapphire waveguides.

Transmission Simulations

As the gapmap only gives an indication of the position of the gap in the layer structure the transmission through the PhC for the real configuration is simulated with Crystal Wave.

For the most accurate results these transmission simulations must be done by 3D FDTD simulations. In 2D FDTD transmission simulations the effective index approximation is used to describe the guided modes with a 2D model. In high index contrast waveguides the effective index changes rapidly by increasing or decreasing the wavelength. It is showed by *Qiu* that the effective index approximation for high index contrast waveguides is only valid in small regions of wavelengths [Qiu2002]. Further more, the holes are only penetrating the GaN layer while the vertical mode profile is extending in the sapphire layer as shown in Figure 5-2.

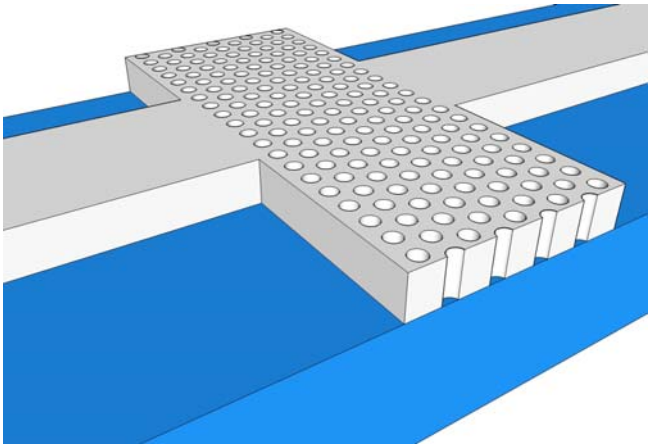

Figure 5-4: the GaN PhC design. The waveguides and holes are etched into the GaN layer.

For technological reasons the PhCs will be designed with a r/a value of 0.3. In the case of infinitely deep holes there is a ΓM stopband for a/λ between 0.29 and 0.38, a ΓK stopband for a/λ between 0.30 and 0.42 and a PBG for a/λ between 0.30 and 0.38 (Figure 5-3).

In Figure 5-5 the results are presented of a 3D FDTD transmission simulation of a ΓM PhC designed as in Figure 5-4. The thickness of the GaN layer is 650 nm, the lattice constant is 557 nm, the r/a value is 0.3 and the number of rows is 11 and 22. The transmission graph shows that at the dielectric band a sharp edge is visible around a/λ is 0.3. This edge is slightly shifted to higher frequencies compared to the edge for the 2D infinite GaN on sapphire PhC (Figure 5-3). The air band edge is expected at $a/\lambda = 0.38$. However no edge is visible and the transmission is gradually increasing. This gradual increase can be explained by the location of the lightline for sapphire. In Figure 5-6 a schematic banddiagram is shown for the ΓM direction. The complete air band of the designed PhC lies above the lightline for sapphire and can therefore leak to the substrate. In Figure 5-5 lines are drawn, showing the frequency on the lightline for air and sapphire at the M-point. Note that this frequency for the lightline for sapphire lies exactly at the spot where the transmission in the gap for the 22 row PhC starts increasing again.

For the 11 row PhC there is still minimal transmission in the PBG. The dielectric band transmission is lower for the 22 row PhC than for the 11 row PhC while the maximum at the air band is almost equal. The difference in transmission at the dielectric band may be caused by losses in the horizontal plane of the PhC. Light entering the PhC from the entrance waveguides is diffracted in the horizontal plane. Part of that light will not be collected in the exit waveguide and will get lost. These losses will be higher for lower frequencies (at the dielectric band) and for longer PhCs. The 22 row PhC is almost twice as long as the 11 row PhC.

Although the suppression of the transmission in the PBG is more than a factor 10 better for the 22 row PhC it is chosen to design the GaN PhC with 11 rows. The simulations do not account for extrinsic losses in experiments which are caused by for instance imperfect holes. These losses can increase for larger PhCs. In the coming sections the transmission diagram of the 11 row PhC will be treated in more depth.

Note that only PhCs for the ΓM direction will be simulated. In this direction no mixing takes place of transmission from ΓK and ΓM directions at the ΓM air band edge, as found by Van der Heijden [VanderHeijden2006].

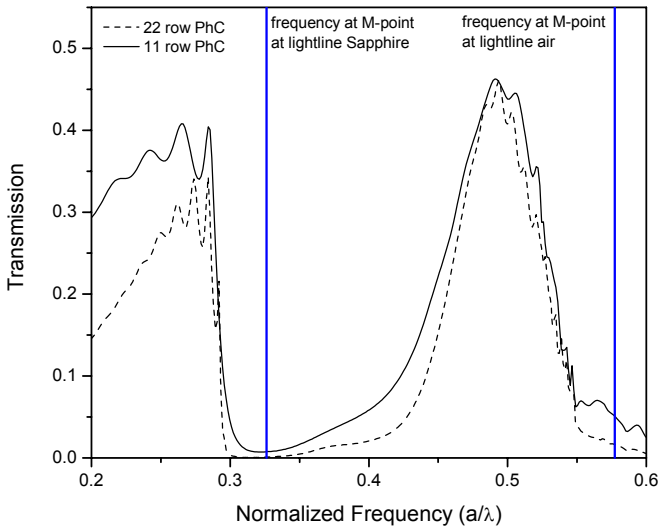

Figure 5-5: results of a 3D FDTD transmission simulation of a GaN on sapphire PhC for an 11 row PhC (continuous line) and a 22 row PhC (dashed line). The thickness of the GaN layer is 650 nm, the lattice constant is 557 nm and the r/a value is 0.3. See Appendix II for simulation parameters.

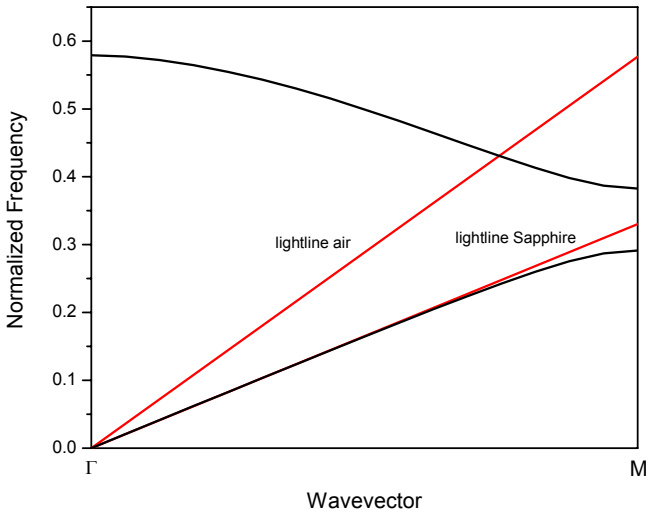

Figure 5-6: schematic representation of the dielectric band and air band of a 2D PhC. The index used in this calculation is the effective index of the fundamental mode of the GaN-sapphire waveguide. The air band lies completely above the lightline for sapphire.

Gallium Nitride Membrane, Semi-membrane and Deep Etched PhC

The transmission diagrams of the 11 and 22 row PhC show a gradual increase in transmission in the air band (Figure 5-5) instead of a sharp onset. It is already explained that light in the air band can leak to the sapphire substrate. In this section the simulated transmission diagrams of a PhC with the holes etched infinitely deep and of a PhC membrane are discussed.

The simulation results are shown in Figure 5-7. For the membrane as well as for the deep hole PhC a clear PBG with a sharp onset at the air band edge $(a/\lambda \sim 0.39)$ is visible. For the membrane the dielectric band and air band modes are guided, a sharp bandgap is therefore visible. In the deep etched PhC the light is also better confined in the guiding layer. This is because the holes are etched through sapphire.

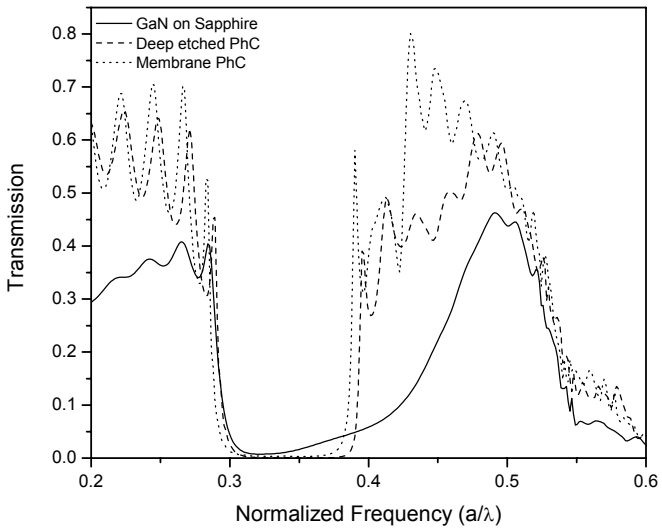

Figure 5-7: relative transmission diagrams for a GaN membrane (dotted line), GaN on sapphire (continuous line) and deep etched GaN-sapphire PhC (dashed line). See Appendix II for simulation parameters.

Single mode and Multimode Waveguides

Up to now a waveguide with a GaN core layer of 650 nm thick on top of a sapphire cladding layer is used in the simulations. The waveguide is in that case single mode in the vertical direction. In reality it is difficult to grow thin GaN layers. The thickness of such layers cannot be controlled precisely. It is therefore investigated how the transmission will change when the thickness of the GaN layer is 450 nm or 850 nm instead of 650 nm.

The result of the transmission simulation for a 450 nm thick GaN layer is plotted in Figure 5-8. The transmission in the air band is lower and in the gap higher than with the 650 nm thick layer. The mode profiles for the 450 nm and 650 nm thick GaN laser are shown in Figure 5-9. The decay length of a mode in the cladding increases with decreasing layer thickness. The evanescent wave of a thinner membrane will therefore penetrate deeper into the claddings. For the dielectric edge this implies the shift to higher frequencies which is observed in the simulation results. The lower effective index for the 450 nm thick layer will also lead to extra losses compared to the 650 nm thick layer.

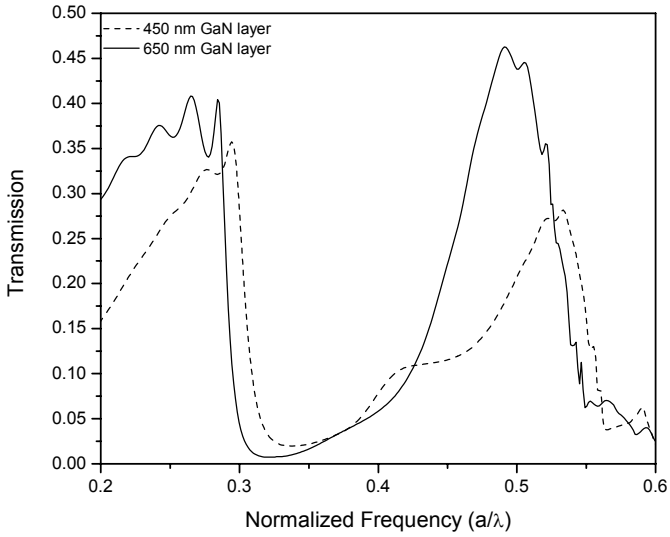

Figure 5-8: the transmission diagram for a GaN on sapphire PhC for a 450 nm (dashed line) and 650 nm (continuous line) thick GaN layer. The thickness of the GaN layer is varied, the lattice constant is 557 nm. In both cases the waveguides are single mode. See Appendix II for simulation parameters.

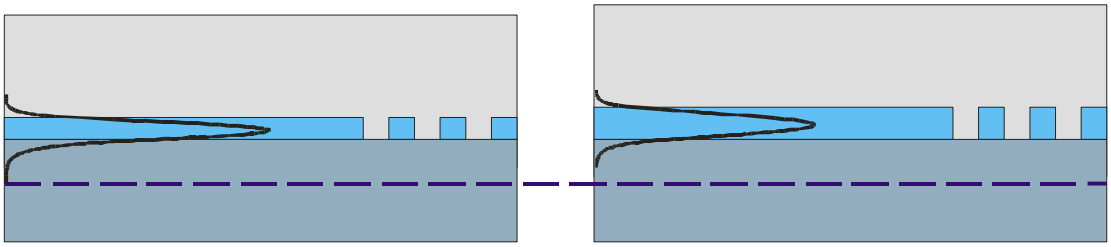

Figure 5-9: vertical intensity profiles of the fundamental mode of a waveguide with an 450 nm thick GaN layer (left) and a 650 nm thick GaN layer (right).

A waveguide with a GaN layer of 850 nm thick is multimode with two modes in the vertical direction (Figure 5-10), the fundamental mode TE0 and TE1. The intensity maxima of mode TE1 are located closer to the core-cladding boundaries while the intensity maximum of the TE0 mode is more confined to the center of the core layer. Crystal Wave simulations are done to show how radical the transmission diagrams changes when all the light is propagating in the TE1[2] mode instead of the TE0 mode. The results are presented in Figure 5-11.

[2] The mode profile of TE1 is calculated with Fimm Wave and imported into Crystal Wave. Fimm Wave is a program developed by Photon Design and is used to calculate mode profiles for waveguides. We thank Luc Augustin from the Opto-Electric Devices group for the use of Fimm Wave.

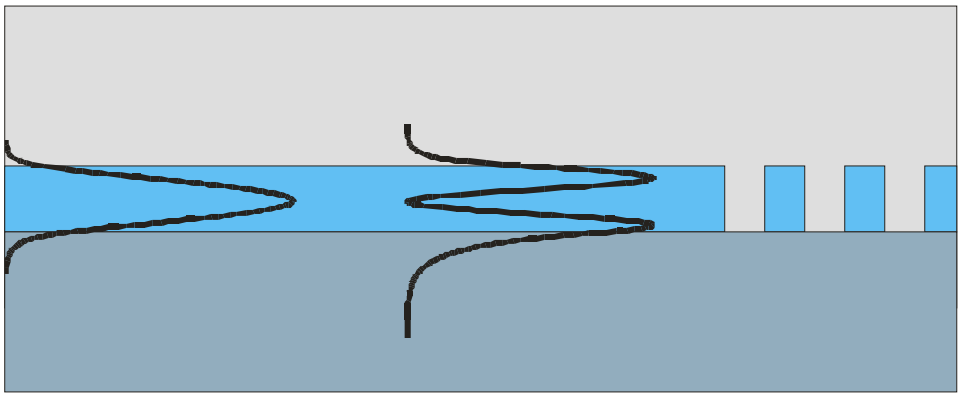

Figure 5-10: intensity mode profile of the vertical modes TE0 and TE1 in a waveguide with an 850 nm thick GaN layer.

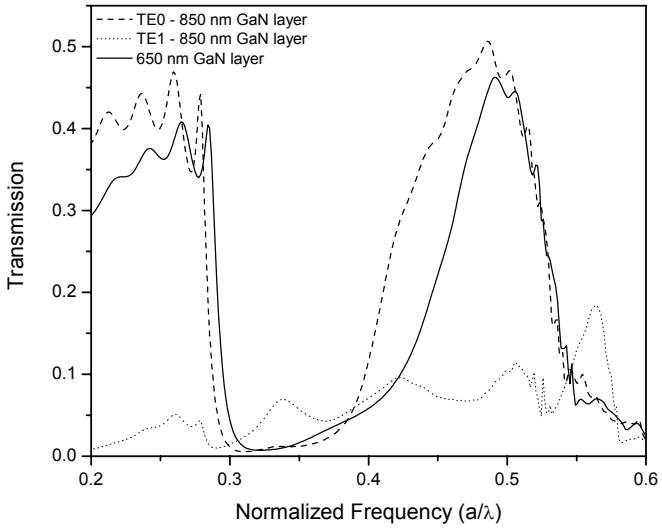

Figure 5-11: transmission diagrams of a GaN on sapphire PhC for a GaN layer of 650 nm thick (continuous line) and 850 nm thick (TE0: dashed line) (TE1: dotted line). The waveguide is multimode for the 850 nm thick layer. The lattice constant is 557 nm. Simulation parameters are shown in Appendix II.

Comparison of the transmission diagrams of the fundamental modes of the 650 nm and 850 nm thick GaN layer shows that with the 850 nm thick layer the transmission will be higher and that the gap has shifted to lower frequencies. This difference in transmission diagram can be explained by looking at the mode profiles. The evanescent wave of the fundamental mode of the 650 nm thick layer is penetrating deeper into the claddings than for the 850 nm thick layer. The effective index of the 850 nm thick layer is higher and the banddiagram is shifted to lower frequencies. As a result the losses will also decrease.

The simulation result clearly shows that almost no light is penetrating through the PhC if it propagates in the TE1 mode. The bandgap is disappeared. In Figure 5-12 the banddiagram of a 2D PhC is shown, calculated with a refractive index of 1.89. This is the effective index of the TE1 mode [Hammer2006]. The dielectric band lays above the lightline for sapphire. No PhC mode is confined in the core layer and almost all the light will couple out to the substrate. This explains the low transmission through the PhC. This situation must be averted [Johnson1999]. Note that not all the light in a

multi-mode waveguide will propagate in higher order modes. The profile of the laser beam that will couple to the entrance waveguide is Gaussian shaped. Due to reasons of symmetry the light will rather couple to the fundamental mode than to TE1. During propagation in the waveguide it is possible that light will be converted into the TE1 mode. Because not all the light will propagate in a higher order mode it is still expected to see a dielectric band and air band for a waveguide with an 850 nm thick GaN layer.

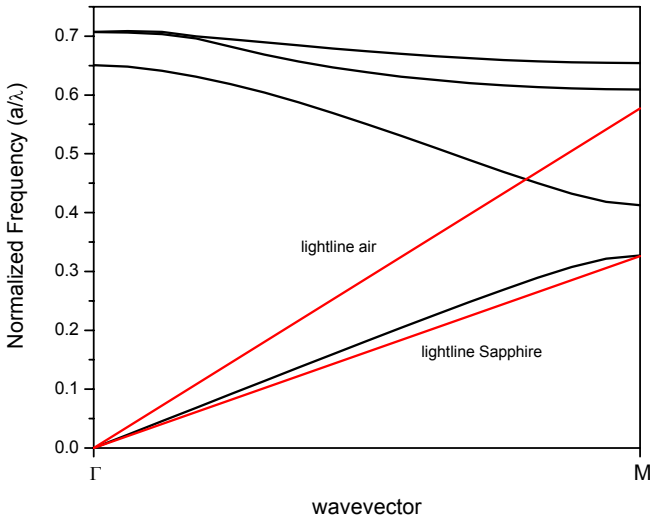

Figure 5-12: banddiagram calculated for a 2D PhC. The effective index used for the calculation is the index of the TE1 mode (n=1.89).

With the simulation results of the 450 nm, 650 nm and 850 nm thick GaN layer the ideal layer thickness can be deduced [Johnson1999]. Simulations showed that for the thinner GaN layer the transmission in the dielectric band and air band is lowered and the transmission in the gap is increased. For a thicker layer the opposite is true. With increasing thickness of the layer the waveguide eventually becomes multimode. Light propagating in a higher order mode through the PhC will get lost. The ideal layer thickness is a thick GaN layer that is still single mode. This thickness is the 650 nm which is used in the simulations.

Lithographic Tuning

So far continuous transmission diagrams were simulated by varying λ and keeping a fixed. This does not represent the experimental situation, since there both λ and a are varied. Since the effective index strongly varies with a, λ and slab thickness d it is necessary to take into account a and λ explicitly instead of only their ratio. In this section the results of transmission simulations for lithographically tuned PhCs are shown.

The transmission through PhCs is measured with an end-fire set-up. The wavelength of the IR laser used in the set-up can be tuned between $\lambda = 1470$ nm and $\lambda = 1570$ nm. For a PhC with $a = 557$ nm only the transmission between $a/\lambda = 0.355$ and

$a/\lambda = 0.379$ can be measured. A method called lithographic tuning is therefore used to measure the complete transmission diagram. The transmission of several PhCs with each a different lattice constant is measured. For each structure a different region of the normalized frequency is measured from which the complete transmission diagram is build up. For 2D PhCs with deeply etched holes and a low index contrast between core and cladding layers the transmission diagram will barely change for different lattice constants and lithographic tuning can be used for measurements [VanderHeijden2006]. With the designed GaN on sapphire PhCs the transmission diagram will however change for different lattice constants. This is shown in Figure 5-13 where two transmission diagrams are plotted, one with $a = 406$ nm and one with $a = 764$ nm.

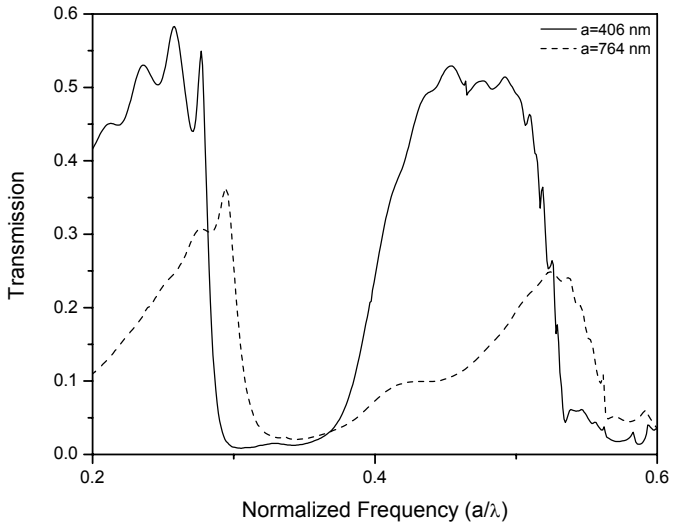

Figure 5-13: simulated transmission diagrams for a lattice constant of 406 nm and of 764 nm. Note that for higher lattice constants the band edges are shifted to the right. Simulation parameters are shown in Appendix II.

The difference in the transmission diagram is explained with the differences in effective index of the modes. Imagine two PhCs, one with lattice constant a and one with $2a$. For a fixed normalized frequency of $a/\lambda = c$ the mode propagating through the structure will have a wavelength of respectively λ or 2λ. For waveguides with large index contrast the effective index will change rapidly for changing wavelengths. Transmission diagrams for the designed GaN on sapphire PhCs are therefore lattice constant dependent. For increasing lattice constants the dielectric band edge will shift to higher frequencies as the effective index decreases for increasing wavelength.

The effect that the transmission diagrams are dependent on lattice constants must be taken into account to find the transmission diagram that would correspond to the lithographic tuning measurements. In Figure 5-14 the transmission diagrams for GaN on sapphire PhCs each with a different a are plotted. It clearly shows that with increasing a the dielectric band edge shifts to higher frequencies just like the air band maximum. The transmission in the air band is lowered with increasing a due to out of plane losses.

For increasing lattice constant the transmission in the dielectric band is successfully higher, lower and again higher than in the air band. This might be due to two distinctive types of losses. The wavelength increases with increasing lattice constant when looking at a fixed normalized frequency $a/\lambda = c$. Losses due to diffraction occurring at the boundary between the waveguide and the PhC in the horizontal plane are larger for increasing wavelengths. These losses will be higher at the dielectric band than at the air band and higher for larger lattice constants. Furthermore with increasing hole size due to increasing lattice constant the out of plane losses will rise. This affects especially the transmission at the air band. These two types of losses might explain the behavior pictured in Figure 5-14.

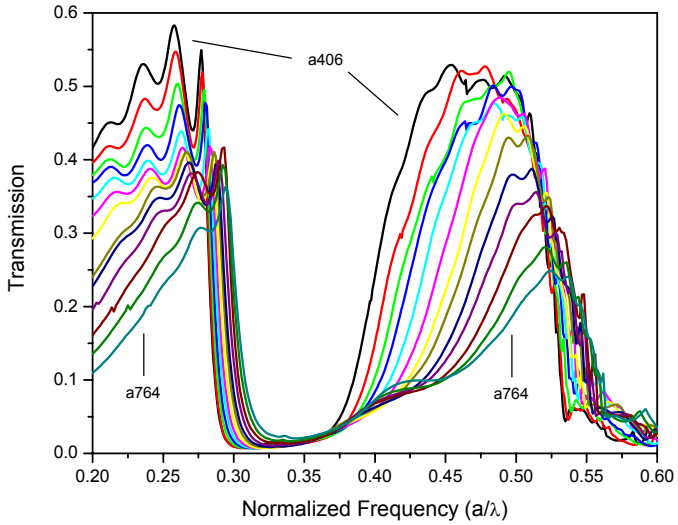

Figure 5-14: transmission diagrams for PhCs with different lattice constants. The r/a value is fixed at 0.3. Note the right shift of the dielectric band edge with increasing lattice constants. From top to bottom on the dielectric band: a406, a428, a451, a475, a501, a528, a557, a587, a619, a652, a687, a724, a764. Simulation parameters are shown in Appendix II.

The lattice constants used in the simulations can be used for lithographic tuning experiments. Table 5-1 shows the lattice constant and the normalized frequency range. For the calculation of the lithographic tuning parameters the tuning range of the laser was taken between 1480 nm and 1560 nm instead of 1470 nm to 1570 nm. In this way overlap in normalized frequency is created between PhCs with its adjacent neighbors.

The transmission diagram that would be measured with lithographic tuning measurements is found by plotting only that range of normalized frequencies that would be measured for each PhC within the tunable range of the laser. The result is plotted in Figure 5-15. A steep dielectric band edge is visible. No air band edge is visible due to substrate losses. Note that between successive PhCs there can be a jump in transmission due to the change in transmission for PhCs with different a.

Table 5-1: Lithographic tuning parameters for the GaN on sapphire PhC.

Lattice constant	Normalized frequency range	
	$a/1570$	$a/1470$
406	0.259	0.276
428	0.273	0.291
451	0.287	0.307
475	0.303	0.323
501	0.319	0.341
528	0.336	0.359
557	0.355	0.379
587	0.374	0.399
619	0.394	0.421
652	0.415	0.444
687	0.438	0.467
724	0.461	0.493
764	0.487	0.520

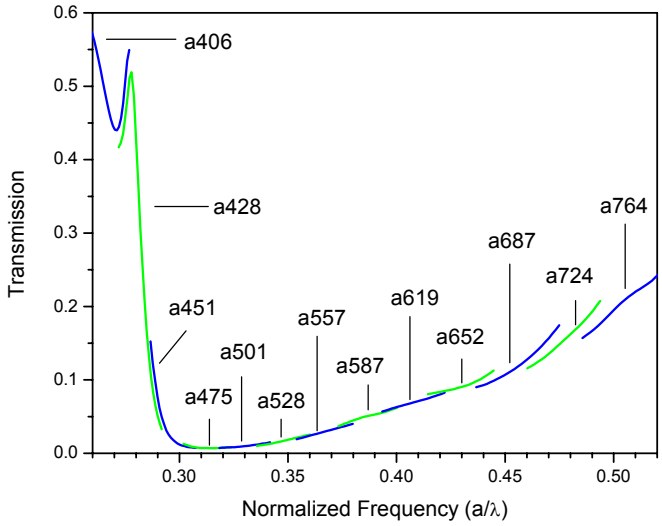

Figure 5-15: transmission diagram corrected for lithographic tuning of the PhCs. See Appendix II for simulation parameters.

Simulations show that it is possible to create a PhC in GaN with a bandgap around 1.55 μm that has a compact mode which is mostly localized in the core layer. The optimum thickness of the GaN layer is the highest that is single mode in our wavelength region, which corresponds to ~650 nm. For lithographic tuning measurements the different lattice constants strongly affect the transmission diagram. This effect must be taken into account for the simulations.

5.2 *Sample Design and Fabrication*

The sample is fabricated at the University of Technology Delft (TU Delft) by Bifeng Rong. Below a basic description of the sample design and fabrication is given. Only the final results as relevant to this report are given.

Gallium Nitride Wafer

GaN wafers are obtained commercially from the USA based company *Technologies and Devices International Inc*. The GaN layer is grown on top of a 60 nm thick AlN buffer layer and a sapphire substrate. Growing thin layers of GaN is difficult. The company can control the growth of thin layers within 200 nm. The thickness of the GaN layers lies therefore between the 450 nm and 850 nm (650±200 nm).

Sample Design

Figure 5-16 shows the sample design. The waveguides are all 2.5 μm wide. On the left and right side of each waveguide a trench of 10 μm is etched down to the sapphire. There are 4 blocks of 4 structures and 1 block of 2 structures. Each block is separated 200 μm and each structure within one block is separated 100 μm from another. On one sample there are 13 PhCs with entrance and exit waveguides and 5 waveguides.

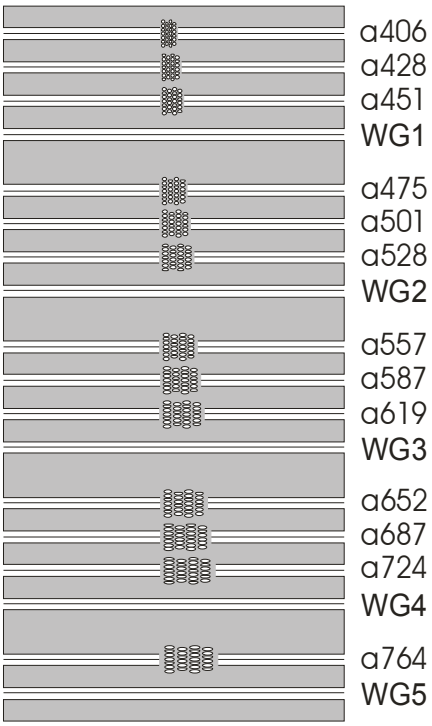

Figure 5-16: sample design. On the right the lattice constant for the PhC is given. WG stands for waveguide.

Fabrication

The sample is fabricated at the TU Delft; one processing step is done at the TU/e.

The first fabrication step is the deposition of a SiN_x mask layer on top of the GaN wafers by plasma enhanced chemical vapor deposition. This is done at the TU/e. On top of the SiN_x mask layer an e-beam resist is spun. The PhC and waveguide pattern is written by e-beam lithography into the resist. After development of the resist the mask pattern is transferred into the SiN_x mask layer by reactive ion etching. The final fabrication step is the transfer of the waveguide and PhC pattern into the GaN layer.

This is done by inductive coupled plasma (ICP) etching. There is still a layer of SiN mask left after the ICP etch step (Figure 5-17).

Before the sample is ready for measurements facets must be cleaved on both sides of the sample. To couple light (efficiently) into a waveguide the facets must be vertical and smooth. GaN and sapphire are however not easy materials to cleave. The preferred cleavage plane is not the c-plane but the r-plane as already shown in Chapter 3. The cleaving of GaN is done at TU Delft using a proprietary process (B. Rong). Tests indicated that the cleaved facets will be smooth and straight enough to couple light into the structure as is shown in Figure 5-17.

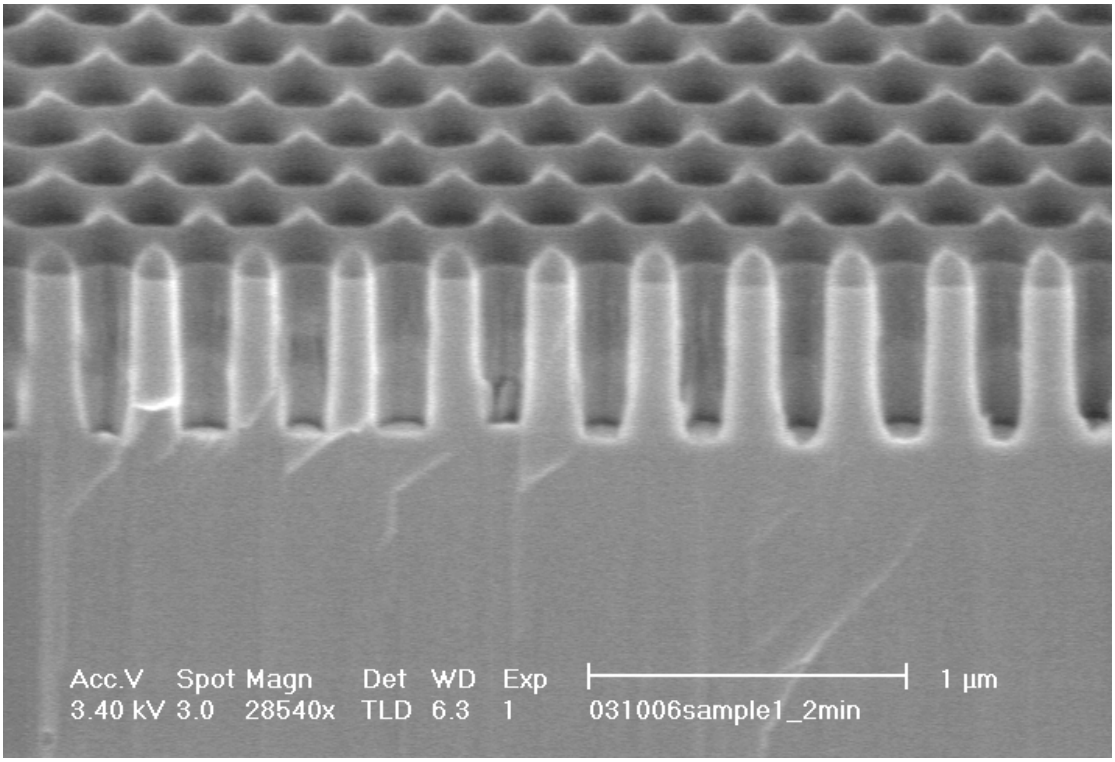

Figure 5-17: tests indicate that the facets will be smooth enough to couple light into the waveguides. On top of the GaN layer a layer of the SiN mask is visible [Bifeng Rong – TU Delft].

5.3 *Measurement Set-up*

Transmission measurements are done with a so called end-fire setup. The schematic view of the set-up is shown in Figure 5-18.

The set-up exists of two lasers. One tunable laser from Tunics with a wavelength range form 1470 nm to 1570 nm and one Helium-Neon alignment laser from Thorlabs with a wavelength of 635 nm. The lasers cannot be used simultaneously. The light from the lasers is transported through a polarization maintaining fiber to the optical set-up. After the fibers the beam passes a positive lens to create a parallel beam and is then transmitted through a Glan Thompson polarizing prism. After passing a chopper the beam is focused through the first objective on the waveguide facet of the sample.

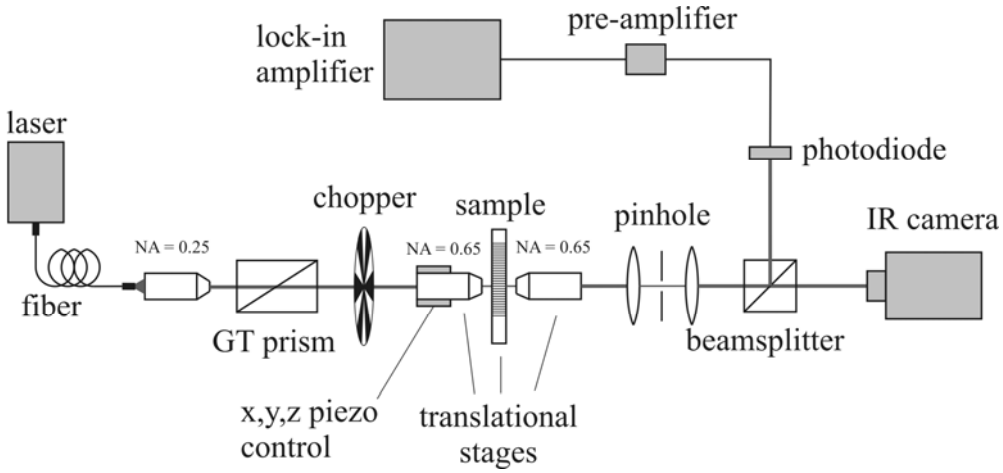

Figure 5-18: schematic view of the measurement set-up [VanderHeijden2006].

After leaving the exit waveguide the beam passes through a second objective which creates a parallel beam. The objectives can be moved by translation stages in the x-, y- and z-directions. For fine tuning piëzo-actuators can be used. The focal point of the objectives is wavelength specific and they have a working distance of 0.4 mm. The sample is lying on a sample holder which can be moved in two directions and be rotated around its center axes. Three sample holders with each a different thickness is available. The setscrews which are used to manually move the objectives have an accuracy of 0.5 µm, those of the sample holder is 5 µm. Above the sample an optical microscope is placed for visual inspection of the sample.

After the second objective, the parallel beam passes a lens-pinhole system acting as spatial filter to remove stray light and a 50/50 beam splitter. The intensity of one arm is projected on a screen through an infrared camera. The intensity of the other arm is received by a photo diode after which the signal travels through a pre-amplifier to the lock-in amplifier. Measurements are controlled by a Lab View based program.

5.4 *Alignment Procedure*

Before the sample is placed on the sample holder the set-up itself must be aligned. Below the alignment procedure is described shortly, since this is critical for the GaN samples with imperfect facets.

The spatial filter and the objectives are removed. The tunable laser is put on and it is checked if the beam hits the photodiode and the IR camera. The place where the beam spot is visible on the screen is marked. The lenses of the pinhole system are placed back in the set-up. When the lenses are placed inside the beam the laser spot must be visible on the same place as without lenses. If not the location of the lenses must be adjusted. The pinhole is placed in the focal point of the lenses. The two objectives are placed on the translation stages. After alignment of the objectives the sample is placed on the sample holder. By viewing through the optical microscope it is made sure that the waveguides are aligned parallel to the laser beam. This is checked by using the alignment laser.

Finding the GaN layer with the tunable laser can be very time consuming. The transparency of GaN for the visible wavelengths comes in handy. The alignment laser is used to find the core layer. It is possible by viewing through the optical microscope

to align a waveguide with the laser beam. First a waveguide is placed near the spot of the laser beam by moving the translation stage of the sample holder. For fine tuning of the alignment the first objective is moved. If the sample is aligned properly a thin red line is visible through the optical microscope: the beam is guided by the waveguides.

The second step is the alignment of the second objective. The beam is guided through the waveguide and is focused by the second objective at a certain point. By placing a paper after the second objective in the beam a large red blurry spot is visible. Inside the large blurry spot there is a small but clear red dot visible: the beam that was guided by the waveguides. By moving the translation stages of the second objective the bright dot can be focused at the camera and the photo diode. Note that focusing at the camera is the same as creating a parallel beam: the bright dot is placed at "infinity".

The alignment laser is replaced by the infrared laser. The two objectives are placed in focus for $\lambda = 1495$ nm or $\lambda = 1525$ nm and the structure is ready to measure. The 100 nm tuning range of the laser can not be exploited in one sweep as the focal point of the two objectives is wavelength specific [VanDerHeijden2006]. The wavelength region over where a measurement is performed is therefore 50 nm instead of 100 nm. For each structure the alignment is therefore done twice, once at 1495 nm (1470 nm - 1520 nm) and once at 1545 nm (1520 nm-1570 nm).

5.5 *Sample Characterization*

Two GaN on sapphire PhC samples are measured. In this paragraph scanning electron microscopy (SEM) images and optical microscope (OM) images of the first sample (S1) are presented. From the evaluation of the SEM images typical properties of S1 can be deduced. For S2 only the hole radius and lattice constants are measured. The end-fire measurement results of S1 and S2 are presented in paragraph 5.6.

5.5.1 Sample 1

Sample Edges and Facets

On both sample edges the waveguides are not standing perpendicular to the sample edge as illustrated by the SEM image in Figure 5-19. The sample edge is also curved on one side. A combination of both properties leads to problems with the sample alignment. This is sketched in Figure 5-20. Due to the non straight sample edges and the waveguides not standing perpendicular to it, it is barely possible to place the objectives at the focal point.

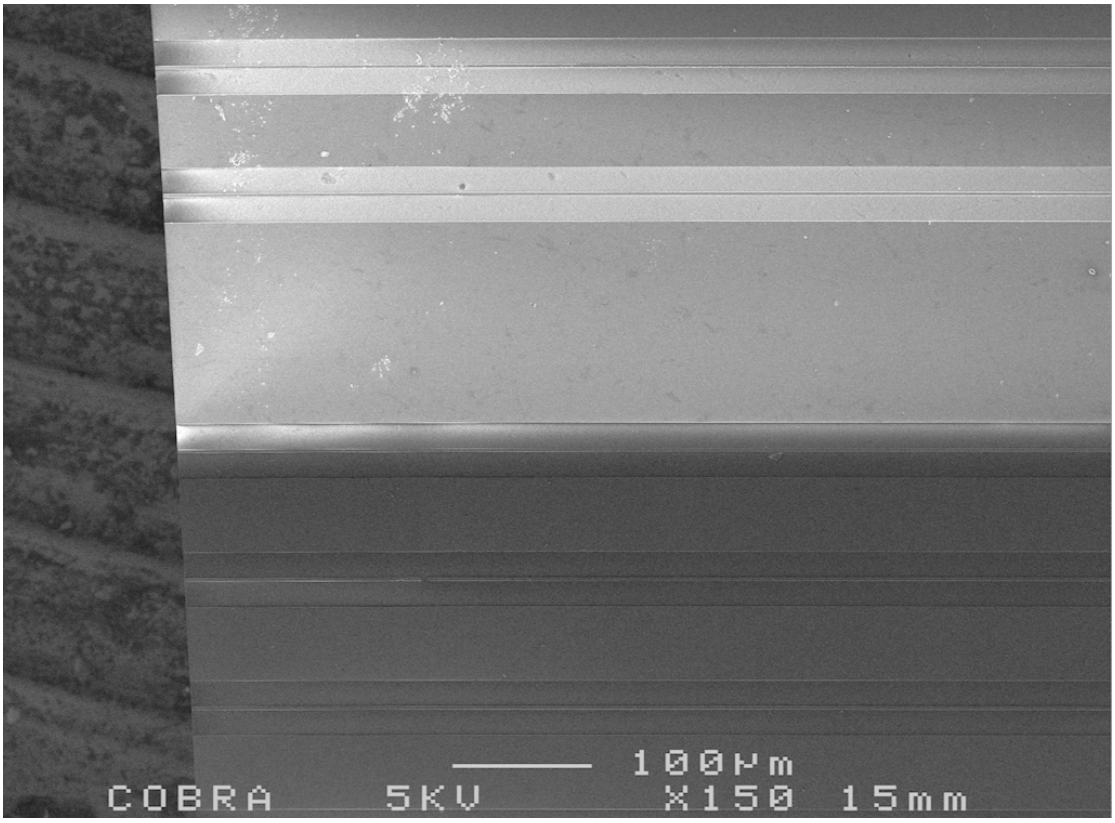

Figure 5-19: the picture clearly shows that the sample edge is not standing perpendicular to the waveguides.

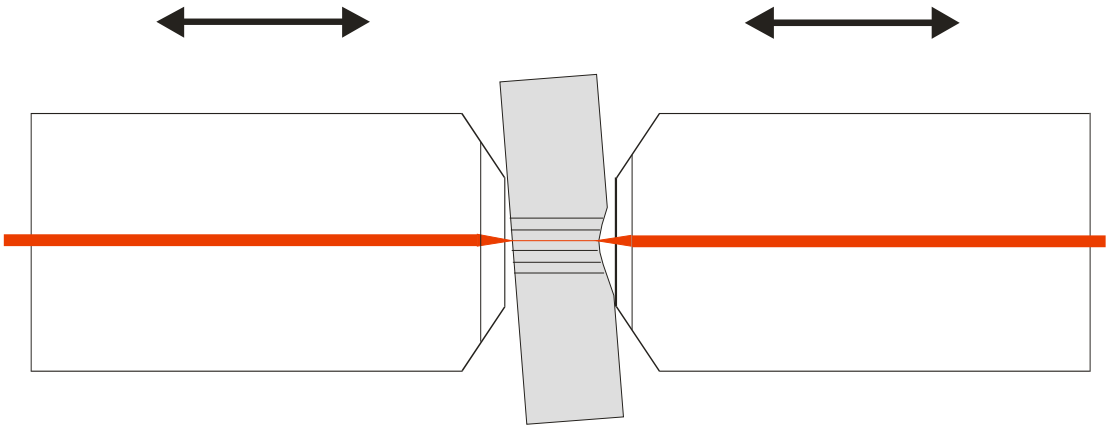

Figure 5-20: for alignment the waveguides must be perpendicular to the objective. Due to the non straight edges one objective is too close to one edge of the sample. Therefore, it is barely possible to place the right objective in the focal point for each measurement. The figure gives an idea of how the sample was placed between the objectives.

The waveguide facets must be as vertical and as smooth as possible for light in coupling. Figure 5-21 shows a typical waveguide facet. Several SEM images indicate that the facets are vertical and smooth enough to couple light into the waveguides.

Layer Structure

There are several layers visible at the SEM image of Figure 5-21. From bottom to top: sapphire, AlN buffer layer (dark layer), GaN and SiN mask layer. The thickness of the layers is measured with the help of SEM images. The results are presented in Table 5-2. Although the thickness of the GaN layer is within the ordered specifications the layer is much thicker than the designed 650 nm. The waveguides will therefore be multi-mode.

Table 5-2: measured layer structure of S1[3].

Measurement	
Layer	Thickness (nm)
Air	
SiN	100
GaN	830
AlN	120
Sapphire	

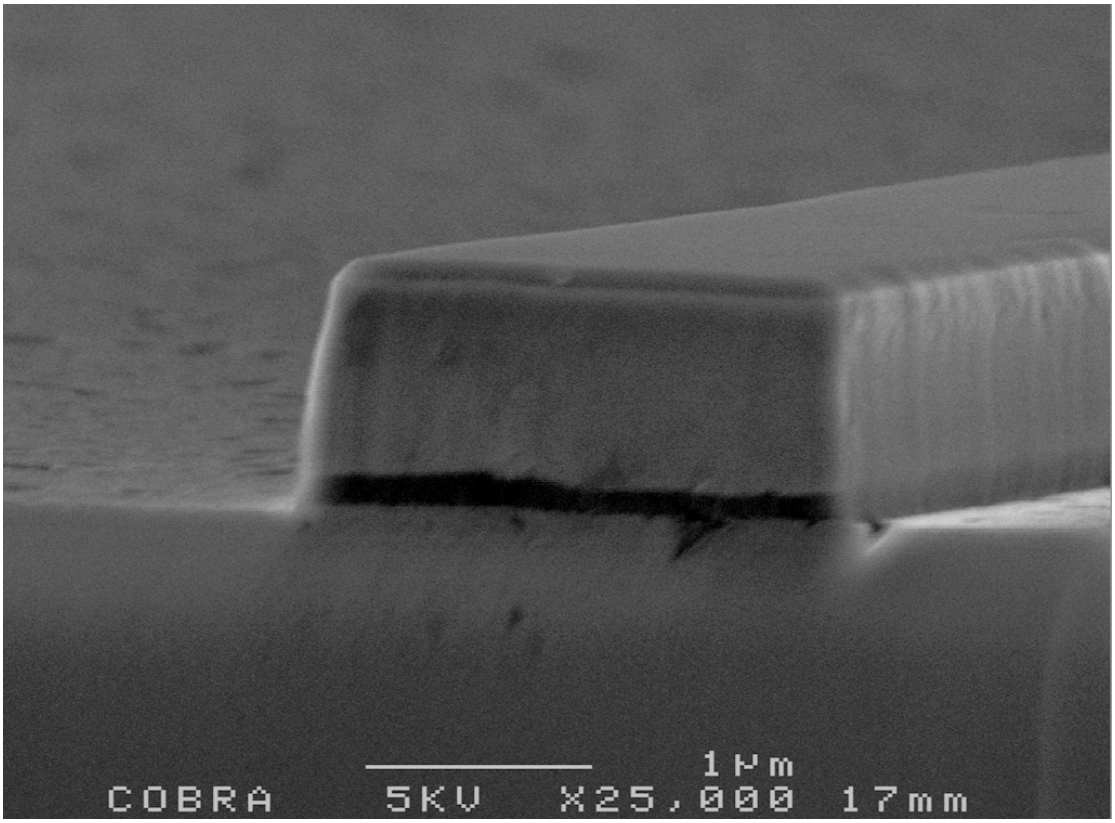

Figure 5-21: the figure shows the facet of the entrance waveguide of structure a406 (if the sample is placed between the objective as shown in Figure 5-20). The darker layer on top of the sapphire substrate is the 120 nm thick AlN buffer layer. On top of the 830 nm thick GaN layer a 100 nm thick layer of SiN mask is left.

[3] Data collected by Bifeng Rong.

Waveguides

Five waveguides of sample 1 could not be used since they were broken: a451, a528, a724, WG5 and a764. Furthermore, the sidewalls of all the waveguides are damaged on several places as shown in Figure 5-22. The damage was already present in the SiN etching mask before the final etch step. Since etching these waveguides is routine procedure for other materials, the damaged areas are attributed to adhesion problems of the SiN mask with the GaN layer.

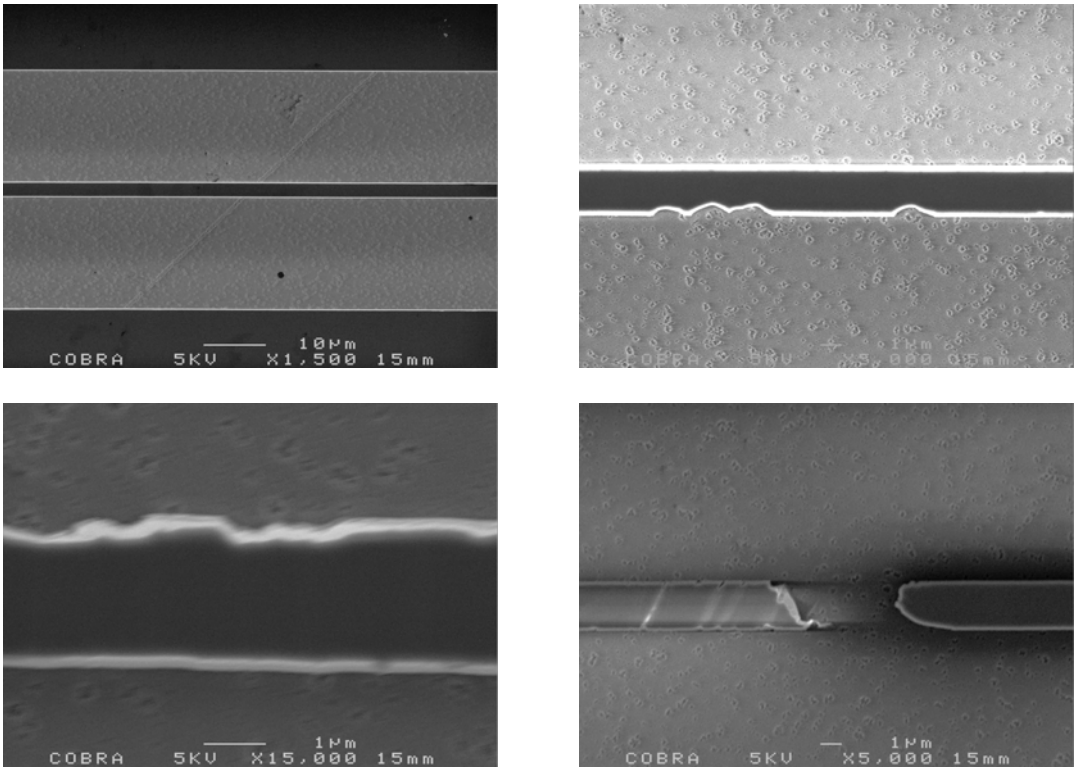

Figure 5-22: the SEM-pictures show the typical waveguide quality. Large parts of the waveguides are of good quality as is shown in the upper left corner. All the structures have however imperfections as is shown in the upper right and lower left corners. In total five waveguides are interrupted. A broken waveguide is shown in the lower right corner. Upper left: a475, upper right: a475, lower left: a406, lower right: a451.

The sidewalls of the waveguides are not straight as can be seen in Figure 5-23. The figure shows that there is an undercut on one side of the waveguide and a sloped sidewall on the other side. It is not known if this is the tendency for all the waveguides.

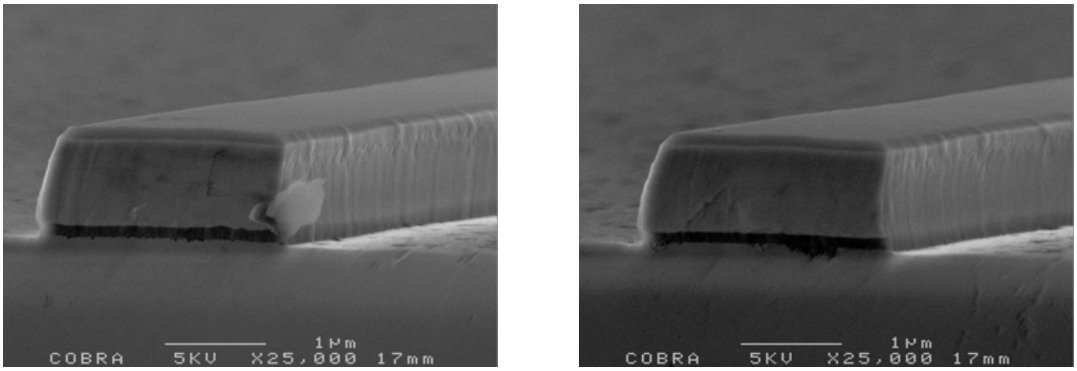

Figure 5-23: X-SEM pictures of the facets of a428 (left) and a451 (right). One sidewall of the waveguides clearly shows an undercut while the other sidewall is sloped.

Photonic Crystals

The majority of the PhC fields are flawless looking from above. However, some PhC fields are damaged. Figure 5-24 shows the SEM images of several fields. In Table 5-3 the actual radius and lattice constants for al the PhCs are shown, acquired by the evaluation of SEM images. There is no data available about the quality of the holes itself. The holes might be not completely etched up to the sapphire and they may also be not completely straight.

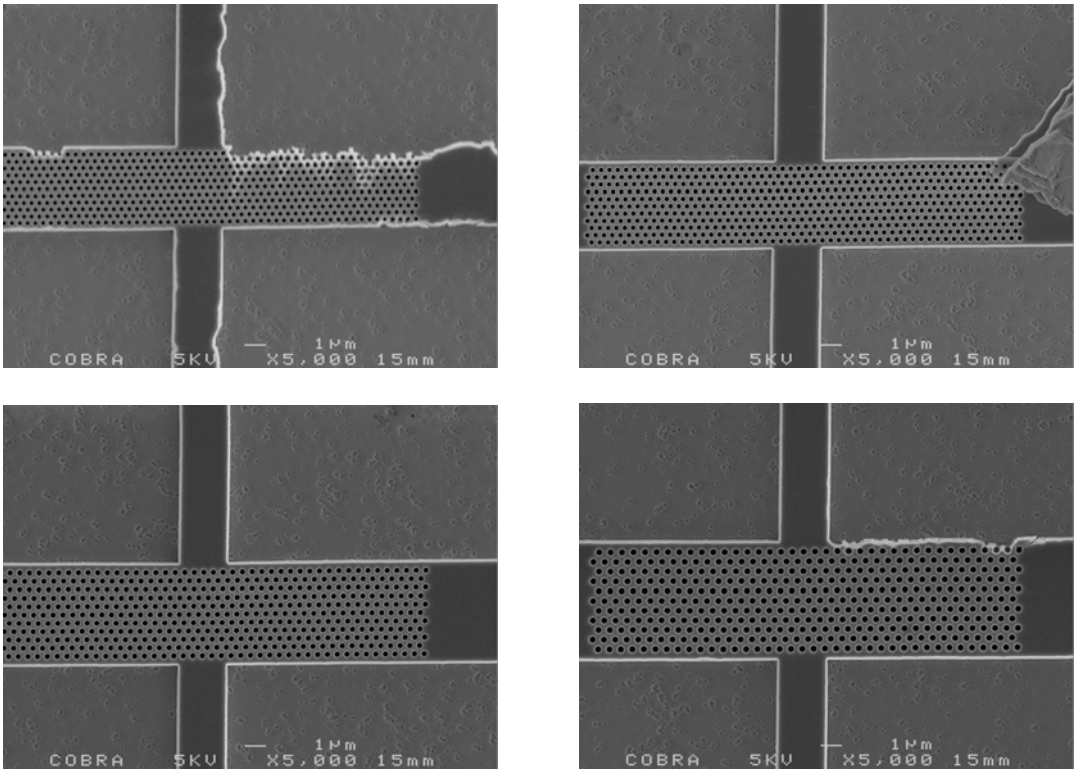

Figure 5-24: top view of PhC fields. Upper left: a406, upper right: a428, lower left: a501, lower right: a587.

Table 5-3: *r*- and *a*-values of the simulated and measured PhCs (S1). The actual r/a values are about 79 % to 87 % of the designed value[4].

Simulation			SEM Measurement		
a	r	r/a	a	r	r/a
406	122	0.3	403	105	0.26
428	128	0.3	423	108	0.25
451	135	0.3	452	113	0.25
475	143	0.3	459	117	0.25
501	150	0.3	495	123	0.25
528	158	0.3	528	129	0.24
557	167	0.3	554	132	0.24
587	176	0.3	583	142	0.24
619	186	0.3	607	149	0.24
652	196	0.3	643	163	0.25
687	206	0.3	677	169	0.25
724	217	0.3	713	176	0.25
764	229	0.3	768	193	0.25

Wafer Quality

In the upper left picture of Figure 5-22 a line is visible which is running from the upper right to the lower left corner of the sample. Little craters on top of or in the sapphire substrate are visible in the SEM image in the upper right corner. Although it is not expected that these irregularities will have a large influence on the optical measurements they will be shortly discussed.

In Figure 5-25 a close-up is shown of the irregularities. The SEM images in Figure 5-23 showed that the waveguides are etched down to the sapphire layer. No piles on top of the Sapphire wafer are visible. The slanting lines visible at the sample (Figure 5-22) also run through under the GaN layer as was observed on OM images. Putting everything together the idea is that the irregularities are little holes in the sapphire wafer. It might be that the irregularities are due to polishing of the sapphire wafer.

[4] Data collected by Bifeng Rong.

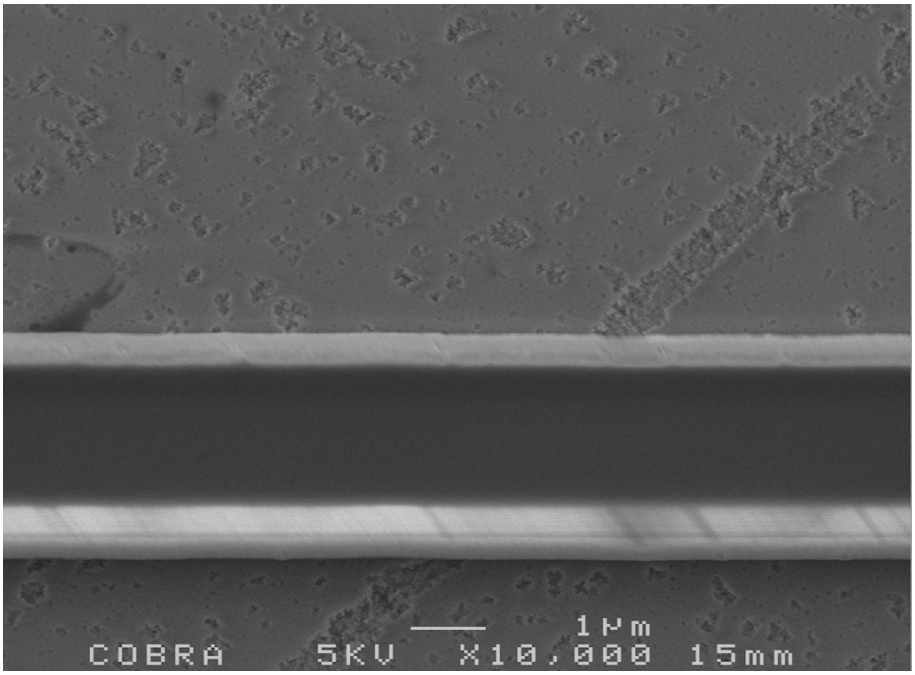

Figure 5-25: close up of irregularities at the surface of the sapphire. Structure: a475.

5.5.2 Sample 2

In Table 5-4 the actual radius and lattice constants for the PhCs of S2 are shown. These values are acquired from the evaluation of SEM images. The actual r/a values of S2 are higher than those of S1 and equal or higher than designed. There is no data available about the quality of the holes itself.

Table 5-4: *r*- and *a*-values of the simulated and measured PhCs (S2). The actual r/a values are about 100 % to 117 % of the designed value[5].

Simulation			SEM Measurement		
a	r	r/a	a	r	r/a
406	122	0.3	402	122	0.30
428	128	0.3	430	148	0.34
451	135	0.3	468	141	0.30
475	143	0.3	468	144	0.31
501	150	0.3	505	167	0.33
528	158	0.3	533	165	0.31
557	167	0.3	552	178	0.32
587	176	0.3	589	190	0.32
619	186	0.3	627	185	0.30
652	196	0.3	652	203	0.31
687	206	0.3	683	238	0.35
724	217	0.3	739	242	0.33
764	229	0.3	758	235	0.31

[5] Data collected by Bifeng Rong.

5.6 *End-fire Measurements*

The lithographic transmission diagram of two samples of GaN on sapphire PhCs is measured. The optical set-up described in paragraph 5.3 is used. The results are presented below.

The wavelength step size of the tunable laser was 0.1 nm for the transmission measurements of S1 and 1 nm for S2. The input power of the tunable laser was 2 mW. Structures with broken waveguides are not measured. The structures of S1 were measured twice on different occasions.

One transmission measurement at a structure of S1 is partly performed with a step size of 0.01 nm to check for Fabry Perot (FP) fringes resulting from reflections from the end facets. No indications were found of their presence. This could indicate lossy waveguides or may be caused by the facets not standing perpendicular to the waveguides. The presence of FP fringes is not investigated for S2.

On each sample five uninterrupted waveguides are etched. The transmission through these waveguides is measured. This data is indicative for the quality of the waveguides and is used to normalize the data of the transmission measurements through the PhCs.

Measurement Results Sample 1

The waveguide transmissions from the first measurement series of S1 are presented in Figure 5-26. On average the transmission through the waveguides is decreasing with increasing wavelength. Large oscillations are visible due to interferences within the structure. These are reproducible patterns and are not random noise.

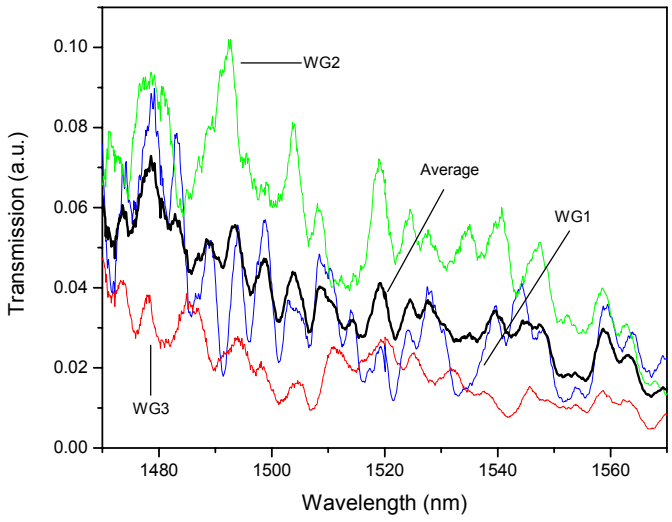

Figure 5-26: transmission through waveguides versus the wavelength. The thick transmission line is the average transmission. Note that only three waveguides are measured.

The results of the transmission measurements through the PhC structures are shown in Figure 5-27. The dielectric band edge is visible around $a/\lambda = 0.27$. A gradual increase in transmission is observed in the air band.

It should be noted that there is substantial variations within a waveguide for varying frequencies, and substantial variations between waveguides. Obviously this will limit the accuracy of the PhC characterization measurements. Gap induced variations in a PhC however, can typically be very large, orders of magnitude in some materials. Despite the variations, it is still reasonable to perform PhC characterization measurements.

The normalized transmission is the transmission through a PhC structure divided by the average transmission through the waveguides. In Figure 5-28 the normalized transmission is plotted versus the normalized frequency. The transmission in the gap is still substantial especially compared to the dielectric and air band. This is due to poor alignment of the sample. With the first measurement series it was chosen to not re-align the second objective with each measurement. With the slightest move in the wrong direction the sample would be touched and moved by the objective as explained in section 5.5. During the measurements it became clear that this choice could lead to non-optimal measurement data. A second series of measurements is therefore performed.

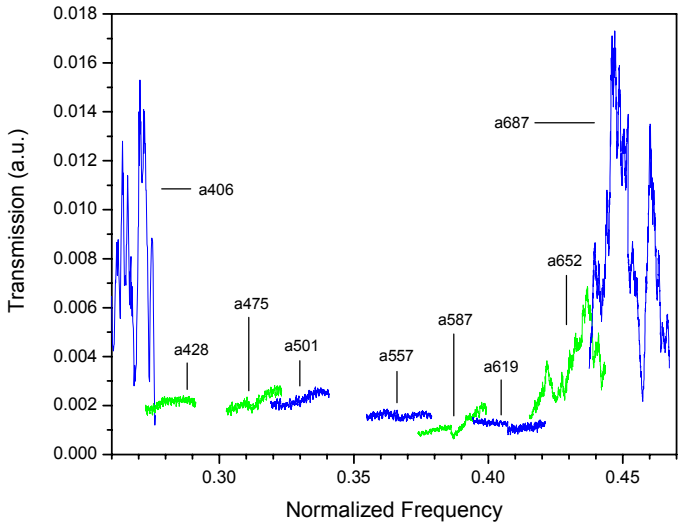

Figure 5-27: first measurement results of the measured transmission through PhCs.

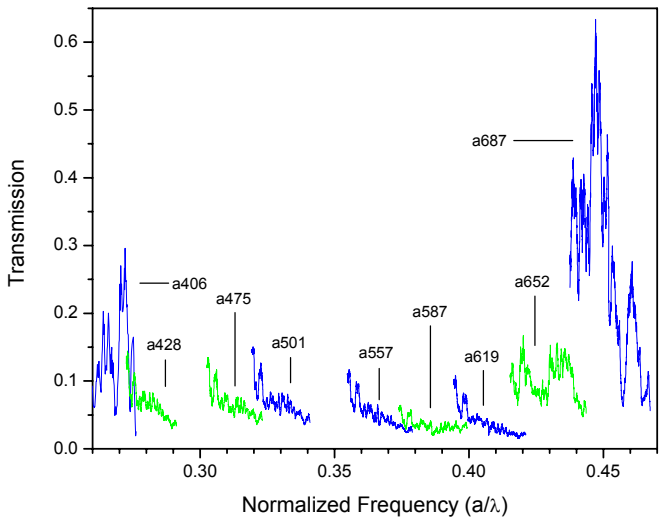

Figure 5-28: normalized transmission versus normalized frequency.

The following alignment procedure is used for the second measurement series. For structures in the PBG the red laser is used for verification of the alignment. A waveguide is placed in the red laser beam. This is checked by viewing through the optical microscope. The IR laser is turned on and the objectives are moved to the point of maximum transmission with the help of the setscrews and the piëzo-actuators. The alignment laser is turned on again and it is checked if the spot of the red laser is still on the waveguide facet. If not the procedure is repeated.

The transmission though the waveguides as measured during the second series is plotted in Figure 5-29 and the transmission through the PhCs in Figure 5-30. Notice that the transmission in the gap is lower in the second series compared to the first series. The absolute transmission through the waveguides and through the air band structures is higher than the first series.

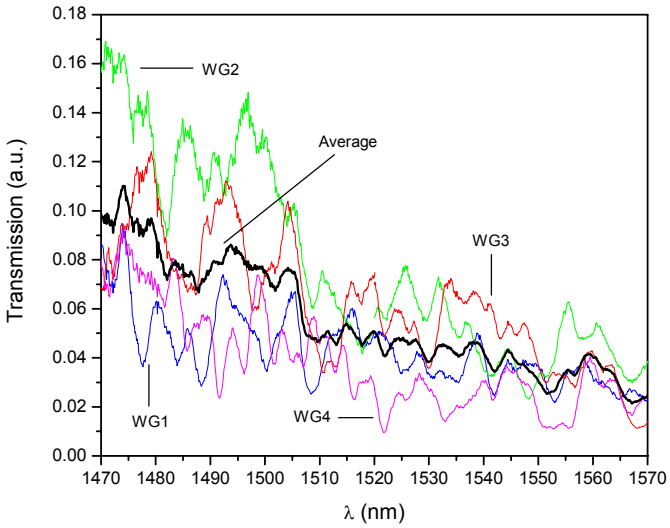

Figure 5-29: the transmission through the waveguides versus the wavelength. The thick line is the average transmission through the waveguides.

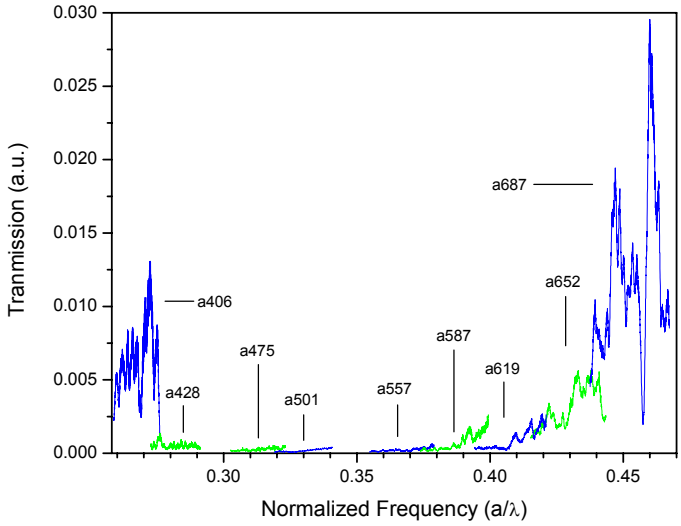

Figure 5-30: second measurement result of the measured transmission through PhCs.

The normalized transmission data is plotted in Figure 5-31. The overall transmission is slightly lower than measured in the first series. However, the transmission in dielectric and air band with respect to the average transmission in the gap is about an order of magnitude larger than in the first series.

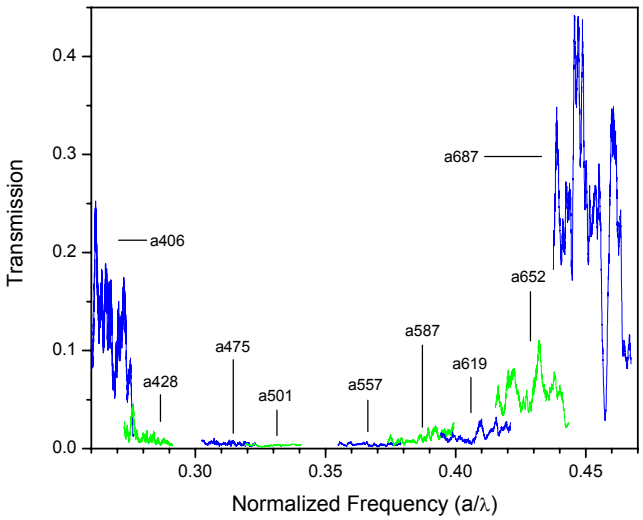

Figure 5-31: the normalized transmission versus the normalized frequency for the second measurement series.

In Figure 5-32 the results of the first and second measurements series are compared with the simulated transmission from Figure 5-15. The graph clearly shows that although there is a difference in transmission between the first and second series that the trend in both measurements is the same.

The dielectric band has a pretty sharp edge around $a/\lambda = 0.275$. This is in disagreement with the simulated dielectric band edge which lies around $a/\lambda = 0.29$. The transmission in the air band is slowly increasing, and large in the last structure (a687). This slow increase is also visible in the simulation results. Note that in both measurement series the transmission in the air band is higher than in the dielectric band.

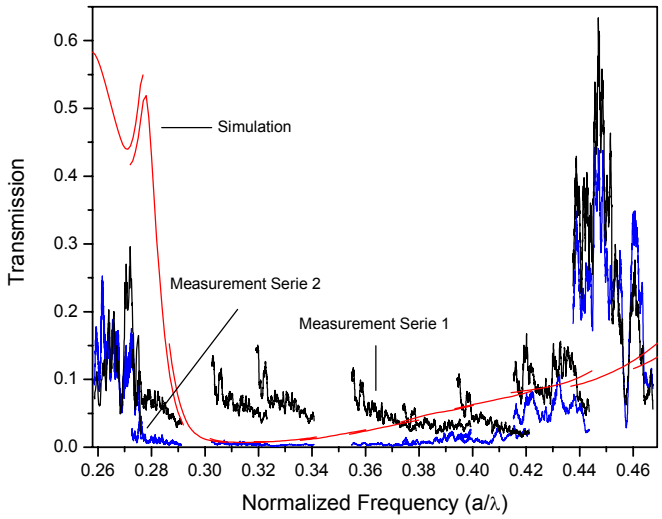

Figure 5-32: normalized measurement data from the first and second measurements series and the simulated transmission diagram. See Appendix II for simulation parameters.

There is a discrepancy in the location of the dielectric band in the simulated transmission diagram and the measured transmission diagrams. The differences in simulations and the actual structures can be found in the layer structure and in the r/a values. The simulations are performed with the r/a value fixed at 0.3. The actual r- and a-values are shown in Table 5-3. In Table 5-5 the simulated layer structure and the actual layer structure are compared. The actual waveguide does consist of five layers instead of the simulated three and is much thicker. The waveguide is in reality multimode in the vertical direction as is shown in Figure 5-33.

Table 5-5: layer structures for the simulated and measured PhCs

Simulation			Measurement		
Layer	Thickness (nm)[6]	n	Layer	Thickness (nm)	n
Air	∞	1	Air	∞	1
			SiN	99	1.93
GaN	650 nm	2.31	GaN	828	2.31
			AlN	116	2.1
Sapphire	∞	1.77	Sapphire	∞	1.77

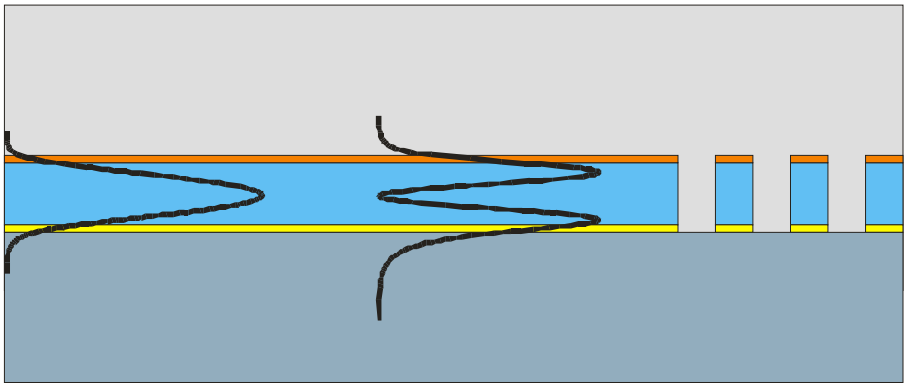

Figure 5-33: intensity profiles of the vertical modes for the actual layer structure (Table 5-5) [Hammer2007].

The simulated structure must come as close as possible to the real structure for honest comparison of the measurement data with the simulation. The specifications of the fabricated PhCs are put into Crystal Wave to simulate the transmission diagram. It is assumed that the holes are etched through the AlN layer. Note that the simulations are only performed for the fundamental mode. Figure 5-34 shows the results. There is a large difference between the original simulation (line a) and the simulation that comes as near to the real structure as possible (line b). The dielectric band edge is shifted from $a/\lambda = 0.29$ to $a/\lambda = 0.275$. This can be explained again with the increasing effective index between the real and the designed structure. Furthermore the transmission at the air band is not gradually increasing. The air band edge appears fairly sharp around $a/\lambda = 0.33$.

To understand the change between simulation a and b two more transmission graphs are simulated, one with the designed layer structure and the measured r- and a-values and one with the measured layer structure and the designed r/a-value (respectively line c and d in Figure 5-34). The results show that the large difference is

[6] The thickness of the air and sapphire layers are not chosen infinitely in Crystal Wave, however the layer is much larger than the penetration depth of the mode.

mainly caused by the change in r/a-value from 0.3 to about 0.25 instead of the change in layer structure. The decrease in radius leads to an increase of the effective index of the guided modes in the air band. Therefore the dielectric band and air band shift to lower frequencies leading to lower losses in the air band. In Figure 5-35 the banddiagrams are shown for a 2D PhC with the designed layer structure and $r/a = 0.3$, and with the actual layer structure and $r/a = 0.25$. It shows that especially the air band is shifted to lower frequencies.

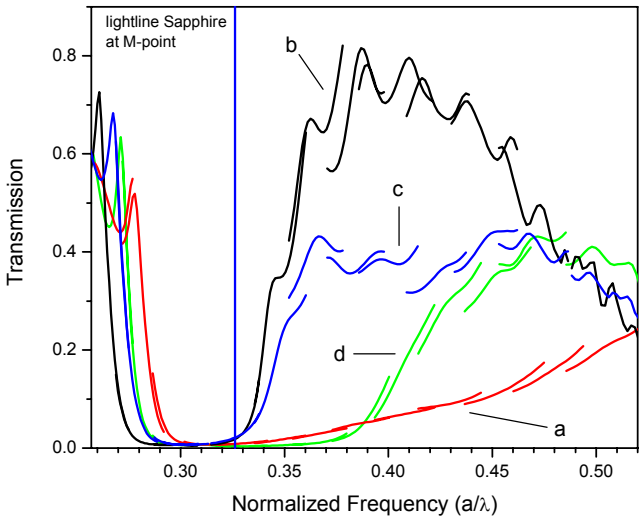

Figure 5-34: lithographic transmission simulations. a: the designed layer structure and designed r/a-value. b: the measured layer structure and measured r/a-value. c: the designed layer structure and measured r/a-value. d: the measured layer structure and designed r/a-value. See Table 5-5 for the designed and measured layer structure. The designed r/a-value is 0.3. In Table 5-3 the measured r- and a-value are shown. See Appendix II for simulation parameters.

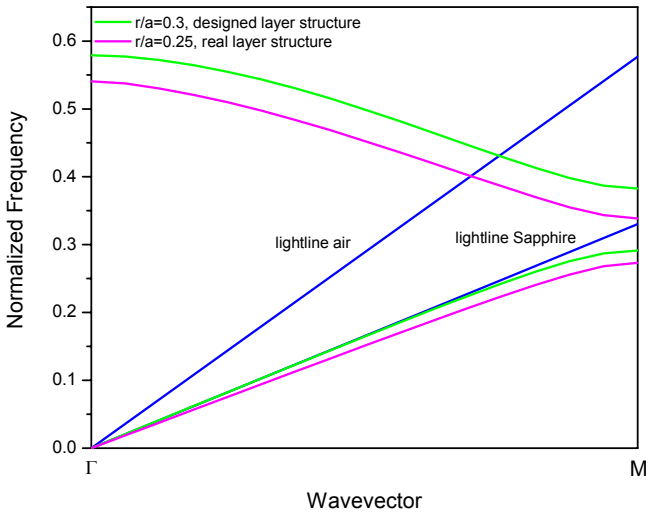

Figure 5-35: banddiagram for a 2D PhC. The effective index used for the calculations is 2.14 for the designed layer structure and 2.20 for the actual layer structure.

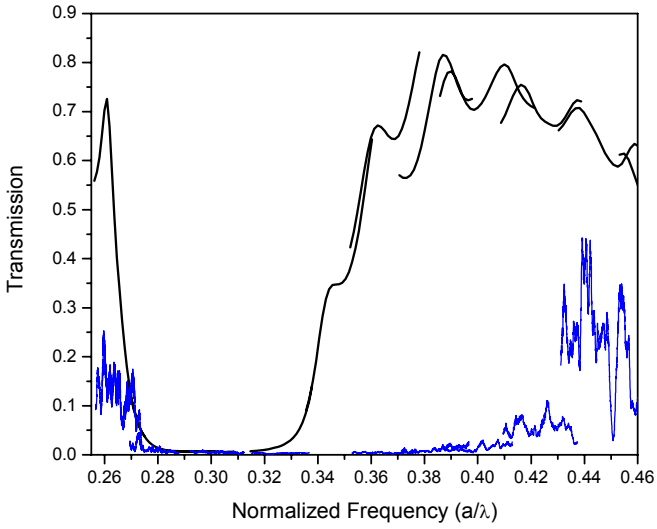

Figure 5-36: measurement data (second series) compared to the simulated data. The dielectric band edges of the simulation and the measurements are overlapping. There is no correspondence between the measurement and the simulation on the air band side. See Appendix II for simulation parameters.

In Figure 5-36 the data from measurement series 2 is compared with the simulation. The simulated location of the dielectric band edge corresponds with the measured location. The transmission in the air band should rise at $a/\lambda = 0.33$ according to the simulations. In reality it rises around $a/\lambda = 0.40$. Apparently the losses in the air band are very high. The simulations already showed that the losses are very sensitive to the r/a-ratio. The losses are probably also sensitive to the shape of the PhC holes. The difference in the air band location is therefore attributed to extrinsic losses in the PhCs: the sidewalls of the holes might not be vertical and might not be etched down

to the sapphire layer. It is also possible that the losses are due to light propagating in a higher order mode.

Measurement Results Sample 2

For S1 the holes were smaller than designed. In S2 this is corrected and the holes are larger than in S1. The actual r- and a-values are shown in Table 5-4. The thickness of the layer structure of sample 2 is not measured yet. Both samples are part of the same GaN wafer. The measured layer structure of S1 is therefore an indication for the layer structure of S2 (Table 5-2). The sample edges are not standing perpendicular to the waveguides. However the problems with alignment were smaller than with S1.

In Figure 5-37 the transmission data through the waveguides are presented. The transmission through the PhCs is shown in Figure 5-38. Although no SEM images of the waveguides are made yet there are two indications that the quality of the waveguides is better than those of S1. First indication is that the level of transmission is higher for the waveguides of S2 than of the waveguides of S1. Second indication is the experimental observation that when the red laser beam couples to the waveguide less light is coupling out due to imperfections for S2 than for S1.

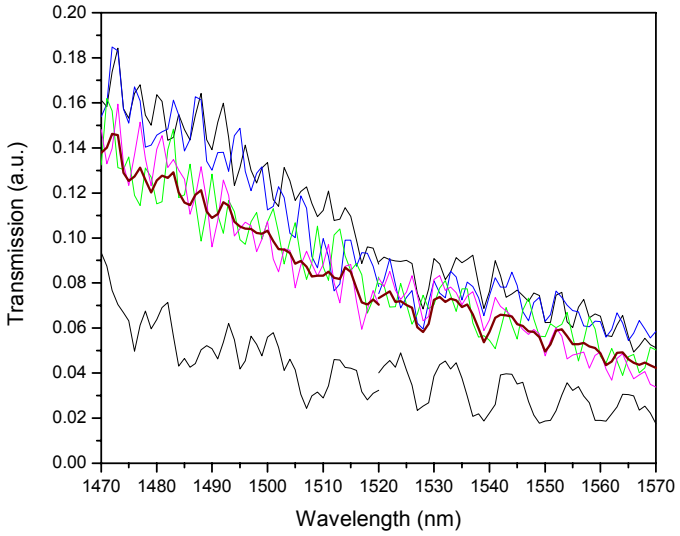

Figure 5-37: transmission through the waveguides of S2. The thick line is the average transmission. A total of 5 waveguides were measured.

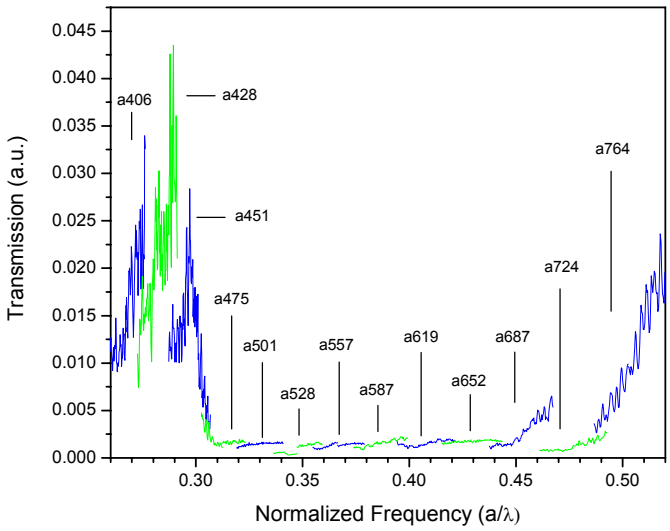

Figure 5-38: transmission versus normalized frequency for S2.

In Figure 5-39 the normalized transmission data is presented. Note that the dielectric band edge is formed by two PhC structures with perfect overlap in transmission. The dielectric band edge lies around $a/\lambda = 0.3$. There is no air band edge present. Just like for S1 the air band is gradually increasing. The measured transmission in the dielectric band is higher than in the air band, contrary to the results of S1. This indicates that losses in the air band are higher in this sample than in S1. This is consistent with the lower effective index of guided modes.

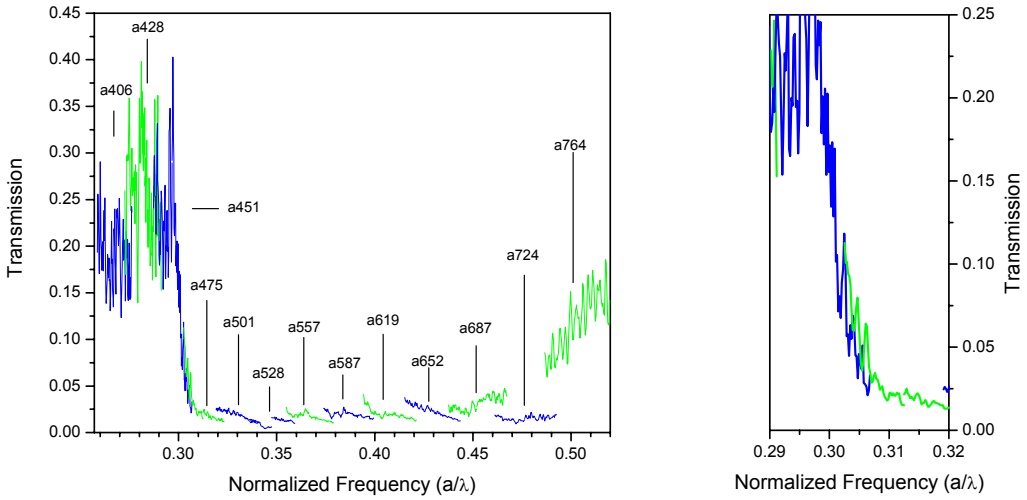

Figure 5-39: normalized transmission versus normalized frequency for S2.

In Figure 5-40 the measurement data of S1 and S2 are compared with each other and with simulations. The transmission diagram of S2 is shifted to higher frequencies. This shift is partially caused by the increase in hole size. The air band edge is also

shifted to higher frequencies compared to the simulation results for the actual layer structure of S1 and the r/a value of 0.3 (d). The dielectric band edge of S2 is measured in the structures a451 and a475. The r/a value for these structures is respectively 0.30 and 0.31. According the simulation d no dielectric band edge is expected in these structures for these r/a values. There is no explanation so far for the large shift in dielectric band edge. The air band of S2 is increasing more gradually and at higher frequencies than the air band of S1. This is in line with the general trend shown by the simulations c and d.

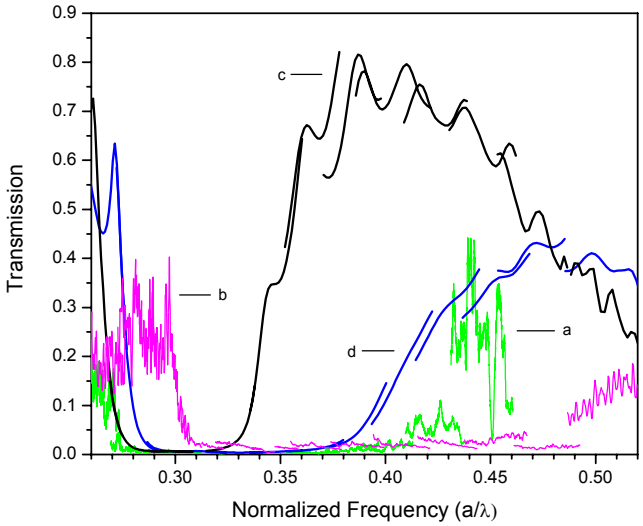

Figure 5-40: a: measurement S1, b: measurement S2, c: simulation with measured layer structure and measured r/a -value of S1, d: simulation with measured layer structure of S1 and r/a -value of 0.3. See Appendix II for simulation parameters.

5.7 *Conclusions*

Simulations have shown that it is possible to design a GaN PhC with a bandgap around the optical telecommunications wavelength with a compact vertical mode. The PhC consist of a 650 nm thick GaN layer with the sapphire substrate and the air layer as claddings. The holes are only puncturing the GaN layer. For lithographic tuning measurements the simulated transmission diagram must be adjusted. This is done by simulating the transmission diagrams of all the lithographic PhCs.

Etch tests in Delft showed that it is technologically possible to fabricate the designed PhC. This is later confirmed by the measurements of S1 and S2. The quality of the cleaved facets is well enough to use for light incoupling. However having the sample edges (and facets) not standing perpendicular to the waveguides lead to alignment problems. It is advised to find other ways of producing smooth facets that stand perpendicular to the waveguides. Sawing and polishing and the use of a laser cutter can be investigated. Another method might be using a focused ion beam (FIB) to etch a deep trench into the sapphire wafer over a long distance and then break the sample. The use of grating couplers for light in- and outcoupling is also possible. A sample specific grating should be designed to optimize the coupling. Changing the objectives

in the set-up for objectives with a larger working distance could of course also relieve the issue.

The measurement results clearly show the existence of the dielectric band and air band in both S1 and S2. The measured dielectric band from S1 coincides with the simulation results. There are however large differences between the simulation and the air band of S1 probably caused by out of plane losses due to imperfections in the holes and the multi-mode waveguide. The dielectric band from S2 is shifted to higher frequencies compared to S1. The layer structure and actual r- and a-values must be investigated before this large shift can be fully understood. It is expected that the shift is partially caused by the larger r/a-value, although this cannot explain the complete shift.

In the original PhC design the r/a-value was set to 0.3 for technological reasons. For S1 the r/a-value was however measured at about 0.25. Simulations showed that the PBG of the PhC with the r/a-value of 0.25 would be better defined than for the PhC with the r/a-value of 0.3. It is critical to increase the effective index of the membrane mode above that of the substrate.

Chapter 6 Conclusions

The aim of this project was to investigate the use of two dimensional (2D) photonic crystals (PhCs) for enhancement of light extraction efficiency in particular in gallium nitride (GaN) light emitting diodes (LEDs) and to start experimenting with GaN 2D PhCs.

PhCs can enhance the external quantum efficiency of LEDs by Purcell enhancement, redistribution of modes and Bragg scattering of light to continuum. A simulation approach used by Fan *et al.* [Fan1997] is proposed to investigate two of these effects: redistribution of modes and Bragg scattering. 2D Finite Difference Time Domain (FDTD) simulations for light extraction from a dielectric slab are performed. It is found that the simulations were consistent and reliable for low normalized frequencies $a/\lambda < 1.5$, with λ the vacuum wavelength of light and a the lattice constant. The relation between extraction efficiency and slab mode density of states as found by Fan was confirmed. Analogous FDTD simulations in 3D for a real PhC slab were unsuccessful due to problems with the simulation software.

A GaN on sapphire PhC with a triangular lattice of holes and with the photonic bandgap (PBG) in the optical telecommunications wavelength is designed and fabricated. PhCs with a PBG in this wavelength region are chosen because they are easier to fabricate and there exist ample reference data for other materials. 3D FDTD simulations show that the complete air band is lying above the lightline for sapphire for $r/a = 0.3$, with r the radius of the holes. A gradual increase in transmission in the air band is therefore expected instead of a sharp edge. For $r/a = 0.25$ the air band is lying slightly above the light line for sapphire. Simulations show a sharp air band edge.
Two samples containing lithographically tuned PhCs are optically characterized by transmission measurements. The measurement results show the existence of a dielectric band with a sharp edge. A gradual increase in transmission is observed in the air band for both samples. The measurement result of one sample is compared with 3D FDTD simulations, confirming the location of the dielectric band edge. The location of the measured air band does not correspond to the location of the simulated air band. This deviation is attributed to losses due to imperfect PhC hole shapes.

Literature

[Bogaerts2001] W. Bogaerts, P. Bienstman, D. Taillaert, R.Baets, D. de Zutter, IEEE Phot. Techn. Lett. **13**, 565 (2001)

[Boroditsky1999-1] M. Boroditsky, T.F. Krauss, R. Coccioli, R. Vrijen, R.Bhat, and E. Yablonovitch, Appl. Phys. Lett. **75**, 1036 (1999)

[Boroditsky1999-2] M. Boroditsky, R. Vrijen, T.F. Krauss, R. Coccioli, R. Bhat, and E. Yablonovitch. Journal of Lightwave and Techn. **17**, 2096 (1999)

[Chao2006] C.-H. Chao, S.L. Chuang, and T.-L. Wu, Appl. Phys. Lett. **89**, 091116 (2006)

[Choi2005] Y.-S. Choi, K. Hennessy, R. Sharma, E. Haberer, Y, Gao, S.P. DenBaars, S. Nakamura, and E.L. Hu, Appl. Phys. Lett. **87**, 243101 (2005)

[Cook2006] Jim Cook, Loomis Incorporate (2006)

[Coquillat1999] D. Coquillat, A. Ribayrol, R.M. de La Rue, P. Girard, O. Briot, R.L. Aulombard, D. Cassagne, and C. Jouanin, Phys. Stat. Sol. (b) **216**, 669 (1999)

[Coquillat2001a] D. Coquillat, A. Ribayrol, R.M. de La Rue, M. Le Vassor D'Yerville, D. Cassagne, and C. Jouanin, Phys. Stat. Sol. (a) **183**, 135 (2001)

[Coquillat2001b] D. Coquillat, A. Ribayrol, R.M. de La Rue, M. Le Vassor D'Yerville, D. Cassagne, and J.P. Albert, Appl. Phys. B **73**, 591-593 (2001)

[CrystalWave2007] Crystal Wave Manual version 4.0, Photon Design, Oxford England

[David2005] A. David, C. Meier, R. Sharma, F.S. Diana, S.P. DenBaars, E.Hu, S. Nakamura, C. Weisbuch, and H. Benisty, Appl. Phys. Lett. **87**, 101107 (2005)

[David2006a] A. David, T. Fujii, R. Sharma, K. McGroddy, S. Nakamura, S.P. DenBaars, E.L. Hu, C. Weisbuch, and H. Benisty, Appl. Phys. Lett. **88**, 061124 (2006)

[David2006b] A. David, T. Fujii, B. Moran, S. Nakamura, S.P. DenBaars, C. Weisbuch, and H. Benisty, Appl. Phys. Lett. **88**, 133514 (2006)

[DOE2003] www.netl.doe.gov/ssl/PDFs/Niche%20Final%20Report.pdf

[Erchak2001] A.A. Erchak, D.J. Ripin, S. Fan, P. Rakich, J.D. Joannopoulos, E.P. Ippen, G.S. Petrich, and L.A. Kolodziejski, Appl. Phys. Lett. **78**, 563 (2001)

[Fan1997] S. Fan, P.R. Villeneuve, J.D. Joannopolous, and E.F. Schubert, Phys. Rev. Lett. **78**, 3294 (1997)

[Fujii2004] T. Fujii, Y. Gao, R. Sharma, E.L. Hu, S.P. DenBaars, and S. Nakamura, Appl. Phys. Lett. **84**, 855 (2004)

[Fujita2005] M. Fujita, S. Takahashi, Y. Tanaka, T. Asano and S. Noda, Science **308**, 1296 (2005)

[Ghent2007] CAMFR, http://camfr.sourceforge.net/ (2007)

[Hammer2007] M. Hammer, http://wwwhome.math.utwente.nl/~hammerm/index.html (2007)

[Hui2003a] R. Hui, S.Taherion, Y. Wan, J. Li, S.X. Jin, J.Y. Lin, and H.X. Jiang, Appl. Phys. Lett. **82**, 1326 (2003)

[Hui2003b] R. Hui, Y. Wan, J. Li, S.X. Jin, J.Y. Lin, and H.X. Jiang, Appl. Phys. Lett. **83**, 1698 (2003)

[Inoue2004] K. Inoue, and K. Ohtaka, Photonic Crystals; Physcis, Fabrication and Applications, Springer–Verlag (2004), ISBN 3-540-20559-4

[Ioffe2007] www.ioffe.rssi.ru/SVA/NSM/Semicond/index.html

[Jackson1962] J.D. Jackson, Classical Electrodynamics, John Wiley & Sons, New York (1962)

[Joannopoulos1995] J.D. Joannopoulos, R.D. Meade, J.N. Winn, Photonic Crystals; Molding the Flow of Light, Princeton University Press (2005), ISBN 0-691-03744-2

[John1987] S. John, Phys Rev. Lett. **58**, 2486 (1987)

[Johnson1999] S.G. Johnson, S. Fan, P.R. Villeneuve, J.D. Joannopoulos, and L.A. Kolodziejski, Phys. Rev. Lett. **60**, 5751 (1999)

[Krames1999] M.R. Krames *et al.*, Appl. Phys. Lett. **75**, 2365 (1999)

[Krauss2006] Thomas. F. Krauss, summer school presentation, 2nd EPS-QEOD Europhoton Conference on Solid-State and Fiber Coherent Light Sources, Pisa, Italy (09-2006)

[Meier2006] C. Meijer, K. Hennessy, E.D. Haberer, R. Sharma, Y.-S. Choi, K. McGroddy, S. keller, S.P. DenBaars, S. Nakamura, and E.L. Hu, Appl. Phys. Lett. **88**, 031111 (2006)

[MellesGriot2007] http://www.mellesgriot.com/products/optics/mp_3_5.htm

[Nakamura2000] Nakamura *et al.*, Introduction to Nitride Semiconductor and Blue Lasers and Light Emitting Diodes, Taylor&Francis (2000), ISBN 0-7484-0836-3

[Oder2003] T.N. Oder, J. Shakya, J.Y. Lin, and H.X. Jiang, Appl. Phys. Lett. **83**, 1231 (2003)

[Oder2004] T.N. Oder, K.H. Kim, J.Y. Lin, and H.X. Jiang, Appl. Phys. Lett. **84**, 466 (2004)

[Peyrade2001] D. Peyrade, Y. Chen, L Manin-Ferlazzo, A. Lebib, N. Grandjean, D. Coquillat, R. Legros, and J-P Lascaray, Microelectronic Eng. **57-58**, 843-849 (2001)

[Peyrade2003] D. Peyrade *et al.*, Physica E **17**, 423-425 (2003)

[Purcell1946] E.M. Purcell, Physical Review **69**, 681 (1946)

[Qiu2002] M. Qiu, Appl. Phys. Lett. **81**, 1163 (2002)

[Rattier2002] M. Rattier, T.F. Krauss, J.-F. Carlin, R. Stanley, U. Oesterle, R. Houdré, C.J.M. Smith, R.M. De La Rue, H. Benisty, and C. Weisbuch, Optical and Quantum Electronics **34**, 79 (2002)

[Saleh1991] B.E.A.Saleh, and M.C. Teich, Fundamentals of Photonics, Chichester : Wiley-Interscience (1991), ISBN 0-471-83965-5

[Shakya2004] J. Shakya, K.H. Kim, J.Y. Lin, and H.X. Jiang, Appl. Phys. Lett. **85**, 142 (2004)

[Shakya2004-2] J. Shakya, J.Y. Lin, and H.X. Jiang, Appl. Phys. Lett. **85**, 2104 (2004)

[Schubert2003] E.F. Schubert, Light-Emitting Diodes, Cambridge University Press (2003), ISBN 0-521-82330-7

[VanderHeijden2006] R.W. van der Heijden, InP-based Planar Photonic Crystals: Process Development, Characterization and Infiltration, PhD thesis, University of Technology Eindhoven (2006)

[Wang2006] W.K. Wang, S.Y. Huang, S.H. Huang, K.S. Wen, D.S. Wuu, and R.H. Horng, Appl. Phys. Lett. **88**, 181113 (2006)

[Watanabe2006] S. Watanabe, N. Yamada, *et al.*, Appl. Phys. Lett. **83**, 4908 (2003)

[Wierer2004] J.J. Wierer, M.R. Krames, J.E. Epler, N.F. Gardner, M.G. Crafor, J.R. Wendt, J.A. Simmons and M.M. Sigalas, Appl. Phys. Lett. **84**, 3885 (2004)

[Yablonovitch1987] E. Yablonovitch, Phys. Rev. Lett. 58, 2059 (1987)

[Zhang1996] H.Y. Zhang, X.H. He, Y.H. Shih, M. Schurman, Z.C. Feng, and R.A. Stall, Optics Lett. **21**, 1529 (1996)

[Zhang2006] Z.S. Zhang, B. Zhang, J. Xu, K. Xu. J. Yang, Z.X. Qin, T.J. Yu, and D.P. Yu, Appl. Phys. Lett. **88**, 171103 (2006)

Appendix I

A fraction of about $1/4n^2$ of light generated in a dielectric slab can escape through the top or bottom surface. The derivation of this approximation is shown below.

Consider a dielectric slab with index n_1, surrounded by a material with lower index n_2. The critical angle for total internal reflection is $\sin\theta_c = n_2/n_1$. Assume that light incident on the boundary between material 1 and 2 with the angle $\theta < \theta_c$ will fully escape to the low index material. Furthermore it is assumed that light is emitted uniformly in all directions.

Figure A1 shows that light incident up the boundary with the angle smaller than the critical angle will escape to medium 2. The fraction of light that can escape is the blue area from the sphere divided by 4π.

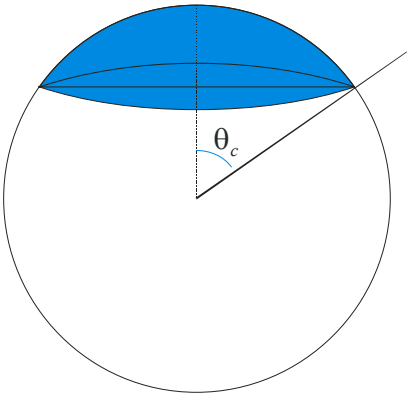

Figure A1: the blue part of the sphere represents the amount of light that is directly extracted from the slab.

The area of the blue part of the sphere can be calculated with $2\pi r^2(1-\cos\theta_c)$. Filling in the critical angle $\theta_c = \sin^{-1}(n_2/n_1)$ and by using $\cos(\sin^{-1}\alpha) = \sqrt{1-\alpha^2}$ the equation $2\pi r^2\left(1-\sqrt{1-(n_2/n_1)^2}\right)$ is obtained.

The output efficiency is $(1/2)\left(1-\sqrt{1-(n_2/n_1)^2}\right)$. Develop the function $\sqrt{1-x}$ with a Taylor series around *0*: $\sqrt{1-x} = 1 - x/2 + x^2/8 + \Re$. Fill in $x = (n_2/n_1)^2$. The fraction of extracted light is than given by: $\frac{1}{2}\left(1-\sqrt{1-(n_2/n_1)^2}\right) \approx \frac{n_2^2}{4n_1^2} - \frac{n_2^4}{16n_1^4} + \Re$. With $n_2 = 1$ (air) we find that a fraction of about $1/4n^2$ will be directly coupled out through the top or bottom surface.

Appendix II

In this appendix the simulation parameters for the 3D FDTD transmission simulations as shown in Chapter 5 are given. With these parameters the simulations can be reconstructed in Crystal Wave.

Figure 5-5

Photonic Crystal		
Parameter	**Value**	**Units**
Lattice Type	Triangular	
Lattice Constant (a)	0.560	µm
Number of Rows	**11 / 22**	
Size Z	**5.789/10.61**	µm
Size X	16	µm

Photonic Crystal Holes		
Parameter	**Value**	**Units**
Material	Air	
r/a value	0.3	
Diameter	0.334	µm
Top Boundary		
YMaxLayer	Top GaN layer	
Bottom Boundary		
YMinLayer	Bottom GaN Layer	

FDTD Calculator		
Parameter	**Value**	**Units**
NumDimensions	3D	
DurationSpec	t/timesteps	
Duration	16384	time steps
Duration	1438	fs
CentralWavelength	0	µm
Grid		
GridType	Match lattice	
Gridspacing	0.0406	µm

Layer Structure			
Material	**Thickness**	**Units**	**n**
Air	2	µm	1
Gallium Nitride	0.65	µm	2.31
Sapphire	2	µm	1.77

Sensor		
Name	Input	
Parameter	**Coordinate**	**Units**
Position Z	3	µm
Position X	0	µm
Angle	0	degrees
Size X	8	µm
Top Boundary		
YMaxCoordinate	3.65	µm
Bottom Boundary		
YMinCoordinate	1	µm

Sensor		
Name	Output	
Parameter	**Coordinate**	**Units**
Position Z	13	Mm
Position X	0	µm
Angle	0	degrees
Size X	8	µm
Top Boundary		
YMaxCoordinate	3.65	µm
Bottom Boundary		
YMinCoordinate	1	µm

Excitor		
Parameter	**Coordinate**	**Units**
Position Z	1	µm
Position X	0	µm
Angle	0	degrees
Top Boundary		
YMaxLayer	Top Air Layer	
Bottom Boundary		
YminLayer	Bottom Sapphire Layer	
Time Domain		
Wavelength	1.55	µm
TimeEnvShape	Sinusoidal pulse	
TimeEnvWidthSpec	Width in femtoseconds	
TimeEnvWidth	20	fs
Mode Excitor		
Width	8	µm
Power	1	W
Phase	0	degrees
ModeSolver	Effective Index Solver	
Effective Index Solver		
Polarisation	TE	
ModeOrder	0	
ProfileMethod	Uniform	

Figure 5-7

Simulation 1

GaN Membrane			
Layer Structure			
Material	**Thickness**	**Units**	**n**
Air	2	µm	1
Gallium Nitride	0.65	µm	2.31
Air	2	µm	1
Photonic Crystal Holes			
Top Boundary			
YMaxLayer	**Top GaN Layer**		
Bottom Boundary			
YMinLayer	**Bottom GaN Layer**		

Simulation 2

GaN Semi Membrane			
Layer Structure			
Material	**Thickness**	**Units**	**n**
Air	2	µm	1
Gallium Nitride	0.65	µm	2.31
Sapphire	2	µm	1.77
Photonic Crystal Holes			
Top Boundary			
YMaxLayer	**Top GaN Layer**		
Bottom Boundary			
YMinLayer	**Bottom GaN Layer**		

Simulation 3

GaN-Sapphire			
Layer Structure			
Material	**Thickness**	**Units**	**N**
Air	2	µm	1
Gallium Nitride	0.65	µm	2.31
Sapphire	2	µm	1.77
Photonic Crystal Holes			
Top Boundary			
YMaxLayer	**Top GaN Layer**		
Bottom Boundary			
YMinLayer	**Bottom Sapphire Layer**		

Photonic Crystal		
Parameter	**Value**	**Units**
Lattice Type	Triangular	
Lattice Constant (a)	0.557	µm
Number of Rows	11	
Size Z	5.789	µm
Size X	16	µm

Photonic Crystal Holes		
Parameter	**Value**	**Units**
Material	Air	
r/a value	0.3	
Diameter	0.334	µm
Top Boundary		
YMaxLayer	**See Table**	
Bottom Boundary		
YMinLayer	**See Table**	

FDTD Calculator		
Parameter	**Value**	**Units**
NumDimensions	3D	
DurationSpec	t/timesteps	
Duration	16384	time steps
Duration	1438	fs
CentralWavelength	0	µm
Grid		
GridType	Match lattice	
Gridspacing	0.0406	µm

Sensor		
Name	Input	
Parameter	**Coordinate**	**Units**
Position Z	3	µm
Position X	0	µm
Angle	0	degrees
Size X	8	µm
Top Boundary		
YMaxCoordinate	3.65	µm
Bottom Boundary		
YMinCoordinate	1	µm

Sensor		
Name	Output	
Parameter	**Coordinate**	**Units**
Position Z	13	µm
Position X	0	µm
Angle	0	degrees
Size X	8	µm
Top Boundary		
YMaxCoordinate	3.65	µm
Bottom Boundary		
YMinCoordinate	1	µm

Excitor		
Parameter	**Coordinate**	**Units**
Position Z	1	µm
Position X	0	µm
Angle	0	degrees
Top Boundary		
YMaxLayer	Top Air Layer	
Bottom Boundary		
YminLayer	Bottom Sapphire Layer	
Time Domain		
Wavelength	1.55	µm
TimeEnvShape	Sinusoidal pulse	
TimeEnvWidthSpec	Width in femtoseconds	
TimeEnvWidth	20	fs
Mode Excitor		
Width	8	µm
Power	1	W
Phase	0	degrees
ModeSolver	Effective Index Solver	
Effective Index Solver		
Polarisation	TE	
ModeOrder	0	
ProfileMethod	Uniform	

Figure 5-8

Simulation 1

GaN 650 nm: See Figure 5-5

Simulation 2

GaN 450 nm			
Layer Structure			
Material	**Thickness**	**Units**	**n**
Air	2	µm	1
Gallium Nitride	0.45	µm	2.31
Sapphire	2	µm	1.77
Photonic Crystal Holes			
Top Boundary			
YMaxLayer	**Top GaN Layer**		
Bottom Boundary			
YMinLayer	**Bottom GaN Layer**		

Photonic Crystal		
Parameter	**Value**	**Units**
Lattice Type	Triangular	
Lattice Constant (a)	0.557	µm
Number of Rows	11	
Size Z	5.789	µm
Size X	16	µm

Photonic Crystal Holes		
Parameter	**Value**	**Units**
Material	Air	
r/a value	0.3	
Diameter	0.334	µm
Top Boundary		
YMaxLayer	Top GaN layer	
Bottom Boundary		
YMinLayer	Bottom GaN Layer	

FDTD Calculator		
Parameter	**Value**	**Units**
NumDimensions	3D	
DurationSpec	t/timesteps	
Duration	16384	time steps
Duration	1438	fs
CentralWavelength	0	µm
Grid		
GridType	Match lattice	
Gridspacing	0.0406	µm

Sensor		
Name	Input	
Parameter	**Coordinate**	**Units**
Position Z	3	µm
Position X	0	µm
Angle	0	degrees
Size X	8	µm
Top Boundary		
YMaxCoordinate	3.45	µm
Bottom Boundary		
YMinCoordinate	1	µm

Sensor		
Name	Output	
Parameter	**Coordinate**	**Units**
Position Z	13	µm
Position X	0	µm
Angle	0	degrees
Size X	8	µm
Top Boundary		
YMaxCoordinate	3.45	µm
Bottom Boundary		
YMinCoordinate	1	µm

Excitor		
Parameter	**Coordinate**	**Units**
Position Z	1	µm
Position X	0	µm
Angle	0	degrees
Top Boundary		
YMaxLayer	Top Air Layer	
Bottom Boundary		
YminLayer	Bottom Sapphire Layer	
Time Domain		
Wavelength	1.55	µm
TimeEnvShape	Sinusoidal pulse	
TimeEnvWidthSpec	Width in femtoseconds	
TimeEnvWidth	20	fs
Mode Excitor		
Width	8	µm
Power	1	W
Phase	0	degrees
ModeSolver	Effective Index Solver	
Effective Index Solver		
Polarisation	TE	
ModeOrder	0	
ProfileMethod	Uniform	

Figure 5-11

Simulation 1

GaN 650 nm: See Figure 5-5

Simulation 2

GaN 850 nm TE0			
Layer Structure			
Material	**Thickness**	**Units**	**n**
Air	2	µm	1
Gallium Nitride	0.85	µm	2.31
Sapphire	2	µm	1.77
Photonic Crystal Holes			
Top Boundary			
YMaxLayer	**Top GaN Layer**		
Bottom Boundary			
YMinLayer	**Bottom GaN Layer**		

Photonic Crystal		
Parameter	**Value**	**Units**
Lattice Type	Triangular	
Lattice Constant (a)	0.557	µm
Number of Rows	11	
Size Z	5.789	µm
Size X	16	µm

Photonic Crystal Holes		
Parameter	**Value**	**Units**
Material	Air	
r/a value	0.3	
Diameter	0.334	µm
Top Boundary		
YMaxLayer	Top GaN layer	
Bottom Boundary		
YMinLayer	Bottom GaN Layer	

FDTD Calculator		
Parameter	**Value**	**Units**
NumDimensions	3D	
DurationSpec	t/timesteps	
Duration	16384	time steps
Duration	1438	fs
CentralWavelength	0	µm
Grid		
GridType	Match lattice	
Gridspacing	0.0406	µm

Sensor		
Name	Input	
Parameter	**Coordinate**	**Units**
Position Z	3	µm
Position X	0	µm
Angle	0	degrees
Size X	8	µm
Top Boundary		
YMaxCoordinate	3.85	µm
Bottom Boundary		
YMinCoordinate	1	µm

Sensor		
Name	Output	
Parameter	**Coordinate**	**Units**
Position Z	13	µm
Position X	0	µm
Angle	0	degrees
Size X	8	µm
Top Boundary		
YMaxCoordinate	3.85	µm
Bottom Boundary		
YMinCoordinate	1	µm

Excitor		
Parameter	**Coordinate**	**Units**
Position Z	1	µm
Position X	0	µm
Angle	0	degrees
Top Boundary		
YMaxLayer	Top Air Layer	
Bottom Boundary		
YminLayer	Bottom Sapphire Layer	
Time Domain		
Wavelength	1.55	µm
TimeEnvShape	Sinusoidal pulse	
TimeEnvWidthSpec	Width in femtoseconds	
TimeEnvWidth	20	fs
Mode Excitor		
Width	8	µm
Power	1	W
Phase	0	degrees
ModeSolver	Effective Index Solver	
Effective Index Solver		
Polarisation	TE	
ModeOrder	0	
ProfileMethod	Uniform	

Simulation 3

GaN 850 nm TE1			
Layer Structure			
Material	**Thickness**	**Units**	**n**
Air	3	µm	1
Gallium Nitride	0.85	µm	2.31
Sapphire	6	µm	1.77
Photonic Crystal Holes			
Top Boundary			
YMaxLayer	**Top GaN Layer**		
Bottom Boundary			
YMinLayer	**Bottom GaN Layer**		

Photonic Crystal		
Parameter	**Value**	**Units**
Lattice Type	Triangular	
Lattice Constant (a)	0.557	µm
Number of Rows	11	
Size Z	5.789	µm
Size X	16	µm

Photonic Crystal Holes		
Parameter	**Value**	**Units**
Material	Air	
r/a value	0.3	
Diameter	0.334	µm
Top Boundary		
YMaxLayer	Top GaN layer	
Bottom Boundary		
YMinLayer	Bottom GaN Layer	

FDTD Calculator		
Parameter	**Value**	**Units**
NumDimensions	3D	
DurationSpec	t/timesteps	
Duration	16384	time steps
Duration	1438	fs
CentralWavelength	0	µm
Grid		
GridType	Match lattice	
Gridspacing	0.0406	µm

Sensor		
Name	Input	
Parameter	**Coordinate**	**Units**
Position Z	3	µm
Position X	0	µm
Angle	0	degrees
Size X	8	µm
Top Boundary		
YMaxCoordinate	7.85	µm
Bottom Boundary		
YMinCoordinate	5	µm

Sensor		
Name	Output	
Parameter	**Coordinate**	**Units**
Position Z	13	µm
Position X	0	µm
Angle	0	degrees
Size X	8	µm
Top Boundary		
YMaxCoordinate	7.85	µm
Bottom Boundary		
YMinCoordinate	5	µm

Excitor		
Parameter	**Coordinate**	**Units**
Position Z	1	µm
Position X	0	µm
Angle	0	degrees
Top Boundary		
YMaxLayer	Top Air Layer	
Bottom Boundary		
YminLayer	Bottom Sapphire Layer	
Time Domain		
Wavelength	1.55	µm
TimeEnvShape	Sinusoidal pulse	
TimeEnvWidthSpec	Width in femtoseconds	
TimeEnvWidth	20	fs
Mode Excitor		
Width	8	µm
Power	1	W
Phase	0	degrees
ModeSolver	**IMPORT FIMMWAVE**	

Figure 5-13, Figure 5-14, Figure 5-15, Figure 5-32, Figure 5-34

Layer Structure			
Material	**Thickness**	**Units**	**n**
Air	2	µm	1
Gallium Nitride	0.65	µm	2.31
Sapphire	2	µm	1.77

Simulations				
Number	**a (µm)**	**r/a**	**diameter (µm)**	**Size Z (µm)**
1	0.406	0.3	0.244	4.2193
2	0.428	0.3	0.257	4.4479
3	0.451	0.3	0.271	4.6869
4	0.475	0.3	0.285	4.9363
5	0.501	0.3	0.301	5.2065
6	0.528	0.3	0.317	5.4871
7	0.557	0.3	0.334	5.7885
8	0.587	0.3	0.352	6.1003
9	0.619	0.3	0.371	6.4328
10	0.652	0.3	0.391	6.7758
11	0.687	0.3	0.412	7.1395
12	0.724	0.3	0.434	7.5240
13	0.764	0.3	0.458	7.9397

Photonic Crystal		
Parameter	**Value**	**Units**
Lattice Type	Triangular	
Lattice Constant (a)	**See Table**	µm
Number of Rows	11	
Size Z	**See Table**	µm
Size X	16	µm

Photonic Crystal Holes		
Parameter	**Value**	**Units**
Material	Air	
r/a value	**See Table**	
Diameter	**See Table**	µm
Top Boundary		
YMaxLayer	Top GaN layer	
Bottom Boundary		
YMinLayer	Bottom GaN Layer	

FDTD Calculator		
Parameter	**Value**	**Units**
NumDimensions	3D	
DurationSpec	t/timesteps	
Duration	16384	time steps
Duration	1438	fs
CentralWavelength	0	µm
Grid		
GridType	Match lattice	
Gridspacing	0.0406	µm

Sensor		
Name	Input	
Parameter	**Coordinate**	**Units**
Position Z	3	µm
Position X	0	µm
Angle	0	degrees
Size X	8	µm
Top Boundary		
YMaxCoordinate	3.65	µm
Bottom Boundary		
YMinCoordinate	1	µm

Sensor		
Name	Output	
Parameter	**Coordinate**	**Units**
Position Z	13	µm
Position X	0	µm
Angle	0	degrees
Size X	8	µm
Top Boundary		
YMaxCoordinate	3.65	µm
Bottom Boundary		
YMinCoordinate	1	µm

Excitor		
Parameter	**Coordinate**	**Units**
Position Z	1	µm
Position X	0	µm
Angle	0	degrees
Top Boundary		
YMaxLayer	Top Air Layer	
Bottom Boundary		
YminLayer	Bottom Sapphire Layer	
Time Domain		
Wavelength	1.55	µm
TimeEnvShape	Sinusoidal pulse	
TimeEnvWidthSpec	Width in femtoseconds	
TimeEnvWidth	20	fs
Mode Excitor		
Width	8	µm
Power	1	W
Phase	0	degrees
ModeSolver	Effective Index Solver	
Effective Index Solver		
Polarisation	TE	
ModeOrder	0	
ProfileMethod	Uniform	

Figure 5-34, Figure 5-36, Figure 5-37, Figure 5-40

Layer Structure			
Material	**Thickness**	**Units**	**n**
Air	2	µm	1
Silicon Nitride	0.099	µm	1.93
Gallium Nitride	0.828	µm	2.31
Aluminum Nitride	0.116	µm	2.1
Sapphire	2	µm	1.77

Simulations				
Number	**a (µm)**	**r/a**	**diameter (µm)**	**Size Z (µm)**
1	0.403	0.26	0.210	4.1881
2	0.423	0.25	0.215	4.3959
3	0.452	0.25	0.226	4.6973
4	0.459	0.25	0.234	4.7701
5	0.495	0.25	0.245	5.1442
6	0.528	0.24	0.258	5.4871
7	0.554	0.24	0.264	5.7573
8	0.583	0.24	0.284	6.0587
9	0.607	0.24	0.297	6.3081
10	0.643	0.25	0.326	6.6823
11	0.677	0.25	0.338	7.0356
12	0.713	0.25	0.351	7.4097
13	0.768	0.25	0.386	7.9813

Photonic Crystal		
Parameter	**Value**	**Units**
Lattice Type	Triangular	
Lattice Constant (a)	**See Table**	µm
Number of Rows	11	
Size Z	**See Table**	µm
Size X	16	µm

Photonic Crystal Holes		
Parameter	**Value**	**Units**
Material	Air	
r/a value	**See Table**	
Diameter	**See Table**	µm
Top Boundary		
YMaxLayer	Top SiN layer	
Bottom Boundary		
YMinLayer	Bottom AlN Layer	

FDTD Calculator		
Parameter	**Value**	**Units**
NumDimensions	3D	
DurationSpec	t/timesteps	
Duration	16384	time steps
Duration	1427	fs
CentralWavelength	0	µm
Grid		
GridType	Match lattice	
Gridspacing	**0.0403**	Mm

Sensor		
Name	Input	
Parameter	**Coordinate**	**Units**
Position Z	3	µm
Position X	0	µm
Angle	0	degrees
Size X	8	µm
Top Boundary		
YMaxCoordinate	Middle Air Layer	
Bottom Boundary		
YMinCoordinate	Middle Sapphire Layer	

Sensor		
Name	Output	
Parameter	**Coordinate**	**Units**
Position Z	13	µm
Position X	0	µm
Angle	0	degrees
Size X	8	µm
Top Boundary		
YMaxLayer	Middle Air Layer	
Bottom Boundary		
YMinLayer	Middle Sapphire Layer	

Excitor		
Parameter	**Coordinate**	**Units**
Position Z	1	µm
Position X	0	µm
Angle	0	degrees
Top Boundary		
YMaxLayer	Top Air Layer	
Bottom Boundary		
YminLayer	Bottom Sapphire Layer	
Time Domain		
Wavelength	1.55	µm
TimeEnvShape	Sinusoidal pulse	
TimeEnvWidthSpec	Width in femtoseconds	
TimeEnvWidth	20	fs
Mode Excitor		
Width	8	µm
Power	1	W
Phase	0	degrees
ModeSolver	Effective Index Solver	
Effective Index Solver		
Polarisation	TE	
ModeOrder	0	
ProfileMethod	Uniform	

Figure 5-34, Figure 5-40

Layer Structure			
Material	**Thickness**	**Units**	**n**
Air	2	µm	1
Silicon Nitride	0.099	µm	1.93
Gallium Nitride	0.828	µm	2.31
Aluminum Nitride	0.116	µm	2.1
Sapphire	2	µm	1.77

Simulations				
Number	**a (µm)**	**r/a**	**diameter (µm)**	**Size Z (µm)**
1	0.406	0.3	0.244	4.2193
2	0.428	0.3	0.257	4.4479
3	0.451	0.3	0.271	4.6869
4	0.475	0.3	0.285	4.9363
5	0.501	0.3	0.301	5.2065
6	0.528	0.3	0.317	5.4871
7	0.557	0.3	0.334	5.7885
8	0.587	0.3	0.352	6.1003
9	0.619	0.3	0.371	6.4328
10	0.652	0.3	0.391	6.7758
11	0.687	0.3	0.412	7.1395
12	0.724	0.3	0.434	7.5240
13	0.764	0.3	0.458	7.9397

Photonic Crystal		
Parameter	**Value**	**Units**
Lattice Type	Triangular	
Lattice Constant (a)	**See Table**	µm
Number of Rows	11	
Size Z	**See Table**	µm
Size X	16	µm

Photonic Crystal Holes		
Parameter	**Value**	**Units**
Material	Air	
r/a value	**See Table**	
Diameter	**See Table**	µm
Top Boundary		
YMaxLayer	Top GaN layer	
Bottom Boundary		
YMinLayer	Bottom GaN Layer	

FDTD Calculator		
Parameter	**Value**	**Units**
NumDimensions	3D	
DurationSpec	t/timesteps	
Duration	16384	time steps
Duration	1438	fs
CentralWavelength	0	µm
Grid		
GridType	Match lattice	
Gridspacing	0.0406	µm

Sensor		
Name	Input	
Parameter	**Coordinate**	**Units**
Position Z	3	µm
Position X	0	µm
Angle	0	degrees
Size X	8	µm
Top Boundary		
YMaxCoordinate	Middle Air Layer	
Bottom Boundary		
YMinCoordinate	Middle Sapphire Layer	

Sensor		
Name	Output	
Parameter	**Coordinate**	**Units**
Position Z	13	µm
Position X	0	µm
Angle	0	degrees
Size X	8	µm
Top Boundary		
YMaxLayer	Middle Air Layer	
Bottom Boundary		
YMinLayer	Middle Sapphire Layer	

Excitor		
Parameter	**Coordinate**	**Units**
Position Z	1	µm
Position X	0	µm
Angle	0	degrees
Top Boundary		
YMaxLayer	Top Air Layer	
Bottom Boundary		
YminLayer	Bottom Sapphire Layer	
Time Domain		
Wavelength	1.55	µm
TimeEnvShape	Sinusoidal pulse	
TimeEnvWidthSpec	Width in femtoseconds	
TimeEnvWidth	20	fs
Mode Excitor		
Width	8	µm
Power	1	W
Phase	0	degrees
ModeSolver	Effective Index Solver	
Effective Index Solver		
Polarisation	TE	
ModeOrder	0	
ProfileMethod	Uniform	

Figure 5-34

Layer Structure			
Material	**Thickness**	**Units**	**n**
Air	2	µm	1
Gallium Nitride	0.650	µm	2.31
Sapphire	2	µm	1.77

Simulations				
Number	**a (µm)**	**r/a**	**diameter (µm)**	**Size Z (µm)**
1	0.403	0.26	0.210	4.1881
2	0.423	0.25	0.215	4.3959
3	0.452	0.25	0.226	4.6973
4	0.459	0.25	0.234	4.7701
5	0.495	0.25	0.245	5.1442
6	0.528	0.24	0.258	5.4871
7	0.554	0.24	0.264	5.7573
8	0.583	0.24	0.284	6.0587
9	0.607	0.24	0.297	6.3081
10	0.643	0.25	0.326	6.6823
11	0.677	0.25	0.338	7.0356
12	0.713	0.25	0.351	7.4097
13	0.768	0.25	0.386	7.9813

Photonic Crystal		
Parameter	**Value**	**Units**
Lattice Type	Triangular	
Lattice Constant (a)	**See Table**	µm
Number of Rows	11	
Size Z	**See Table**	µm
Size X	16	µm

Photonic Crystal Holes		
Parameter	**Value**	**Units**
Material	Air	
r/a value	**See Table**	
Diameter	**See Table**	µm
Top Boundary		
YMaxLayer	Top SiN layer	
Bottom Boundary		
YMinLayer	Bottom AlN Layer	

FDTD Calculator		
Parameter	**Value**	**Units**
NumDimensions	3D	
DurationSpec	t/timesteps	
Duration	16384	time steps
Duration	1427	fs
CentralWavelength	0	µm
Grid		
GridType	Match lattice	
Gridspacing	**0.0403**	Mm

Sensor		
Name	Input	
Parameter	**Coordinate**	**Units**
Position Z	3	µm
Position X	0	µm
Angle	0	degrees
Size X	8	µm
Top Boundary		
YMaxCoordinate	Middle Air Layer	
Bottom Boundary		
YMinCoordinate	Middle Sapphire Layer	

Sensor		
Name	Output	
Parameter	**Coordinate**	**Units**
Position Z	13	µm
Position X	0	µm
Angle	0	degrees
Size X	8	µm
Top Boundary		
YMaxLayer	Middle Air Layer	
Bottom Boundary		
YMinLayer	Middle Sapphire Layer	

Excitor		
Parameter	**Coordinate**	**Units**
Position Z	1	µm
Position X	0	µm
Angle	0	degrees
Top Boundary		
YMaxLayer	Top Air Layer	
Bottom Boundary		
YminLayer	Bottom Sapphire Layer	
Time Domain		
Wavelength	1.55	µm
TimeEnvShape	Sinusoidal pulse	
TimeEnvWidthSpec	Width in femtoseconds	
TimeEnvWidth	20	fs
Mode Excitor		
Width	8	µm
Power	1	W
Phase	0	degrees
ModeSolver	Effective Index Solver	
Effective Index Solver		
Polarisation	TE	
ModeOrder	0	
ProfileMethod	Uniform	

Dankwoord

Ik wil hierbij Huub bedanken voor het mogelijk maken van dit afstudeerproject, voor alle ideeën, hulp en commentaar en voor het helpen nadenken over wat te doen na mijn studie. Ik heb dat zeer gewaardeerd. Rob bedankt voor de fantastische begeleiding. Jou ideeën en opmerkingen hebben zeker bijgedragen aan een beter begrip van mijn kant en aan het succes van de GaN PhC fabricage.

Bifeng, thank you for all the work you have done. Without your excellent expertise on etching of GaN I would not have been able to measure any GaN PhC samples. I have appreciated all your comments and help and overall it was nice working with you.

Ik bedank natuurlijk ook mijn (oud)-kamergenoten dr. ir. Robbie, Harm en Johan voor alle gezelligheid. Dit ondanks het oude pepermuntjes ritueel [VanderHeijden2006]. En verder (maar zeker niet minder belangrijk): Margriet voor alle hulp en ondersteuning en veel meer dan dat, Peter voor de SEM plaatjes, Frans voor de nodige technische ondersteuning, Carl Fredrich voor de gezelligheid en het opdampen van SiN, Luc Augustin voor Fimm Wave, Els Kok voor de nuttige opmerkingen, Fouad Karouta voor de informatie over het klieven van GaN, Tjibbe de Vries voor de gegevens van SiN en alle groepsgenoten voor de gezelligheid. Van de TU Delft wil ik graag Jaap Caro, Felipe Bernal en Emiel van der Drift bedanken voor hun bijdrage en opmerkingen.

Als laatste wil ik alle vrienden bedanken en vooral mijn vriendin Elise voor alle gezelligheid en ondersteuning (en geduld).

Bedankt allemaal!